Effectiveness of Inductive Vehicle Charging to Alleviate EV Range Anxiety

Final Report

05/20/2026

Prepared For:

Michigan Department of Transportation

Research Administration

8885 Ricks Rd.

P.O. Box 30049

Lansing MI 48909

Prepared By:

Sina Bahrami

Manzi Li

Yafeng Yin

The Regents of the University of Michigan

Office of Research and Sponsored Projects

Wolverine Tower

First Floor, Room 1058

3003 South State Street

Ann Arbor, Michigan 48109-1274

TECHNICAL REPORT DOCUMENTATION PAGE

1. Report No.	2. Government Accession No.	3. Recipient's Catalog No.
SPR-1768	N/A	

4. Title and Subtitle	5. Report Date
Effectiveness of Inductive Vehicle Charging to Alleviate EV Range Anxiety	05/20/2026
	6. Performing Organization Code N/A

7. Author(s)	8. Performing Organization Report No.
Sina Bahrami, Ph.D. https://orcid.org/0000-0002-0049-8326 Manzi Li, Ph.D. https://orcid.org/0000-0002-8155-5010 Yafeng Yin, Ph.D. https://orcid.org/0000-0003-3117-5463	N/A

9. Performing Organization Name and Address	10. Work Unit No.
The Regents of the University of Michigan Office of Research and Sponsored Projects Wolverine Tower First Floor, Room 1058 3003 South State Street Ann Arbor, Michigan 48109-1274	N/A
	11. Contract or Grant No. Contract #2022-0433 Z4

12. Sponsoring Agency Name and Address	13. Type of Report and Period Covered
Michigan Department of Transportation (MDOT) Research Administration 8885 Ricks Road P.O. Box 33049 Lansing, Michigan 48909	Final Report, 5/20/2024 – 5/20/2026
	14. Sponsoring Agency Code N/A

15. Supplementary Notes

Conducted in cooperation with the U.S. Department of Transportation, Federal Highway Administration. MDOT research reports are available at www.michigan.gov/mdotresearch.

16. Abstract

This study evaluates the efficacy, optimal placement, and economic viability of Inductive Vehicle Charging (IVC) technology as a strategic solution to facilitate electrification of the Michigan transportation sector. Motivated by the need to mitigate range anxiety and support high-utilization electric fleets, the research employs a multi-methodological approach combining economic modeling, transit network analysis, and macroscopic highway optimization. The findings demonstrate that while stationary IVC chargers are sufficient for smaller transit agencies, in-motion IVC is critical for larger, high-frequency transit systems to maintain operational continuity without fleet expansion. For intercity travel, optimization models reveal that high-power dynamic charging on key arterial corridors specifically in Southeast Michigan maximizes social welfare by complementing the existing DC fast-charging network. The study concludes that IVC offers a distinct economic advantage in scenarios characterized by high traffic density and fleet utilization, recommending targeted investment in shared infrastructure for transit and freight corridors.

17. Key Words	18. Distribution Statement
Electric vehicles; Charging infrastructure; Wireless charging technology	No restrictions. This document is also available to the public through the Michigan Department of Transportation.

19. Security Classif. (of this report)	20. Security Classif. (of this page)	21. No. of Pages	22. Price
Unclassified	Unclassified	127	N/A

Acknowledgments

The authors would like to express their gratitude to the Michigan Department of Transportation (MDOT) for sponsoring this research. Special appreciation is extended to Michele Mueller, Project Manager, and Caitlin Mackay, Co-Project Manager, whose support were instrumental to the success of the work. The authors are also grateful to Mary Hoffmeyer (Research Manager), Janet Geissler, and Kelly Bartlett for their valuable comments and feedback during progress meetings, which significantly enhanced the clarity and quality of this report. In addition, the authors would like to thank Karen Faussett, and Jesse Frankovich for assisting with access to the State network and travel model, which greatly supported the intercity highway case study.

Disclaimer

This material is based upon work supported by the Federal Highway Administration under SPR-1768. Any opinions, findings and conclusions or recommendations expressed in this publication are those of the author(s) and do not necessarily reflect the views of the Federal Highway Administration.

Table of Contents

List of Tables

List of Figures

Executive Summary

The transportation sector accounts for approximately one-third of greenhouse gas (GHG) emissions in the United States. While the transition to electric vehicles (EVs) is a crucial strategy for decarbonization, widespread adoption is hindered by range anxiety. The Michigan Department of Transportation (MDOT) commissioned this study to explore Inductive Vehicle Charging (IVC) as a potential solution. IVC allows vehicles to charge wirelessly while stationary or in motion, potentially eliminating charging downtime and reducing the need for large batteries.

The primary objective of this project was to identify high-impact use cases for IVC technology implementation. The research team assessed current IVC capabilities through literature review and manufacturer consultations, and developed detailed optimization models to determine optimal locations for implementation in real-world cases.

The state of the art for stationary IVC charging capability is comparable to plug-in fast charging; however, in-motion (dynamic) IVC charging capability is currently lower. Therefore, the study concludes that transit systems are the premier use case for this technology due to their high vehicle utilization and repetitive driving over the same routes. However, analyses of major urban Michigan transit agencies indicate that smaller agencies can electrify using only stationary plug-in chargers. In contrast, larger agencies face operational bottlenecks that require either fleet expansion, service reduction, or stationary or in-motion IVC. The choice depends on a specific cost-benefit analysis of infrastructure versus fleet and service operations. The deployment of stationary and in-motion IVC was found to render 100% of transit electrification feasible, eliminating the need for fleet expansion or schedule adjustments. A web-based decision-support tool was developed to assist agencies in optimizing charger locations. For personal intercity travel, the benefits of IVC are limited by extended EV ranges and recommended rest stops during long trips. However, optimal placement revealed that IVC is most effective when deployed on high-volume corridors. At higher power and available budget levels, optimal infrastructure placement consolidates around key urban centers like Southeast Michigan. In these locations, IVC complements the existing DC fast-charging network by enabling EVs to extend their range without stopping.

Based on these findings, the report recommends targeted pilot projects on transit routes where the cost of fleet expansion outweighs IVC infrastructure investment. These focused investments will maximize the return on infrastructure spending, effectively mitigate range anxiety for critical user groups, and support the robust electrification of Michigan's transportation network. In addition, it is important for planners to stay adaptable and

closely follow progress in battery technology and ultra-fast charging, as these innovations may diminish the necessity for in-motion charging in the future.

1 Introduction

1.1 Background

Greenhouse gas (GHG) emissions have been on a constant rise since the 19th century, peaking in 2019. The Paris Agreement, enacted in 2015, set an ambitious goal to limit the global temperature increase to 2°C above pre-industrial levels. However, with the current emission patterns, projected infrastructure developments, and national level policy commitments, achieving the targets set by the Paris Agreement has become increasingly challenging. In the US, approximately one-third of GHG emissions are produced by the transportation sector (Morrow et al., 2010). To decrease transportation GHG emissions, the shift to electric vehicles (EVs) due to their energy efficiency and reduced emissions has been prioritized in the Infrastructure Investment and Jobs Act (IIJA). However, the limited driving range of EVs, shortage of charging stations, and long charging times, often referred to as range anxiety, hinder their widespread usage. To alleviate EV users' range anxiety, over 1200 public stations with around 3000 ports have been established throughout Michigan as shown in Figure 1 (Alternative Fuels Data Center, 2023).

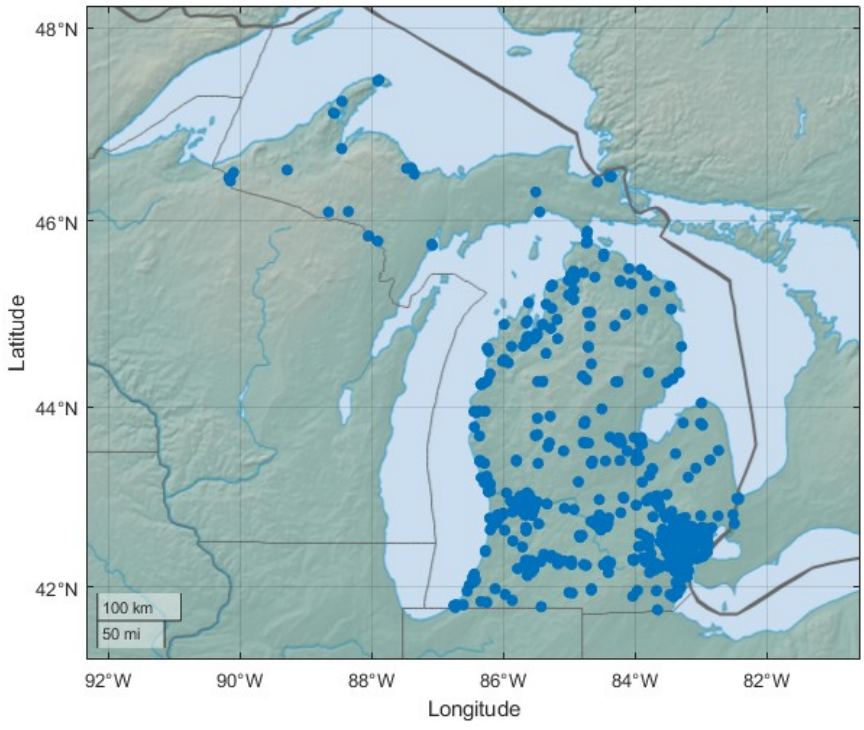

Figure 1: Location of public charging stations in Michigan.

These charging stations utilize Level 1, Level 2, and direct current (DC) fast charging. However, even with DC fast charging, EV charging time is still relatively high compared to refueling at gas stations. For instance, Level 2 chargers typically take one hour to add 10–20 miles of driving range, and DC fast charging can take 30 minutes to get from 20% to 80% charge, which is unsuitable for en-route charging. Currently, most fast charging stations are located along highways to facilitate long-distance travel (Charge up Michigan Program, 2023). Consequently, the Michigan Department of Transportation (MDOT) is exploring the potential of inductive vehicle charging (IVC) technology, which enables EVs to wirelessly charge, as an innovative solution. Throughout this report, the terms IVC and wireless charging will be used interchangeably to describe this technology.

Thus, IVC technology could eliminate the need for long stoppages for recharging, potentially reduce the range anxiety of EVs, and improve EV adoption rates. Wireless charging for EVs was first proposed and tested in the 1990s by California's PATH program (Shladover, 1992). Although the pilot demonstrated the possibility of charging while driving, commercialization of the concept was not achieved due to low power transfer efficiency and high construction and maintenance costs. The Korea Advanced Institute of Science and Technology (KAIST) successfully developed the first commercial dynamic (in-motion) IVC technology in its campus shuttle system in 2009, demonstrating 80% charging efficiency and cost savings by reducing the fleet and battery size of buses (Lee et al., 2010; Jeong et al., 2015; Suh and Cho, 2017). Since then, numerous pilots worldwide have been announced to test the feasibility of IVC technology including an electrified test track at Utah State University (Morris, 2015), in Gotland, Sweden (Smart Road Gotland, 2023), and in Detroit, Michigan (State of Michigan, 2022). A comprehensive list of these demonstration projects and their properties is presented by Jang (2018). In addition, researchers are investigating various aspects of IVC technology. One major research stream examines the optimal location of IVC lanes through micro and macro models. The micro models focus on a specific route like a transit route to find the optimal section for IVC technology (Ko and Jang, 2013; Jang et al., 2015; Ko et al., 2015; Hwang et al., 2018; Liu and Song, 2017). These models employ realistic driving patterns and energy usage, which may contribute to optimizing EV battery capacity. Conversely, macro models strive to determine the optimal link to introduce IVC technology into a network to either maximize flow coverage (Riemann et al., 2015), minimize the cost to satisfy all trips considering EV range (Fuller, 2016), or minimize the total network travel time (Chen et al., 2016). These studies use approximations and generalizations like average trip length or EV range and generally consider private fleets with flexible route choices. While IVC technology could reduce the need for lengthy recharge times and decrease range anxiety, it may not be the best charg-

ing option for all EV users. Alternative charging methods may be more suitable depending on various factors such as vehicle and trip characteristics. For instance, a commuter with access to a charger at home or work might not benefit from IVC. However, another commuter without such access or with a commute distance greater than their vehicle's driving range could make effective use of IVC, where possible, negating the need for extra trips or lengthy waits at charging stations. Certain characteristics need consideration to ensure the effectiveness of IVC technology such as the less flexible routes of delivery trucks or the fixed routes of transit buses. Moreover, IVC technology's potential benefits are not restricted to mitigating recharging times and range anxiety, as it could also reduce fleet operating costs by, e.g., reducing fleet size via eliminating charging downtime of buses in a transit agency. This highlights the need to further explore IVC technology, systematically identify its use cases, and develop decision-support tools for optimal location implementation. This project will assess, analyze, and validate IVC technology's effectiveness for different light- and heavy-duty vehicle use cases, and it will provide insights on where IVC charging lanes are more effective.

1.1.1 Objectives

This project aims to evaluate the efficacy of IVC in overcoming range anxiety for different EV users. It systematically categorizes different light- and heavy-duty transportation user groups and investigates their use cases where these various users can reap benefits from IVC implementation. Considering different EV user groups, this project provides proof of concept for locations or scenarios in which IVC technology effectively removes range anxiety for light- to heavy-duty vehicles. In addition, the project investigates the current IVC technology characteristics. Subsequently, the project conducts a cost-benefit analysis for the selected high-impact IVC use cases, taking into account the cost of the technology and its benefits. This will determine the economic sustainability of IVC and the feasibility of its broader implementation. Such evaluation will assist MDOT and policymakers in their planning endeavors to promote electric mobility.

1.1.2 Scope

The scope of this project is structured around five major tasks.

Task 1: Identification of IVC Use Cases

This task aims to identify different IVC use cases targeting various types of EV users, specify scenarios under which IVC technology can effectively overcome users' range anxiety or will be favored over charging stations, and assess the potential benefits of IVC

technology for each use case.

Task 2: Investigation of IVC Technology State-of-the-Art

This task involves collecting and analyzing data on IVC technology by reviewing the literature, examining the industry, meeting with IVC technology manufacturer(s), and gathering information from the IVC pilots.

Task 3: Determine Ideal Locations

Following the definition of the high-impact use case for targeted user groups in Task 1, and harnessing the information gathered on IVC technology properties from Task 2, we will research and establish mathematical models to identify the optimal locations for implementing IVC technology, with the objective of mitigating range anxiety for the selected high-impact use case. A single model cannot fully encapsulate the details of various use cases. For example, if the intercity highways or transit routes are identified as the high-impact use cases, the charging scenarios for both are distinct. In the bus transit route case, buses could charge while in transit or during scheduled stops for passenger boarding and alighting. In contrast, on intercity highways, vehicles can only charge while in motion. Consequently, in the transit routes use case, the strategic decision to be addressed by the model is whether to assign IVC locations to stops or routes, taking into account both in-motion and stationary charging efficiencies of IVC. However, in the intercity highways use case, charging occurs solely when in motion, and therefore the model needs to incorporate traffic speed profiles to identify optimal sections of the highways for IVC implementation. Therefore, a custom model will be created tailored to meet the requirements of the chosen high-impact use case. This model can then act as a decision-support tool for MDOT when selecting optimal locations for IVC technology implementation.

Task 4: Assess Implementation Cost and Expansion Feasibility

Finally, we calculate the IVC implementation cost based on the information collected in Task 3 to conduct a cost-benefit analysis for the selected high-impact use case. We provide a conceptual cost-benefit analysis for the selected high-impact use case to help MDOT in their return-on-investment analysis.

1.2 Statement of Hypotheses

This study tests the following hypotheses regarding the ability of IVC to mitigate EV range anxiety and support economically feasible deployment.

H1: Range Anxiety Mitigation

For targeted EV user groups, access to IVC along relevant routes/scenarios reduces range anxiety relative to a charging-stations-only baseline (e.g., fewer/shorter charging-

related delays), and the magnitude of range-anxiety reduction provided by IVC differs across user groups.

H2: Technical Sufficiency of Current IVC

State-of-the-art IVC technology (e.g., power delivery, efficiency, reliability) is sufficient to produce a meaningful net energy gain for at least one high-impact Michigan use case spanning light- to heavy-duty vehicles. Also, incorporating IVC reduces the required on-board battery capacity and/or plug-in charging needs to meet service requirements, enabling electrification of operations that are otherwise infeasible or impractical under a plug-in charging-only strategy.

H3: Existence of High Impact Locations

For the selected high-impact use case(s), an optimization model can identify a limited set of roadway segments and/or stops where IVC deployment yields a disproportionate share of achievable range-anxiety reduction.

2 Literature review

2.1 Review of Previous Research

The widespread adoption of EVs is hindered by several factors. Among the most significant is range anxiety, a concern stemming from the limited range of EVs, long recharging times, and the scarcity of charging stations (Bahrami et al., 2017; Niroumand et al., 2023). Recent advancements in battery technology have increased the maximum range of light-duty EVs to over 500 miles, with a median range approaching 300 miles (Fuel Economy, 2024), which is comparable to traditional internal combustion engine vehicles. However, long-distance trips for light-duty vehicles, such as cross-country travel, often exceed the driving range of EVs. In contrast, heavy-duty vehicles are driven for long hours on a daily basis (Bahrami et al., 2020). These extended trips, along with unplanned journeys without a fully charged battery, can deter potential buyers from adopting EVs.

In efforts to address these challenges, numerous public and private charging stations have been established across the nation. However, charging times are still relatively lengthy compared to refueling at gas stations, even with fast charging options. For example, DC fast chargers usually take between 30 minutes to an hour to fully charge EVs. As a result, wireless charging, particularly in-motion wireless charging which allows vehicles to recharge while driving over charging pads embedded in the pavement, is gaining attention as an innovative alternative to traditional charging methods to potentially eliminate extended stops for recharging.

The concept of wireless electricity transmission traces its origins back to the latter half of the 19th century, with Nikola Tesla's pioneering work laying the foundational principles. By the late 20th century, the practical applications of this technology began to emerge, notably illustrated by California's PATH program, showcasing the potential of wireless technology in extending the range of electric vehicles (Shladover, 1992). Later, the KAIST implemented the first real-world wireless charging lane (WCL) for electric buses. This milestone achievement was recognized as one of "the 50 Best Inventions of 2010" by TIME Magazine, highlighting the potential of WCL to remove the range anxiety of EVs.

He et al. (2013a) were the first to explore wireless charging in transportation networks, assuming full network coverage and examining how charging prices for each link could impact users' route choices and reduce congestion. Later, Riemann et al. (2015) investigated the selection of optimal locations for placing wireless chargers among candidate sites to maximize the number of EVs that can use them on the shortest paths between origins and destinations. Fuller (2016) examined the minimum wireless charging requirements to facilitate travel between all origins and destinations by EVs, using California as a case study. Chen et al. (2016) considered that the amount of charging in WCL depends on travel time, which is a function of speed. They explored the trade-off between travel time and charging time to determine the optimal location of charging lanes for minimizing total travel times.

With the proliferation of public charging stations, researchers have turned their attention to the competitiveness and integration of wireless charging technologies alongside charging stations. Chen et al. (2017a) examined the competitiveness of WCLs in contrast to charging stations along a corridor and identified a critical threshold in the value of time for EV users, beyond which charging lanes become the preferred option. Liu and Wang (2017) developed a tri-level problem where, at the upper level, the government decides the location and type of charging provision; at the middle level, users choose between plug-in or wireless charging for their EVs; and at the lower level, the network route choice equilibrium is considered. Their numerical analysis indicated that with a limited budget, the government should invest in charging stations. However, as the budget increases, a combination of charging stations and WCLs becomes desirable. Sun et al. (2020) similarly investigated the deployment of charging stations and lanes, taking into account the interaction between transportation and electricity networks, where electricity prices are determined by the providers' locational marginal prices. They showed that building charging stations can provide more coverage, especially when the transportation network topology has a high node degree, or a large number of links connected to each node.

Since then, researchers have aimed to relax some assumptions in the previously men-

tioned models, addressing issues such as partial link coverage for wireless charging (Ngo et al., 2020), the reduction in link capacity due to slowdowns on charging lanes (He et al., 2020), optimizing electricity prices (Liu et al., 2021; Lai et al., 2024), optimizing wireless charging power (Mubarak et al., 2021), dynamic traffic assignment (Tran et al., 2022), and EVs discharging/selling electricity back to the network (Nasr Esfahani et al., 2022; Hossain et al., 2023). Additionally, to enhance the benefits of wireless charging while reducing implementation costs, its effect on decreasing EV battery size and cost (Liu et al., 2024b) or fleet sizes due to reduced charging downtime are considered. These are specially advantageous for fleets such as public transit (Liu et al., 2017; Liu and Song, 2017; Yang et al., 2018; Hwang et al., 2018; Iliopoulou and Kepaptsoglou, 2019; Luo and Fan, 2023; Wang et al., 2023; Liu et al., 2024a) and delivery fleets (Deflorio and Castello, 2017; Mouhrim et al., 2019; He et al., 2023; Ouyang and Wang, 2025).

Early research on wireless charging within transportation networks and its location problem in the 2010s was motivated by the limited range of EVs, with the median range being less than 100 miles until 2015 (Fuel Economy, 2024). This research was further driven by the long recharging times associated with Level 1 and Level 2 chargers and the predicted potential for high in-motion wireless charging power in future years. Table 1 provides details on the EV ranges and the power levels of plug-in and wireless charging considered in these earlier studies. However, the range of newer EV generations has significantly increased in recent years, alongside improvements in fast charging power and their availability through the transportation network. These advancements could reduce the competitiveness of wireless charging for EV users, which is the focus of our study.

Table 1: Assumed driving range and charging powers in literature.

Study	EV driving range [mi]	Plug in charging power [kW]	wireless charging power [kW]
Riemann et al. (2015)	25-45	—	—
Fuller (2016)	100-300	—	20-200
Chen et al. (2016)	60-85	—	6-90
Chen et al. (2017a)	60	100	100
Sun et al. (2020)	120	100	66
Ngo et al. (2020)	30	—	—
Tran et al. (2022)	2	—	20
Nasr Esfahani et al. (2022)	20-100	—	12-24

2.2 Summary of State-of-the-art

Several commercial manufacturers, including WAVE (now part of Ideanomics), InductEV, and Electreon, have deployed high-power inductive charging systems and demonstrated real-world performance across multiple power levels for light- and heavy-duty vehicles.

The discussion that follows is based on information gathered during meetings with manufacturer representatives and on technical documents provided by the manufacturers describing their deployments and measured performance, supplemented by relevant Society of Automotive Engineers (SAE) International standards (Hybrid - EV Committee, 2022, 2024).

Wireless vehicle charging is based on electromagnetic induction, whereby an alternating magnetic field generated by a primary coil induces current in a secondary coil. Contemporary systems typically employ resonant inductive coupling, in which both coils operate at a tuned resonant frequency to increase effective coupling and improve power transfer across practical air gaps (on the order of several centimeters). Although Maxwell's equations provide the theoretical foundation for induction phenomena, practical implementation depends on resonant power converters, frequency control, and high-efficiency power electronics operating in the tens-of-kilohertz range.

A typical wireless charging installation comprises a ground subsystem connected to the electrical grid and a vehicle subsystem integrated into the electric drivetrain. The ground subsystem generally includes the primary coil (ground pad), power-electronics enclosure, thermal management components, and digital control systems for communication, safety monitoring, and energy management. Because the ground pad is typically sealed beneath a protective surface, the installation is comparatively robust to weather, ice, debris, and vandalism. In contrast to plug-in (conductive) charging, the absence of mechanical contacts also reduces susceptibility to fatigue, corrosion, and vandalism. Commercial deployments report reliable operation across a wide range of climates with minimal weather-related performance degradation over evaluated testing periods.

On the vehicle side, the secondary (receiving) coil is integrated into the vehicle underbody and connected to on-board power electronics that interface with the vehicle battery management system. Reliable communication between the ground and vehicle subsystems is essential for authentication, interlocks, alignment confirmation, and charge control. Current deployments use a combination of CAN-based interfaces, vendor-specific protocols, and increasingly standardized approaches (e.g., within the ISO 15118 family, including ISO 15118-20).

Inductive systems regulate power delivery and maintain safety through coordinated control and sensing functions, including active alignment detection, foreign-object detection, and real-time converter control. Performance is sensitive to pad alignment. Consequently, inductive systems employ alignment detection and communication feedback to verify positioning before initiating power transfer. While lateral misalignment reduces coupling and efficiency, experiments report that modern systems can maintain grid-to-battery

efficiencies in the range of approximately 88–91% even under intentional lateral offsets of up to ±200 mm.

Commercial wireless systems are no longer limited to the low power levels associated with early research prototypes. Multiple manufacturers report static (stationary) inductive charging at power levels up to approximately 450 kW via modular installations, with real-world efficiencies near 90% across deployment sites. For dynamic (in-motion) charging, reported power levels are up to approximately 100 kW, depending on vehicle size and the number of receiving coils installed on the vehicle.

To date, the most widespread adoption of high-power inductive charging has been in transit applications. Antelope Valley Transit Authority in California implemented WAVE wireless chargers across multiple bus routes, enabling extended daily operation of electric buses. According to WAVE's case study, the system enabled more than 2.39 million miles of zero-emission operation, saved over 613,000 gallons of diesel, and avoided nearly 14.5 million pounds of CO_2 emissions. The same analysis reports annual operational savings exceeding US$1 million, attributable to reduced fuel costs, fewer required vehicles, and decreased maintenance relative to diesel operations.

In heavy-duty and freight contexts, InductEV reports installations for logistics operators, ports, and transit agencies using wireless systems rated up to 450 kW. Company documentation emphasizes peak-demand mitigation and energy-cost optimization through integrated energy management software that schedules charging events to reduce utility charges. These demonstrations suggest that demand management, together with high-power transfer capability, can strengthen the economic case for wireless charging within broader fleet electrification strategies.

Dynamic wireless charging remains at an earlier stage of deployment but has attracted substantial global interest. Electreon's projects in Europe and Israel demonstrate charging while driving, and the company's Detroit pilot represents a notable milestone for dynamic charging in the United States. The Detroit project integrates both static and dynamic inductive segments and has undergone performance validation using passenger shuttles and commercial fleet vehicles. Collectively, these demonstrations provide evidence of technical feasibility in real-world conditions and inform potential scaling to future broader applications.

3 Methodology

3.1 Economic Comparison

Current EVs rely on large battery packs to satisfy range requirements, resulting in substantial upfront acquisition and lifecycle maintenance costs. Conversely, WCL facilitates in-motion charging, thereby enabling the deployment of vehicles with significantly smaller and more cost-effective battery capacities. This technology enables the continuous power essential for future autonomous and commercial fleets, allowing them to operate near 24/7 without the productivity loss of charging stops (He et al., 2013b; Ahmad et al., 2017; Wang et al., 2024). The evaluation of this emerging technology requires solving a classic infrastructure optimization problem that trades off vehicle battery size against the density of charging opportunities (Nie and Ghamami, 2013; Chen et al., 2017b). Research on this new paradigm has logically split into two main streams. First, extensive work exists on technical component-level studies, such as hardware optimization for coil design and power transfer efficiency (Bosshard and Kolar, 2016; Tavakoli et al., 2021). The second stream provides foundational economic analyses, which have successfully confirmed the technology's potential in high-utilization scenarios like urban buses (Jeong et al., 2015; Chen et al., 2018) and heavy-duty freight (Liao et al., 2024; Ye et al., 2024). However, a systematic comparative evaluation of this inductive technology is largely absent. While essential for establishing initial viability, existing economic studies are fragmented. The most relevant work is limited to case-by-case analyses, such as deployment on a single corridor (Chen et al., 2017b) or for a specific bus system (Chen et al., 2018). Therefore, these studies do not provide a general model that defines the fundamental, underlying cost functions governing the infrastructure-to-battery trade-off. Consequently, a key strategic question remains unanswered: under what specific conditions is it more valuable to build a WCL versus investing in more conventional plug-in chargers? Building on these foundational insights, this section's objective is to provide the general framework needed to systematically answer this question.

To do so, we developed a general, parsimonious cost-competitiveness framework to strategically compare plug-in (conductive) charging station (CS) and WCL systems. Our model minimizes total societal cost by synthesizing governing variables across four domains: engineering (e.g., transfer efficiency), economics (e.g., infrastructure vs. battery costs), traffic dynamics (e.g., density, speed), and operations (e.g., fleet utilization). By explicitly modeling the trade-off between infrastructure investment, battery cost, and users' time cost, we identify the conditions under which each technology yields cost efficiency.

The key input parameters used throughout this analysis are summarized in Table 2.

Table 2: Key input parameters for economic comparison model.

Parameter	Description	Unit
System & Traffic Parameters		
m	Total VMT per hour	veh-miles/hr
l	Total length of roads in the network	miles
λ_{jam}	Traffic jam density	veh/mile
v_f	Free-flow speed	mph
v	Average vehicle speed	mph
λ	Traffic density	veh/mile
n	Total fleet size	veh
u	Fleet utilization factor	dimensionless
τ_a	Access time overhead for CS	hours
Technology Parameters		
d_w	Length of a single WCL charging segment	miles
ρ_{max}	Maximum allowable average occupancy for CS	dimensionless
β	Vehicle energy consumption rate	kWh/mile
θ	Usable battery fraction (depth of discharge)	dimensionless
γ	WCL power transfer efficiency	dimensionless
Economic Cost Parameters		
c_b	Amortized cost per kWh of battery capacity per hour	$/kWh-hr
c_1^w	Amortized fixed cost of WCL infra per hour	$/mile-hr
c_2^w	Amortized variable cost of WCL infra per hour	$/kW-mile-hr
c_1^s	Amortized fixed cost of a CS infra per hour	$/station-hr
c_2^s	Amortized variable cost of a CS infra per hour	$/kW-station-hr
ω	Value of travel time	$/hr

3.1.1 Transport System Characteristics

Our model analyzes a bounded transportation system, flexibly representing diverse application domains from general-purpose urban zones (e.g., city centers, corporate campuses) to commercial systems like municipal bus networks, regional freight arteries, and airport/seaport logistics fleets. The primary input for this system is the total hourly vehicle miles traveled (VMT) denoted by m, the average trip length denoted by $\bar{d}$, travel speed denoted by v, and total fleet size denoted by n. This definition allows the framework to flexibly represent either a future all-electric fleet or the EV component of a transitional, mixed-traffic system. Adopting a top-down macroscopic approach, we derive several key system parameters from fundamental traffic flow principles.

Given the system input, the trip generation rate r and average trip time t are:

$$r = \frac{m}{\bar{d}} \tag{1}$$

$$t = \frac{\bar{d}}{v} \tag{2}$$

By Little's Law, the average number of traveling vehicles $n_a = rt = m/v$. Thus, the fleet's utilization rate u and the total fleet size n are:

$$u = \frac{n_a}{n} \quad \Rightarrow \quad n = \frac{m}{vu} \tag{3}$$

This relationship correctly accounts for the large number of parked vehicles that constitute the total fleet but are not actively contributing to traffic at any given moment. For instance, a personally owned car might only be driven 5% of the day ($u = 0.05$), while a commercial robotaxi could be active 50% of the time ($u = 0.50$).

Finally, for a network with a total road length of l, the traffic density, λ is given by:

$$\lambda = \frac{n_a}{l} = \frac{m/v}{l} = \frac{m}{vl} \tag{4}$$

3.1.2 CS System Design Model

We model a CS system where a network of stations is deployed to serve the EV fleet. The decision variables for this system are the number of stations (N_s), the required battery size for each vehicle (E_s), and the aggregate power capacity of a charging station (P_s). We assume all stations in the network are deployed with this same optimal power level. We define the total system cost (J_s) as the sum of infrastructure investment, battery costs, and user travel time costs. In this section, we focus on the trade-off between infrastructure amount and battery size. Since the travel time is independent of the specific hardware layout at this stage, minimizing the hourly amortized technology cost C_s is equivalent to minimizing J_s.The optimization problem is formulated as:

$$\min_{N_s, E_s, P_s} C_s = c_s(P_s)N_s + c_b E_s n + \omega n_{charge} \tau_a \tag{5}$$

where $c_s(P_s)$ represents the amortized hourly cost of a single charging station as a function of its power P_s, while c_b is the amortized hourly cost per unit of battery capacity per hour. The total number of vehicles in the fleet is denoted by n. For this analysis, we model the station cost using a linear function: $c_s(P_s) = (c_1^s + c_2^s P_s)$, where c_1^s represents

a fixed cost per station, and c_2^s reflects the variable cost that scales with power (such as the charging hardware and power electronics themselves). While the number of stations N_s is inherently an integer, we relax this constraint and treat it as a continuous variable to facilitate the optimization. The term n_{charge} denotes the frequency of charging stops per hour for the entire fleet and τ_a represents the average access time per stop (e.g., deceleration, queuing ingress, plug-in latency). ω is a time-weighting parameter, which is set to a small positive value to serve as a regularization term, ensuring the optimization penalizes excessive delays without allowing time costs to dominate the infrastructure investment decisions. And the user travel time cost would be $\omega\frac{m}{v}$, whose effect will be analyzed in section 3.1.5.

We assume that vehicles adopt a minimum-stop strategy to minimize the total access penalty. In a co-optimized system, this implies that infrastructure and onboard storage are matched perfectly; vehicles utilize the full range provided by the station spacing, stopping at each station along their route. Consequently, the stop frequency is strictly determined by the infrastructure density:

$$n_{charge} = \frac{m}{l/N_s} = \frac{m}{l}N_s \tag{6}$$

Substituting this relation into the objective function reveals that the aggregate access cost scales linearly with the number of stations N_s. We therefore define the effective fixed station cost, $\hat{c}_1^s$, which internalizes the operational access penalty into the infrastructure cost:

$$\hat{c}_1^s = c_1^s + \omega\tau_a\left(\frac{m}{l}\right) \tag{7}$$

The optimization of the CS system is subject to two primary constraints that guarantee a minimum level of service and physical feasibility:

1. Spatial Energy Sufficiency Constraint: A vehicle's usable battery energy (θE_s) must be sufficient to cover the energy needed to travel the average distance between charging stations. In a network of length l with N_s stations, we approximate this distance as l/N_s. The energy required to travel this distance is therefore $\beta(l/N_s)$.

$$\theta E_s \geq \beta\frac{l}{N_s} \tag{8}$$

2. System Energy Balance Constraint: This constraint ensures the daily energy supplied to an average vehicle meets its daily demand. It incorporates a quality-of-

service guarantee via the maximum allowable average occupancy rate (ρ_{max}), a policy parameter that ensures sufficient reserve capacity to prevent excessive queuing.

We derive the constraint by balancing the energy required during the driving period ($u \cdot 24$ hours) against the energy supplied during the non-driving period ($(1-u) \cdot 24$ hours). The total effective network power ($N_s P_s \rho_{\text{max}}$) is averaged across the fleet (n) and compared to the average vehicle's consumption rate ($vu\beta$). The final power balance equation is given as:

$$\underbrace{\frac{N_s P_s \rho_{\text{max}}}{n}(1-u)}_{\text{Effective Energy Supply Rate}} \geq \underbrace{vu\beta}_{\text{Energy Demand Rate}} \tag{9}$$

3.1.3 WCL System Design

The WCL system allows vehicles to charge while in motion, which fundamentally alters the design problem. Our model determines the most cost-effective lane deployment strategy by balancing the high capital outlay for road electrification against the reduced cost of onboard energy storage for the vehicle fleet.

The decision variables are the number of charging lane segments (N_w), the required vehicle battery size (E_w), and the WCL power (P_w). Each segment has a fixed length, d_w, and we assume these N_w segments are distributed uniformly across the road network of total length l.

Similar to the CS system, the objective of minimizing the total societal cost J_w is equal to minimizing the total hourly technology cost (C_w), which is the sum of the infrastructure cost for all deployed lane segments and the aggregate battery cost for the fleet of n vehicles:

$$\min_{N_w, E_w, P_w} C_w = c_w(P_w) N_w d_w + c_b E_w n \tag{10}$$

where $c_w(P_w)$ is the amortized hourly cost per unit length of a charging lane as a function of its power P_w, and c_b is the amortized hourly cost per unit of battery capacity. The number of segments N_w is treated as a continuous variable to facilitate optimization. We also assume a linear model for the infrastructure cost as $c_w(P_w) = c_1^w + c_2^w P_w$.

The system design is subject to the following engineering and physical constraints:

1. Physical Boundary Constraint: The total length of all deployed charging segments

cannot exceed the total length of the road network.

$$N_w d_w \leq l \tag{11}$$

2. Energy Sufficiency Constraint: To ensure continuous operation, the energy supplied to a vehicle on a single charging segment must be sufficient to power it until it reaches the next one. We approximate the average distance between segments as l/N_w.

$$\underbrace{\gamma P_w \frac{d_w}{v}}_{\text{Energy Supplied}} \geq \underbrace{\beta \frac{l}{N_w}}_{\text{Energy Required}} \tag{12}$$

   Here, γ is the power transfer efficiency ($0 < \gamma \leq 1$), v is the average vehicle speed, and β is the energy consumption rate (e.g., in kWh/mile).

3. Battery Sizing Constraint: The vehicle's battery must be large enough to buffer the net energy surplus gained while on a charging segment. This surplus is the energy transferred from the lane minus the energy simultaneously consumed for propulsion.

$$\theta E_w \geq \underbrace{\gamma P_w \frac{d_w}{v}}_{\text{Energy Gained}} - \underbrace{\beta d_w}_{\text{Energy Consumed}} \tag{13}$$

   The parameter θ represents the battery's maximum depth-of-discharge, which is the usable fraction of its total capacity E_w (e.g., 0.8 for 80%).

3.1.4 Optimal Design Schemes

In this section, we derive closed-form analytical solutions that minimize the total societal cost for both charging paradigms.

Optimization of CS System

For the static charging system, the optimization seeks to minimize the total cost C_s with respect to three decision variables: the number of stations (N_s), the station charging power (P_s), and the vehicle battery capacity (E_s).

We first observe that the energy sufficiency constraint (8) will be binding at the optimum, as any excess battery capacity only adds cost without providing system-wide benefits. This allows us to express the optimal battery size E_s^* as a function of the number of

stations:

$$E_s^* = \frac{l\beta}{\theta N_s} \tag{14}$$

Substituting this into the objective function reduces it to a cost function of N_s:

$$C_s(N_s) = (\hat{c}_1^s + c_2^s P_s)N_s + c_b n \frac{l\beta}{\theta N_s} \tag{15}$$

The function in (15) is convex in N_s and has an unconstrained economic minimum. However, the final solution for the number of stations must also satisfy the lower bound imposed by the system energy balance constraint (9), which leads to the following optimal solution.

Lemma 1 (General Optimal Solution)**.** *For a given charging power P_s and maximum occupancy rate $\rho_{\max}$, the optimal system design is determined by:*

$$N_s^* = \max\left(\underbrace{\sqrt{\frac{c_b n l \beta}{(\hat{c}_1^s + c_2^s P_s)\theta}}}_{\text{Economics-Driven: } N_{s,\text{econ}}^*}, \quad \underbrace{\frac{m\beta}{P_s \rho_{\max}(1-u)}}_{\text{Performance-Driven: } N_{s,\text{perf}}^*} \right) \tag{16}$$

$$E_s^* = \frac{l\beta}{\theta N_s^*} \tag{17}$$

The structure of this solution reveals that the system design is governed by one of two distinct regimes.

Regime-1: Economics-Driven Regime

This regime occurs when the unconstrained economic optimum is sufficient to meet the performance target ($N_{s,\text{econ}}^* > N_{s,\text{perf}}^*$). The design is determined purely by the cost trade-off between infrastructure and batteries.

Lemma 2 (Optimal Solution in the Economics-Driven Regime)**.** *If the system is economics-driven, the optimal design and total cost are:*

$$N_s^* = \sqrt{\frac{c_b n l \beta}{(\hat{c}_1^s + c_2^s P_s)\theta}} \tag{18}$$

$$E_s^* = \sqrt{\frac{(\hat{c}_1^s + c_2^s P_s) l \beta}{c_b n \theta}} \tag{19}$$

$$C_s^* = 2\sqrt{\frac{c_b n l \beta}{\theta}(\hat{c}_1^s + c_2^s P_s)} \tag{20}$$

Regime-2: Performance-Driven Regime

This regime occurs when total VMT is high, making the economic optimum insufficient to meet the desired quality of service ($N^*_{s,\text{perf}} \geq N^*_{s,\text{econ}}$). The occupancy constraint becomes binding, forcing the system to build more stations than is economically ideal to prevent congestion.

Lemma 3 (Optimal Solution in the Performance-Driven Regime)**.** *If the system is performance-driven, the optimal design and total cost are:*

$$N^*_s = \frac{m\beta}{P_s \rho_{\text{max}}(1-u)} \tag{21}$$

$$E^*_s = \frac{lP_s\rho_{\text{max}}(1-u)}{\theta m} \tag{22}$$

$$C^*_s = (\hat{c}^s_1 + c^s_2 P_s)\left(\frac{m\beta}{P_s\rho_{\text{max}}(1-u)}\right) + c_b n\left(\frac{lP_s\rho_{\text{max}}(1-u)}{\theta m}\right) \tag{23}$$

The boundary between these two regimes is defined by a critical power threshold, $P_{s,\text{crit}}$, found by setting the two terms in the max function equal ($N^*_{s,\text{econ}} = N^*_{s,\text{perf}}$). Solving this equality for P_s yields:

$$P_{s,\text{crit}} = \frac{m^2\beta\theta c^s_2 + \sqrt{(m^2\beta\theta c^s_2)^2 + 4(c_b n l \rho^2_{\text{max}})(m^2\beta\theta\hat{c}^s_1)}}{2c_b n l \rho^2_{\text{max}}(1-u)^2} \tag{24}$$

For a given system, if the station power $P_s > P_{s,\text{crit}}$, the design will be economics-driven. If $P_s \leq P_{s,\text{crit}}$, it will be performance-driven.

The analysis of the two regimes reveals that the total cost $C^*_s(P_s)$ is a continuous, piecewise function, which allows for a final optimization over the charging power, P_s. As proven in Appendix 8.2, the global cost minimum is always found within the performance-driven regime. This is because the cost in the economics-driven regime is strictly increasing with power, making any such solution inherently suboptimal. Therefore, the globally optimal charging power, P^*_s, is the unconstrained minimum of the performance-driven cost function. Substituting this optimal P^*_s into the performance-driven equations yields the final, globally optimal system design and uncovers a remarkably simple principle for infrastructure planning:

Proposition 1 (Optimal Charging Power for the Plug-in Charging System)**.** *There exists a unique, cost-minimizing charging power, P^*_s, for the CS system, which is the unconstrained*

minimum of the performance-driven cost function:

$$P_s^* = \frac{m}{\rho_{\max}(1-u)} \sqrt{\frac{\hat{c}_1^s \beta \theta}{c_b n l}} \tag{25}$$

This proposition reveals that the globally optimal design is always governed by the performance-driven regime. Intuitively, this is because the cost in the economics-driven regime is strictly increasing with power; it is never optimal to over-power stations beyond the minimum required for performance. This holds true under the extreme case: if utilization is high and approaches 1, the performance-driven power to support a near-continuously operating fleet should be extremely high to enable instant charging during the vehicles' very short downtime.

Corollary 1.1 (Scale-Independent Design Principle for Plug-in Charging)**.** *The optimal station density, $\delta_s^* = N_s^*/l$, is determined by the character of the traffic in a specific area (such as its density and how heavily the vehicles are used), not by the overall size of the entire road network or the total miles traveled on it:*

$$\delta_s^* = \sqrt{\frac{c_b \beta \lambda}{\hat{c}_1^s \theta u}} \tag{26}$$

The proof is provided in the Appendix 8.3. Corollary 1.1 establishes the optimal station density not as a static target, but as an economic equilibrium quantifying the trade-off between fleet capital and infrastructure capital. The numerator ($c_b \beta \lambda$) represents the economic pressure to densify infrastructure to reduce onboard storage costs, while the denominator ($\hat{c}_1^s \theta u$) represents the capital resistance enforcing sparsity.

This derivation reveals two critical strategic insights:

- The Square-Root Law: The dependence on $\sqrt{\lambda}$ implies that infrastructure requirements grow significantly slower than traffic volume. This indicates strong economies of aggregation: high-density corridors achieve superior capital efficiency because the infrastructure investment is amortized over a disproportionately larger fleet, lowering the unit cost per vehicle.

- Technological Substitution: The direct sensitivity to battery cost (c_b) proves that charging infrastructure functions economically as a substitute for onboard energy storage. The optimal design is strictly coupled with vehicle technology. High battery prices drive the system toward denser, distinct charging networks to minimize

fleet capital, whereas low battery prices naturally shift the equilibrium toward sparser infrastructure and larger onboard buffers.

Optimization of WCL System

For the WCL system, optimization is governed by the trade-off between the extent of roadway electrification and vehicle battery size. The decision variables are the number of charging segments (N_w), segment length (d_w, treated here as a fixed module size), and lane power (P_w).

We first analyze the battery sizing constraint (13), which should be binding at the optimum and the optimal battery size E_w^* can be obtained as:

$$E_w^* = \frac{\gamma P_w d_w - \beta d_w v}{\theta v} \tag{27}$$

Substituting this expression for E_w^* into the total cost function transforms the problem into an optimization over the number of segments N_w, if we first fix charging power P_w. The objective is to minimize $C_w(N_w)$ subject to the feasible range for N_w defined by the physical and energy sufficiency constraints:

$$\frac{l\beta v}{\gamma P_w d_w} \leq N_w \leq \frac{l}{d_w} \tag{28}$$

For this range to be valid, the lower bound must not exceed the upper bound. This requirement establishes a critical feasibility condition on the charging power:

$$\frac{l\beta v}{\gamma P_w d_w} \leq \frac{l}{d_w} \quad \Longrightarrow \quad P_w \geq \frac{\beta v}{\gamma} \tag{29}$$

If the charging power is below this threshold, a feasible system cannot be constructed.

Within the feasible range, we observe that the objective function $C_w(N_w)$ is a linearly increasing function of N_w, as the infrastructure cost is directly proportional to the number of segments. Therefore, the total cost is always minimized by selecting the smallest possible value for N_w, which corresponds to the lower bound of its feasible range. This key insight leads to the following result.

Lemma 4 (Optimal Wireless Charging Segment Number)**.** *For any feasible charging*

power $P_w \geq \frac{\beta v}{\gamma}$, the optimal number of charging segments that minimizes cost is:

$$N_w^* = \frac{l\beta v}{\gamma P_w d_w} \tag{30}$$

The cost function $C_w^*(P_w)$ is now a convex function of P_w, which allows us to find a unique, cost-minimizing power level:

Proposition 2 (Optimal Wireless Charging Power and Minimized Cost)**.** *For the WCL system, there exists a unique optimal charging power, P_w^* and the corresponding minimal societal cost, C_w^*:*

$$P_w^* = \frac{v}{\gamma}\sqrt{\frac{c_1^w l\beta\theta}{c_b n d_w}} \tag{31}$$

$$C_w^*(d_w) = 2\sqrt{\frac{c_1^w l\beta c_b n d_w}{\theta}} + \frac{c_2^w l\beta v}{\gamma} - \frac{c_b n d_w \beta}{\theta} \tag{32}$$

With the optimal power P_w^* determined, we can now analyze the physical structure of this optimized network by defining the optimal electrification ratio, $\alpha^* = N_w^* d_w / l$. This dimensionless parameter represents the fraction of the total network that must be equipped with wireless charging. Substituting the underlying expressions for the optimal number of segments (N_w^*) into this definition reveals a powerful insight into the nature of the network's design, which we formalize below.

Corollary 2.1 (Scale-Independent Design for Wireless Charging)**.** *The optimal electrification ratio, $\alpha^* = N_w^* d_w / l$, is governed by the traffic density ($\lambda = un/l$) and fleet utilization ($u = m/(vn)$), instead of the network's overall size, such as its total road length (l) and total vehicle-miles traveled (m):*

$$\alpha^* = \sqrt{\frac{d_w \beta c_b \lambda}{c_1^w \theta u}} \tag{33}$$

This proposition reveals a scale-independent design principle that follows a similar square-root law and exposes a fundamental economic trade-off. High battery costs (c_b) favor a more extensive network of lower-power chargers (P_w^*), whereas high infrastructure costs (c_1^w) favor a less extensive network of higher-power chargers. This provides a clear design rule, showing how the system optimally balances network density against technological power based on the relative costs of batteries and infrastructure.

3.1.5 Strategic Comparison and Viability Analysis

With the overall optimal solutions and metrics summarized in Table 3, we can derive the strategic conditions under which one paradigm is economically superior. This analysis focuses on three key areas: the system's asymptotic properties with traffic density and vehicle utilization, the economic indifference frontier for charging option selection, and a practical benchmark for the infrastructure cost of WCL technology.

Table 3: Optimal system configuration and generalized cost functions.

Variable	Static Plug-in (CS)	Dynamic Wireless (WCL)
Optimal Power (P^*)	$P_s^* = \frac{\lambda v}{\rho_{\max}(1-u)}\sqrt{\frac{\hat{c}_1^s \beta \theta u}{c_b \lambda}}$	$P_w^* = \frac{v}{\gamma}\sqrt{\frac{c_1^w \beta \theta u}{c_b d_w \lambda}}$
Infrastructure Unit (N^*)	$N_s^* = \sqrt{\frac{c_b n l \beta}{\hat{c}_1^s \theta}}$	$N_w^* = \sqrt{\frac{c_b l n \beta}{c_1^w \theta d_w}}$
Infrastructure Density (N^*/l)	$\bar{N}_{s,l}^* = \sqrt{\frac{c_b \beta \lambda}{\hat{c}_1^s \theta u}}$	$\bar{N}_{w,l}^* = \sqrt{\frac{c_b \beta \lambda}{c_1^w \theta d_w u}}$
Battery Size (E^*)	$E_s^* = \sqrt{\frac{\hat{c}_1^s \beta u}{c_b \theta \lambda}}$	$E_w^* = \frac{d_w}{\theta}\left(\sqrt{\frac{c_1^w \beta \theta u}{c_b d_w \lambda}} - \beta\right)$
Minimized Hourly Cost (C^*)	$C_s^* = 2\sqrt{\frac{c_b n l \beta \hat{c}_1^s}{\theta}} + \frac{c_2^s \beta \lambda v l}{\rho_{\max}(1-u)}$	$C_w^* = 2\sqrt{\frac{c_1^w c_b n l \beta d_w}{\theta}} + \frac{c_2^w l \beta v}{\gamma} - \frac{c_b n d_w \beta}{\theta}$
Travel Time Cost (C_{time})	$\omega \cdot \frac{m}{v}$	$\omega \cdot \frac{m}{v}$
Generalized Societal Cost (J^*)	$J_s^* = C_s^* + C_{time}$	$J_w^* = C_w^* + C_{time}$
Cost per VMT (J^*/m)	$\bar{J}_{s,m}^* = \frac{2}{v}\sqrt{\frac{c_b \beta \hat{c}_1^s}{\theta \lambda u}} + \frac{c_2^s \beta}{\rho_{\max}(1-u)} + \frac{\omega}{v}$	$\bar{J}_{w,m}^* = \frac{2}{v}\sqrt{\frac{c_b \beta c_1^w d_w}{\theta \lambda u}} + \frac{c_2^w \beta}{\gamma \lambda} - \frac{c_b d_w \beta}{\theta u v} + \frac{\omega}{v}$

Average Cost and Asymptotic Analysis

To evaluate the long-term economic performance of each system, we define the cost per VMT as the primary efficiency metric. This metric captures the fundamental trade-off between upfront infrastructure investment and operational utility, allowing for a direct comparison normalized by service output.

Proposition 3 (Scale-Independent Average Cost Functions)**.** *The optimal average costs per VMT for the two charging paradigms are scale-independent and given by:*

$$\bar{J}_{s,m}^* = \frac{2}{v}\sqrt{\frac{c_b \beta \hat{c}_1^s}{\theta \lambda u}} + \frac{c_2^s \beta}{\rho_{\max}(1-u)} + \frac{\omega}{v} \tag{34}$$

$$\bar{J}^*_{w,m} = \frac{2}{v}\sqrt{\frac{c_1^w \beta c_b d_w}{\theta \lambda u}} + \frac{c_2^w \beta}{\gamma \lambda} - \frac{c_b d_w \beta}{\theta v u} + \frac{\omega}{v} \tag{35}$$

While both metrics are governed by operational parameters, the internal structure of these cost functions reveals a divergence in their capital allocation mechanisms:

- Static Charging (Inverse-Utilization Dependency): The static cost function contains a term scaled by the power unit cost c_2^s that is inversely proportional to idle time $(1-u)$. This structure reflects a rigid physical constraint: as fleet uptime u increases, the time available for charging shrinks. To deliver the same daily energy in this reduced window, the required charging power rate must increase hyperbolically, driving up the total power infrastructure cost regardless of specific parameter values.
- Wireless Charging (Asset Substitution and Sharing): The wireless cost function is distinguished structurally by two features. First, it contains a subtractive term related to c_b and d_w, implying that infrastructure investment mathematically offsets the vehicle capital cost rather than purely adding to it. Second, the power infrastructure term scales with λ^{-1}, identifying the dynamic charging lane as a shared resource where the cost burden is divided among the aggregate traffic flow.

To rigorously evaluate the performance of these mechanisms, we define two distinct operational regimes for the analysis. The exogenous speed regime represents scenarios with steady operating speeds, such as scheduled transit corridors, where velocity v is treated as a design constant. Conversely, the endogenous speed regime captures urban traffic dynamics using the Macroscopic Fundamental Diagram (MFD), where speed degrades linearly with density:

$$v = v_f \left(1 - \frac{\lambda}{\lambda_{jam}}\right) \tag{36}$$

where v_f is the free-flow speed and λ_{jam} is the jam density of the network. This formulation introduces a convex trade-off in the total societal cost: increasing fleet density improves infrastructure amortization but degrades travel speed. These regimes form the basis for the following comparative asymptotic analysis.

Proposition 4 (Comparative Efficiency with respect to Traffic Density)**.** *The asymptotic behavior of system cost with respect to traffic density (λ) is fundamentally determined by the modeling regime:*

1. ***Under the Exogenous Speed Regime:***

- *WCL (Strong Economies of Density): Exhibits rapid cost decay driven by the amortization of shared roadway infrastructure. Both the battery-optimization term ($\mathcal{O}(\lambda^{-1/2})$) and the power-track term ($\mathcal{O}(\lambda^{-1})$) decrease with density, creating a hyperbolic amortization curve.*
- *CS (Weak Economies of Density): Exhibits slower cost decay driven exclusively by battery optimization ($\mathcal{O}(\lambda^{-1/2})$), resulting in a sub-linear amortization curve.*

2. ***Under the Endogenous Speed Regime:***

- *WCL (High Congestion Sensitivity): The combination of steep initial amortization and high sensitivity to speed collapse ($1/v$) creates a highly convex, deep U-shaped profile with a unique global minimum.*
- *CS (Low Congestion Sensitivity): The combination of weak initial amortization and lower sensitivity to congestion (infrastructure efficiency is speed-independent) results in a flatter convex profile with a unique global minimum.*

The proof is provided in Appendix 8.4. This proposition highlights that the economic efficiency of each system is governed by opposing dominant regimes. The superior amortization of WCL stems from the fundamental distinction between shared versus dedicated resources. In the WCL paradigm, the high capital cost of the electrified roadway (c_1^w) is an intensive property shared by the aggregate flow; thus, adding vehicles reduces the fixed infrastructure cost per VMT, driving the curve downward ($\propto 1/\lambda$). In contrast, the static system is constrained by a structural floor. Because charging power is a dedicated resource that cannot be simultaneously shared, the aggregate infrastructure requirement scales linearly with the total VMT. Consequently, even in ideal density conditions, the average cost per VMT cannot vanish but converges to an irreducible floor determined by the power electronics and battery variables.

However, this amortization advantage in WCL is bounded by a compound congestion penalty. In the CS system, congestion represents a pure diseconomy that erodes travel speed without offering any compensating utility. In the WCL system, congestion strikes twice: it incurs the same time penalty but also degrades the system's throughput efficiency (as energy transfer capacity is speed-coupled). This creates the pronounced U-shape: WCL is economically dominant only within a specific efficiency window $[\underline{\lambda}, \bar{\lambda}]$, bounded by insufficient amortization at the low end and excessive congestion inefficiencies at the high end.

Proposition 5 (Comparative Stability with Fleet Utilization)**.** *The asymptotic behavior of system cost with respect to fleet utilization (u) reveals a fundamental asymmetry in operational resilience:*

1. ***CS Instability:*** *$J_s(u)$ possesses a vertical asymptote at $u \to 1$. The cost diverges according to $\mathcal{O}((1-u)^{-1})$, reflecting the prohibitive power capacity required to charge within vanishingly small dwell times.*
2. ***WCL Stability:*** *$J_w(u)$ remains bounded and exhibits economies of utilization as $u \to 1$.*

The proof is provided in Appendix 8.5. This asymmetry identifies a critical operational limit for the CS paradigm. The divergence of $J_s(u)$ reveals that the stop-and-charge model faces an irreducible conflict between asset utilization and capital cost. As fleets strive for maximum uptime ($u \to 1$), the time window available for energy replenishment vanishes. To maintain energy balance, the system must compensate with a power surge, sharply increasing the charging rate (kW) to deliver the full daily energy demand in mere minutes. This creates an asymptotic cost barrier driven by the prohibitive capital cost of the ultra-fast charging hardware required to support such intensity.

In contrast, WCL serves as an operational stabilizer by physically decoupling energy transfer from vehicle downtime. Because energy is transferred during the revenue-generating phase (u), the infrastructure capacity requirement is independent of the dwell time constraint. This confirms that while static charging is sufficient for private vehicles (low u), WCL is structurally essential for next-generation mobility-on-demand systems that target near-continuous operation, effectively removing the capacity barrier that bounds the CS paradigm.

Indifference Frontier and Strategic Benchmarks

While the asymptotic analysis reveals the fundamental structural limits of each paradigm, practical infrastructure planning requires precise identification of the transition zone between them. To determine exactly where the economic advantage shifts from static to dynamic charging, we formalize the decision boundary between the two paradigms as an indifference frontier. This represents the set of operational points (λ, u) where the optimized societal costs of the two systems are equal:

$$\bar{J}^*_{w,m}(\lambda, u) = \bar{J}^*_{s,m}(\lambda, u) \tag{37}$$

Proposition 6 (Properties of the indifference frontier)**.** *Assuming the existence of a non-empty solution set (i.e.,* $\min(\bar{J}_w^* - \bar{J}_s^*) < 0$*), the intersection of the cost functions defines a continuous indifference frontier in the* (λ, u) *plane with the following properties:*

1. *Density Projections: For a fixed fleet utilization* u*:*
   - *Exogenous Speed: The boundary projects to a unique lower threshold* λ_{crit}*. WCL is economically superior for all* $\lambda > \lambda_{crit}$*.*
   - *Endogenous Speed: The boundary projects to a closed WCL-dominant interval* $[\underline{\lambda}, \bar{\lambda}]$*. WCL is economically superior only within this window, bounded below by amortization requirements and above by congestion-induced efficiency loss.*
2. *Utilization Projection: For a fixed traffic density* λ*, the boundary projects to a unique critical utilization* u_{crit}*. WCL is viable if and only if the fleet utilization exceeds this break-even floor (*$u > u_{crit}$*).*
3. *Sensitivity: The position and shape of this multi-dimensional frontier shift in response to system parameters as summarized in Table 4.*

Table 4: Sensitivity analysis: traffic density and fleet utilization boundaries.

Parameter	Description	Exogenous	Endogenous Regime (MFD)			Fleet Regime
		Critical Density (λ_{crit})	Lower Bound ($\underline{\lambda}$)	Upper Bound ($\bar{\lambda}$)	WCL-dominant Region	Critical Utilization (u_{crit})
WCL System Parameters						
c_1^w, c_2^w	Infrastructure Cost	↑	↑	↓	Contracts	↑
γ	Transfer Efficiency	↓	↓	↑	Expands	↓
CS System Parameters						
$\hat{c}_1^s, c_2^s$	Infrastructure Cost	↓	↓	↑	Expands	↓
ρ_{max}	Max Occupancy	↑	↑	↓	Contracts	↑
Environmental Parameters						
ω	Value of Time	↓	↓	↑	Expands	↓

- **Direction:** (↑) Parameter increase raises the threshold; (↓) Parameter increase lowers the threshold.
- **Region:** "Expands" implies the interval $[\underline{\lambda}, \bar{\lambda}]$ widens.

The proof is provided in Appendix 8.6. The existence of the critical thresholds $(\lambda_{crit}, u_{crit})$ exposes a fundamental deployment paradox for dynamic infrastructure. Unlike static plug-in chargers, which can be deployed incrementally to match dispersed demand, WCL exhibits a strict intensity threshold: it requires a critical mass of either aggregated traffic density (λ) or high-intensity fleet operations (u) to overcome its fixed capital barrier (c_1^w).

Crucially, the WCL-dominant interval $[\underline{\lambda}, \bar{\lambda}]$ is not guaranteed to exist. If the WCL capital costs are too high relative to the CS baseline, the cost curves may never intersect,

rendering the viability set empty. This implies a market entry barrier: there is a maximum allowable infrastructure cost above which the technology cannot compete, regardless of traffic density. This binary nature that viability is either non-existent or conditional on high density implies that WCL deployment is system-dependent and best suited for high-load corridors (such as BRT guideways or freight highways) where high utilization is guaranteed by design, rather than dispersed general traffic networks. Furthermore, within the viable regime, the boundary's sensitivity to ρ_{max} reveals that WCL acts as an operational stabilizer. Its economic value peaks precisely when the static system becomes unreliable (i.e., when queuing constraints bind at high utilization), identifying dynamic charging not merely as an energy alternative, but as a resilience strategy for essential fleets that cannot tolerate the service volatility of congested charging stations.

Beyond these structural thresholds, the sensitivity results in Table 4 highlight a critical asymmetry in how the viability window behaves under the endogenous regime. While lowering the adoption thresholds ($\underline{\lambda}, u_{\text{crit}}$) is a matter of overcoming fixed capitalization costs, extending the upper bound ($\bar{\lambda}$) represents a technological defense against congestion. Parameters that raise $\bar{\lambda}$ (such as improved transfer efficiency γ or higher value of time ω) effectively allow the WCL system to buy more operational time in varying traffic speeds before speed collapse renders infrastructure amortization inefficient. The positive sensitivity to the value of time is particularly notable: it indicates that WCL is disproportionately valuable in high-wage, high-density metropolitan economies where the generalized cost of any friction, whether static charging downtime or congestion, is magnified.

To provide a practical target for industry research and development, we define the critical WCL infrastructure cost ($c_1^{w,\text{crit}}$) as the maximum allowable fixed cost per unit length for WCL to be competitive. This benchmark can also be analytically derived as:

Corollary 6.1 (Critical Cost Benchmark)**.** *For WCL to be competitive at a given operational point* (λ, u)*, its fixed cost must satisfy* $c_1^w \leq c_1^{w,\text{crit}}$*, where:*

$$c_1^{w,\text{crit}} = \frac{v^2 \theta \lambda u}{4 c_b d_w} \left(\frac{2}{v} \sqrt{\frac{c_b \hat{c}_1^s}{\theta \lambda u}} + \frac{c_2^s}{\rho_{\text{max}}(1-u)} - \frac{c_2^w}{\gamma \lambda} + \frac{c_b d_w}{\theta v u} \right)^2 \tag{38}$$

This benchmark reveals that the target price for WCL is adaptive. In high-density, high-utilization environments (high λ, u), $c_1^{w,\text{crit}}$ is higher, meaning congested transit networks can justify paying a premium for WCL. Conversely, cheap batteries lower the threshold, requiring WCL developers to reduce costs aggressively to remain competitive. However, the quadratic form of Corollary 6.1 also exposes a non-linear return on operational efficiency. Small marginal improvements in power transfer efficiency (γ) translate into dis-

proportionately larger increases in the allowable capital budget, offering a high-leverage incentive for research and development. Yet, this relationship simultaneously reveals a degradation risk regarding battery technology. Since WCL functions economically as a substitute for on-board energy storage, a reduction in battery costs (c_b) erodes the primary value proposition of the infrastructure. As $c_b \to 0$, the allowable infrastructure cost collapses, implying that WCL technology must effectively race against battery chemistry improvements to remain a financially viable alternative.

3.2 Single Trip

Current light-duty EV generation can travel distances of up to 500 miles on a single charge, which typically equates to 6-8 hours of continuous driving. Despite these capabilities, it is widely recommended that drivers take regular breaks during extended trips to mitigate the risk of fatigue-related accidents (Williamson et al., 2011; Li et al., 2019). In particular, commercial driving regulations stipulate that drivers must take a mandatory break of at least 30 minutes after every 8 hours of driving to ensure safety and well-being (Federal Motor Carrier Safety Administration, 2024). These breaks can be strategically utilized for charging purposes to complete long-distance trips. Therefore, we develop a model to evaluate the time-saving benefits of wireless charging, assuming that: (i) EVs take a break after driving for a maximum number of hours; (ii) fast chargers are available at every rest stop; and (iii) even with wireless charging, EVs recharge their batteries using fast chargers when stopping, due to their higher efficiency and power.

3.2.1 Model

We use the following notation in this section:

Nomenclature

Parameters

E	Battery capacity
α_w	Wireless charging efficiency
α_p	Plug-in charging efficiency
β	Distance travel on each unit of battery
θ	Initial state of charge
p_w	Wireless charging power
p_p	Plug-in charging power
L	Total trip distance

T	Maximum driving time without rest
σ_t	Value of time
σ_w	Cost of building wireless charging per unit of distance
t^r	Rest time
v	Driving speed
n	Maximum number of driving periods
Decision variables	
l_i^w	Length of i^{th} wireless charging lane
t_i^d	Duration of i^{th} driving period
r_i	Binary variable equal to 1 if take i^{th} rest period and 0 otherwise
s_i	Battery state of charge at the end of i^{th} rest period

$$min\, Z = \sigma_w \cdot \sum_{i=1}^{n} l_i^w + \sigma_t \cdot t_r \cdot \sum_{i=1}^{n-1} r_i \tag{39}$$

$$\text{s.t.} \quad \sum_{i=1}^{n} t_i^d = \frac{L}{v} \tag{40}$$

$$\theta \cdot E + \alpha_w \cdot p_w \cdot \frac{l_1^w}{v} \geq v \cdot t_1^d \cdot \beta \tag{41}$$

$$s_1 \leq \theta \cdot E + \alpha_w \cdot p_w \cdot \frac{l_1^w}{v} - v \cdot t_1^d \cdot \beta + \alpha_p \cdot p_p \cdot r_1 \cdot t^r \tag{42}$$

$$s_i + \alpha_w \cdot p_w \cdot \frac{l_{i+1}^w}{v} \geq v \cdot t_{i+1}^d \cdot \beta \qquad \forall i \in 2, 3, \dots, n-1 \tag{43}$$

$$s_i \leq s_{i-1} + \alpha_w \cdot p_w \cdot \frac{l_i^w}{v} - v \cdot t_i^d \cdot \beta + \alpha_p \cdot p_p \cdot r_i \cdot t^r \qquad \forall i \in 2, 3, \dots, n-1 \tag{44}$$

$$t_i^d \leq T \cdot t_{i-1}^d \qquad \forall i \in 2, 3, \dots, n \tag{45}$$

$$t_{i+1}^d \leq r_i \cdot \frac{L}{v} \qquad \forall i \in 1, 2, \dots, n-1 \tag{46}$$

$$0 \leq l_i^w \leq L \qquad \forall i \in 1, 2, \dots, n \tag{47}$$

$$0 \leq t_i^d \leq T \qquad \forall i \in 1, 2, \dots, n \tag{48}$$

$$s_i \leq E \qquad \forall i \in 1, 2, \dots, n-1 \tag{49}$$

$$r_i \in [0, 1] \qquad \forall i \in 1, 2, \dots, n-1 \tag{50}$$

Objective function (39) aims to minimize both the total length of the wireless charging lanes and trip time. The weights σ_w and σ_t can be adjusted to prioritize each component and compare the two charging technologies. For example, by assigning a large value to the weight of travel time (σ_t), the model focuses on minimizing total trip time by construct-

ing wireless charging lanes to reduce the number of stops. Conversely, by assigning a large value to the charging lane length weight (σ_w), the model adds stops into the trip to ensure feasibility without relying on wireless charging. Constraint (40) ensures that the total driving time equals the trip distance divided by the average driving speed. Constraints (41) and (43) indicate that the energy required to complete a driving period must be less than the energy stored in the battery at the start of the period, plus any energy gained from in-motion wireless charging during that period, for both the initial driving period and any subsequent ones. Constraints (42) and (44) monitor the battery's state of charge following the initial stop and any subsequent stops, respectively. Constraints (45) and (46) ensure a rest period between consecutive driving periods. Finally, Constraints (47) to (50) define the range of the decision variables. The model is a mixed-integer linear programming problem that can be solved using commercial solvers.

3.3 Transit System

In this section, we focus on developing a model to compare plug-in and wireless chargers in facilitating the electrification of transit fleets without changes in their schedules or fleet size.

3.3.1 Model

This section focuses on identifying the optimal types and locations for charging infrastructure needed to support the electrification of a transit agency, while ensuring there are no changes required to its existing schedule, routes, or fleet size. To align with the current operations of the transit agency, we utilize General Transit Feed Specification (GTFS) data, a standardized format that shares transit schedules and associated geographic information. A critical component of GTFS data for our analysis is the concept of *blocks*, which represent the sequence of routes completed by a single vehicle. Additionally, GTFS provides detailed scheduling information, which allows us to calculate the time a bus is stationary between the completion of one route and the commencement of the next in its block schedule. This information is essential for determining feasible locations and times for charging, thus facilitating a seamless transition to electric vehicles without disrupting transit operations.

We define the set of all blocks as $\mathcal{B}$, and for each block $b \in \mathcal{B}$, we define its ordered set of routes as $\mathcal{R}_b = \{r_{b,1}, r_{b,2}, \dots, r_{b,n_b}\}$, where n_b is the number of routes in block b. The

total distance for each block, L_b, can be calculated as:

$$L_b = \sum_{i=1}^{n_b} l_{r_{b,i}} \tag{51}$$

where l_r represents the total distance of route r. When considering the electrification of the transit fleet, if the total distance of a block is less than the driving range of the electric bus, then en-route charging is unnecessary. However, if the block distance exceeds the driving range of the electric bus, charging will be required to ensure that the bus can complete its routes without alterations to the schedule or operations. This logic provides a basis for determining when and where charging infrastructure is needed to support uninterrupted operation with an electrified transit fleet.

In the context of electrifying a transit agency's fleet, buses can be charged using either in-motion wireless chargers while driving or stationary chargers at stops. The stationary charging options include both wireless and plug-in chargers, with differences primarily in the time required to initiate charging and power delivery. Stationary wireless chargers have the advantage of starting the charging process immediately as the bus arrives at a stop. In contrast, plug-in chargers require the driver to exit the vehicle and physically connect the charging cord, resulting in a few minutes of additional time before charging can commence. The choice between these methods involves considering various factors, such as the available dwell time at stops, the energy needs of the bus, and the convenience and infrastructure costs associated with each type of charger. Therefore, the problem of determining the optimal locations and types of chargers for a transit agency's electrification can be formulated similarly to a facility location problem. The primary objective is to identify which charging facilities should be established and where, to ensure that the transit agency can complete all its blocks with electric vehicles that have a limited driving range.

We denote the node at the end of each route r as i_r. For stationary charging, we define a binary decision variable x_i, which equals 1 if a stationary charger is placed at node i and 0 otherwise. In addition, we break each route into a series of consecutive segments, denoted as $\mathcal{K}_r = \{k_{r,1}, k_{r,2}, ..., k_{r,m_r}\}$, where m_r is the number of segments in route r. These segments represent the minimum viable length for installing in-motion wireless charging tracks. For each segment k, we define another binary decision variable, y_k, which equals 1 if an in-motion wireless charging track is installed in segment k, and 0 otherwise. We also define $s^k_{b,r}$ as the bus state of charge after traversing segment k of route r in block b, and $s_{b,r}$ as the state of charge right before starting route r.

$$min\, Z = \sum_i c_i \cdot x_i + \sum_k c_k \cdot y_k \tag{52}$$

s.t.
$$s_{b,r_{b,1}} = \theta \cdot E \qquad \forall b \in \mathcal{B} \tag{53}$$
$$s_{b,r_{b,n}} \leq s^{m_r}_{b,r_{b,n-1}} + \alpha_i \cdot p_i \cdot t_{b,r_{b,n}} \cdot x_i \qquad \forall b \in \mathcal{B}, n = 2, \dots, n_b \tag{54}$$
$$s^1_{b,r} \leq s_{b,r} - l_k \cdot \beta + \alpha_w \cdot p_w \cdot \frac{l_k}{v} \cdot y_k \qquad \forall b \in \mathcal{B}, r \in \mathcal{R}_b \tag{55}$$
$$s^k_{b,r} \leq s^{k-1}_{b,r} - l_k \cdot \beta + \alpha_w \cdot p_w \cdot \frac{l_k}{v} \cdot y_k \qquad \forall b \in \mathcal{B}, r \in \mathcal{R}_b, k = 2, \dots, m_r \tag{56}$$
$$s_{b,r} \leq E \qquad \forall b \in \mathcal{B}, r \in \mathcal{R}_b \tag{57}$$
$$s^k_{b,r} \leq E \qquad \forall b \in \mathcal{B}, r \in \mathcal{R}_b, k \in \mathcal{K}_r \tag{58}$$
$$s^k_{b,r} \geq 0 \qquad \forall b \in \mathcal{B}, r \in \mathcal{R}_b, k \in \mathcal{K}_r \tag{59}$$

The objective function (52) minimizes the construction cost of stationary chargers at nodes (stops) and in-motion chargers at route segments. Constraints (53) ensure the initial state of charge of buses at the beginning of their blocks, where E is the battery capacity and θ is the charge level. Constraints (54) and (57) monitor the state of charge of buses at the start of each route within their respective blocks. Constraints (54) assert that this state of charge must be less than or equal to the level at the end of the previous route's last segment in the block, plus energy obtained from charging if a charger is present at that point. α_i and p_i denote the charging efficiency and power at node i, respectively. Furthermore, $t_{b,r_{b,n}}$ represents the dwell time for the bus assigned to block b at point i before commencing route $r_{b,n}$, which can be predetermined using the block schedule from the GTFS dataset. We also account for charger setup time (wireless versus plug-in) by subtracting this from the dwell time. Constraints (57) guarantee that the bus's state of charge, when recharged at a node, is limited by the battery capacity. Constraints (55), (56), and (58) similarly track the bus's state of charge through each route segment for all blocks, ensuring that if buses receive in-motion charging, their state of charge does not exceed battery capacity. Finally, constraints (59) ensure the feasibility of using electric buses to complete trips by maintaining a positive state of charge at all times. The model is a mixed-integer linear programming problem that can be solved using commercial solvers such as Gurobi.

3.4 Intercity Highway Network

Given the median range of electric vehicles and the range of daily travel distances, IVC technology can help enable intercity journeys on highways and major roads where travel distances are longer. Accordingly, we developed a model to identify the best placement of in-motion wireless charging facilities, accounting for the existing distribution of fast charging stations.

3.4.1 Multi-class Network Equilibrium (MCNE) Problem

We consider a regional or metropolitan road network represented as a graph $G(N, A)$, where N is the set of nodes (e.g., intersections or specific locations) and A is the set of links (i.e., road segments). Each link $a \in A$ connects a starting node i to an ending node j, denoted $a = (i, j)$, where $i, j \in N$. The physical length of link a is d_a. Travel demand occurs between specified origin-destination (O-D) pairs, collectively denoted by the set W. For each O-D pair $w \in W$, $o(w)$ is its origin node and $d(w)$ is its destination node. EVs can traverse a set of available paths $\hat{P}^w$ to travel from $o(w)$ to $d(w)$. The relationship between paths and links is defined by the path-link incidence variable $\delta_{a,p}$, which equals 1 if path p uses link a, and 0 otherwise.

The total traffic flow on any link $a \in A$ is denoted by v_a. The travel time on link a, $t_a(v_a)$, is a strictly increasing function of this flow. A commonly used representation is the Bureau of Public Roads (BPR) function:

$$t_a(v_a) = t_a^0 \left[1 + 0.15 \left(\frac{v_a}{c_a} \right)^4 \right] \tag{60}$$

where t_a^0 is the free-flow travel time and c_a is the capacity of link a.

The network is equipped with charging infrastructure to support EVs. A subset of links, $\tilde{A} \subseteq A$, may offer dynamic charging capabilities. Additionally, a subset of nodes, $\tilde{N} \subseteq N$, may host static charging stations.

We consider K distinct types of EV drivers, indexed by $k \in K$. Each driver type k may have different characteristics, such as their monetary value of travel time, β_k (e.g., \$/hour). The travel demand for type-k drivers between an OD pair w is q_k^w. The flow of type-k drivers on a path $p \in \hat{P}^w$ for OD pair w is $f_{p,k}^w$. The collection of all such path flows for all types, paths, and OD pairs constitutes the flow vector $\mathbf{f} = \{f_{p,k}^w : \forall p \in \hat{P}^w, \forall k \in K, \forall w \in W\}$.

The total traffic flow $v_a(\mathbf{f})$ on any link $a \in A$ is the aggregation of flows from all driver types whose paths use that link:

$$v_a(\mathbf{f}) = \sum_{w \in W} \sum_{p \in \hat{P}^w} \sum_{k \in K} f_{p,k}^w \delta_{a,p} \tag{61}$$

The MCNE problem aims to find equilibrium flow distribution **f**. At equilibrium, for each O-D pair and EV driver type, all utilized paths are usable (i.e., an EV can complete the path, possibly with intermediate recharging). Moreover, the generalized travel costs on all such utilized paths are equal and are no greater than the costs on any unutilized usable paths for the same O-D pair and driver type. The MCNE problem minimizes a system-level objective function, where β is a general parameter converting aggregate travel time to a monetary equivalent, and $s_{p,k}^w$ is the class-specific generalized cost of recharging for type-k drivers on path p for OD pair w:

$$\min_{\mathbf{f}} \left(\sum_{a \in A} \int_0^{v_a(\mathbf{f})} t_a(z)\, dz + \sum_{k \in K} \sum_{w \in W} \sum_{p \in \hat{P}^w} \frac{s_{p,k}^w f_{p,k}^w}{\beta_k} \right) \tag{62}$$

$$\text{S.t.:} \sum_{p \in \hat{P}^w} f_{p,k}^w = q_k^w \quad \forall w \in W, \forall k \in K \tag{63}$$

$$f_{p,k}^w \geq 0 \quad \forall p \in \hat{P}^w, \forall w \in W, \forall k \in K \tag{64}$$

Constraint (63) ensures that for each driver type k and OD pair w, path flows sum to the specified demand q_k^w. Constraint (64) ensures all path flows are non-negative.

Shortest Usable Path (SP) Problem

The generalized cost $s_{p,k}^w$ for a type-k driver on path p for OD pair w is found by solving an SP problem. This sub-problem, given link travel times $t_a(\tilde{v}_a)$ from a current network flow solution $\tilde{\mathbf{v}}$, determines the optimal path and charging strategy. The decision variables for this SP problem (for a given w, k) include: binary path selection variables $x_{a,k}^w \in \{0, 1\}$ (1 if link a is used, 0 otherwise); dynamic charging duration $g_{a,k}^w \geq 0$ on links $a \in \tilde{A}$; static charging duration $h_{i,k}^w \geq 0$ at nodes $i \in \tilde{N}$; the state of charge (SOC) $L_{i,k}^w$ representing the SOC upon arrival at node i; and an auxiliary energy balance variable $\rho_{a,k}^w$.

The minimal recharging cost is:

$$s_{p,k}^w = \left(\sum_{a \in \tilde{A}} g_{a,k}^w e_a p^l + \sum_{i \in \tilde{N}} h_{i,k}^w (\beta_k + s_i p^s) \right) \tag{65}$$

Therefore, the SP problem can be defined mathematically as:

$$\min_{\mathbf{x}_k,\mathbf{g}_k,\mathbf{h}_k,\mathbf{L}_{k,k}} \left(\sum_{a\in A} \beta_k t_a(\tilde{v}_a) x^w_{a,k} + \sum_{a\in \tilde{A}} g^w_{a,k} e_a p^l + \sum_{i\in \tilde{N}} h^w_{i,k}(\beta_k + s_i p^s) \right) \tag{66}$$

$$\text{S.t.:} \sum_{a\in N^{out}_j} x^w_{a,k} - \sum_{a\in N^{in}_j} x^w_{a,k} = \begin{cases} 1 & \text{if } j = o(w) \\ -1 & \text{if } j = d(w) \\ 0 & \text{otherwise} \end{cases} \qquad \forall j \in N \tag{67}$$

$$L^w_{o(w),k} = L_{0,k} \tag{68}$$

$$L^w_{j,k} - (L^w_{i,k} + h^w_{i,k} s_i) + d_a \varpi - g^w_{a,k} e_a = \rho^w_{a,k} \qquad \forall a = (i,j) \in A \tag{69}$$

$$-K(1 - x^w_{a,k}) \le \rho^w_{a,k} \le K(1 - x^w_{a,k}) \qquad \forall a \in A \tag{70}$$

$$L^w_{i,k} + h^w_{i,k} s_i \le B_k \qquad \forall i \in N \tag{71}$$

$$L^w_{i,k} \ge L_{min} \qquad \forall i \in N \tag{72}$$

$$\begin{cases} g^w_{a,k} = 0 & \forall a \notin \tilde{A} \\ 0 \le g^w_{a,k} \le t_a(\tilde{v}_a) & \forall a = (i,j) \in \tilde{A} \end{cases} \tag{73}$$

$$\begin{cases} h^w_{i,k} = 0 & \forall i \notin \tilde{N} \\ h^w_{i,k} \ge 0 & \forall i \in \tilde{N} \end{cases} \tag{74}$$

$$x^w_{a,k} \in \{0,1\} \qquad \forall a \in A \tag{75}$$

where ϖ is energy consumption rate of EVs. e_a is the charging rate on dynamic link $a \in \tilde{A}$ with an electricity price p^l , while s_i is the charging rate at static station $i \in \tilde{N}$ with an electricity price p^s. β_k is the value of time for type-k drivers. N^{out}_j is the set of links originating at node j, and N^{in}_j is the set of links terminating at node j. The EV's initial SOC for type k at the origin $o(w)$ is $L_{0,k}$. The maximum battery capacity for a type-k EV is B_k, and L_{min} is its minimum acceptable SOC during the trip. K are sufficiently large positive constants for the Big-M method.

Constraint (67) ensures the selected links $x^w_{a,k}$ form a continuous path. Equation (68) sets the arrival SOC at the origin $o(w)$ to the given initial SOC, $L_{0,k}$. The SOC evolution is primarily governed by constraint (69): the arrival SOC at node j, $L^w_{j,k}$, is determined by the departure SOC from node i (which is $L^w_{i,k} + h^w_{i,k} s_i$, i.e., arrival SOC at i plus any static charging at i), less the energy $d_a \varpi$ consumed on link $a = (i,j)$, plus any energy $g^w_{a,k} e_a$ gained from dynamic charging on that link. The auxiliary variable $\rho^w_{a,k}$, constrained by (70), ensures this balance strictly holds (i.e., $\rho^w_{a,k} = 0$) if link a is chosen ($x^w_{a,k} = 1$).

The SOC after any static charging at node i, $L^w_{i,k} + h^w_{i,k} s_i$, must not exceed the battery capacity B_k, as enforced by (71). The arrival SOC at any node i, $L^w_{i,k}$, must not be below the minimum threshold L_{min}, enforced by (72). Constraints (73) and (74) limit charging durations. Dynamic charging $g^w_{a,k}$ is limited by link travel time $t_a(\tilde{v}_a)$ and the battery's capacity to store charge, considering the SOC after consumption on the link but before dynamic charging begins. Static charging $h^w_{i,k}$ is limited by the energy required to fill the battery from the arrival SOC $L^w_{i,k}$. Finally, equation (75) defines $x^w_{a,k}$ as binary variables.

3.4.2 Path-based Model Formulation

Each driver aims to minimize their own generalized travel cost, which is a combination of the value of travel time, the value of time spent charging, and the monetary cost of electricity. For a given path p and a set of link travel times $t_a(\tilde{v}_a)$ resulting from network congestion, a type-k driver solves the following optimization problem to determine the least-cost charging strategy for that path. The decision variables are the dynamic charging duration $g^p_{a,k} \geq 0$ on links $a \in \tilde{A}$ and the static charging duration $h^p_{i,k} \geq 0$ at nodes $i \in \tilde{N}$. The SOC upon arrival at node i is $L^p_{i,k}$.

Let $C^w_{p,k}(\mathbf{v})$ be the minimum generalized cost for a type-k driver on path $p \in \hat{P}^w$, given the link flows $\mathbf{v}$ (which determine the link travel times $t_a(v_a)$). This cost is the optimal objective value from the path-based optimization problem subject to the physical and operational constraints:

$$C^w_{p,k}(\mathbf{v}) = \min_{\mathbf{g}^p_k, \mathbf{h}^p_k} \left\{ \sum_{a \in A(p)} \beta_k t_a(v_a) + \sum_{a \in A(p) \cap \tilde{A}} g^p_{a,k} e_a p^l + \sum_{i \in N(p) \cap \tilde{N}} h^p_{i,k} (\beta_k + s_i p^s) \right\} \tag{76}$$

$$L^p_{o(w),k} = L_{0,k} \tag{77}$$

$$L^p_{j,k} - (L^p_{i,k} + h^p_{i,k} s_i) + d_a \varpi - g^p_{a,k} e_a = 0 \qquad \forall a = (i,j) \in A(p) \tag{78}$$

$$L^p_{i,k} + h^p_{i,k} s_i \leq B_k \qquad \forall i \in N(p) \tag{79}$$

$$L^p_{i,k} \geq L_{min} \qquad \forall i \in N(p) \tag{80}$$

$$\begin{cases} g^p_{a,k} = 0 & \forall a \notin \tilde{A} \\ 0 \leq g^p_{a,k} \leq t_a(\tilde{v}_a) & \forall a \in A(p) \cap \tilde{A} \end{cases} \tag{81}$$

$$\begin{cases} h^p_{i,k} = 0 & \forall i \notin \tilde{N} \\ h^p_{i,k} \geq 0 & \forall i \in N(p) \cap \tilde{N} \end{cases} \tag{82}$$

where $A(p)$ and $N(p)$ are the sets of links and nodes in path p. The first term is the monetized cost of travel time, the second term is the monetary cost of dynamic charging, and the last term is generalized cost of static charging, including the monetized value of time spent charging and the electricity cost.

Constraint (77) initializes the State of Charge (SOC) for a type-k EV at the origin node $o(w)$ of its path to a predetermined starting level, $L_{0,k}$. Constraint (78) tracks the EV's SOC across each link $a = (i, j)$ of the path. The SOC upon arrival at the destination node j, $L^p_{j,k}$, is equal to the SOC at the start node i after any static charging ($L^p_{i,k}+h^p_{i,k}s_i$), minus the energy consumed for traversing the link ($d_a\varpi$), plus any energy gained from dynamic charging along the link ($g^p_{a,k}e_a$). Constraint (79) ensures that the SOC at any node i, after completing a potential static charging session, does not exceed the vehicle's maximum battery capacity, B_k. Constraint (80) enforces that the SOC upon arriving at any node i along the path must remain above a specified minimum threshold, L_{min}. This prevents the vehicle from becoming stranded due to a depleted battery. Constraint (81) governs dynamic charging. It specifies that dynamic charging time $g^p_{a,k}$ can only be positive on links equipped with dynamic charging technology ($a \in \tilde{A}$). Furthermore, the duration of charging on a link cannot exceed the time taken to travel across that link, $t_a(\tilde{v}_a)$. Constraint (82) governs static charging. It dictates that static charging time $h^p_{i,k}$ can only be positive at nodes equipped with charging stations ($i \in \tilde{N}$) and must be a non-negative value.

Therefore, we can define the network equilibrium conditions as follows:

$$\sum_{p\in\hat{P}^w} f^w_{p,k} = q^w_k \qquad \forall w \in W, k \in K \tag{83}$$

$$v_a = \sum_{w\in W}\sum_{p\in\hat{P}^w}\sum_{k\in K} f^w_{p,k}\delta_{a,p} \qquad \forall a \in A \tag{84}$$

$$f^w_{p,k} \geq 0 \qquad \forall p \in \hat{P}^w, w \in W, k \in K \tag{85}$$

$$\left(\sum_{a\in A(p)} \beta_k t_a(v_a) + \sum_{a\in A(p)\cap\tilde{A}} g^p_{a,k}e_a p^l + \sum_{i\in N(p)\cap\tilde{N}} h^p_{i,k}(\beta_k + s_i p^s) - \mu^w_k\right) f^w_{p,k} = 0 \qquad \forall p \in \hat{P}^w, w \in W \tag{86}$$

$$\sum_{a\in A(p)} \beta_k t_a(v_a) + \sum_{a\in A(p)\cap\tilde{A}} g^p_{a,k}e_a p^l + \sum_{i\in N(p)\cap\tilde{N}} h^p_{i,k}(\beta_k + s_i p^s) \geq \mu^w_k \qquad \forall p \in \hat{P}^w, w \in W \tag{87}$$

where μ^w is an auxiliary variable, representing the equilibrium trip generalized cost for O-D pair $w \in W$.

We assign a Lagrangian multiplier to each constraint: $\theta^p_{o(w),k}$ (for 77), $\kappa^p_{a,k}$ (for 78), $\xi^p_{i,k}$ (for 79), $\beta^p_{i,k}$ (for 80), $\pi^p_{a,k}$ and $\omega^p_{a,k}$ (for 81), and $\eta^p_{i,k}$ (for 82). The Lagrangian function $\mathcal{L}$ is:

$$\begin{aligned}\mathcal{L} = &\left(\sum_{a\in A(p)} \beta_k t_a(v_a) + \sum_{a\in\tilde{A}} g^p_{a,k} e_a p^l + \sum_{i\in\tilde{N}} h^p_{i,k}(\beta_k + s_i p^s)\right) + \theta^p_{o(w),k}(L^p_{o(w),k} - L_{0,k}) \\ &+ \sum_{a=(i,j)\in A(p)} \kappa^p_{a,k}(L^p_{j,k} - L^p_{i,k} - h^p_{i,k}s_i + d_a\varpi - g^p_{a,k}e_a) + \sum_{i\in N(p)} \xi^p_{i,k}(L^p_{i,k} + h^p_{i,k}s_i - B_k) \\ &+ \sum_{i\in N(p)} \beta^p_{i,k}(L_{min} - L^p_{i,k}) + \sum_{a\in\tilde{A}} \pi^p_{a,k}(g^p_{a,k} - t_a(v_a)) + \sum_{a\in\tilde{A}} \omega^p_{a,k}(-g^p_{a,k}) + \sum_{i\in\tilde{N}} \eta^p_{i,k}(-h^p_{i,k})\end{aligned} \tag{88}$$

Therefore, the stationary conditions are:

$$\frac{\partial\mathcal{L}}{\partial L^p_{i,k}} = \kappa^p_{qi,k} - \kappa^p_{ij,k} + \xi^p_{i,k} - \beta^p_{i,k} = 0 \tag{89}$$

$$-\kappa^p_{o(w)j,k} + \xi^p_{o(w),k} + \theta^p_{o(w)} - \beta^p_{o(w),k} = 0 \tag{90}$$

$$\kappa^p_{qd(w),k} + \xi^p_{d(w),k} - \beta^p_{d(w),k} = 0 \tag{91}$$

$$\frac{\partial\mathcal{L}}{\partial g^p_{a,k}} = e_a p^l - \kappa^p_{a,k}e_a + \pi^p_{a,k} - \omega^p_{a,k} = 0 \tag{92}$$

$$\frac{\partial\mathcal{L}}{\partial h^p_{i,k}} = (\beta_k + s_i p^s) - \kappa^p_{a_{out},k}s_i + \xi^p_{i,k}s_i - \eta^p_{i,k} = 0 \tag{93}$$

The complementary slackness conditions are:

$$\xi^p_{i,k}(L^p_{i,k} + h^p_{i,k}s_i - B_k) = 0 \tag{94}$$

$$\beta^p_{i,k}(L_{min} - L^p_{i,k}) = 0 \tag{95}$$

$$\pi^p_{a,k}(g^p_{a,k} - t_a(v_a)) = 0 \tag{96}$$

$$\omega^p_{a,k}g^p_{a,k} = 0 \tag{97}$$

$$\eta^p_{i,k}h^p_{i,k} = 0 \tag{98}$$

The solution must satisfy all original constraints (77) - (82). Thus, the multipliers for all inequality constraints must be non-negative ($\xi^p_{i,k}, \beta^p_{i,k}, \pi^p_{a,k}, \omega^p_{a,k}, \eta^p_{i,k} \geq 0$).

3.4.3 Network Equilibrium with Variational Inequality (NE-VI)

The vector x contains all path flows and all multipliers from the driver's Karush-Kuhn-Tucker (KKT) subproblem: $x = (\mathbf{f}^*, \mathbf{v}^*, \boldsymbol{\kappa}^*, \boldsymbol{\xi}^*, \boldsymbol{\beta}^*, \boldsymbol{\theta}^*, \boldsymbol{\pi}^*)$. The feasible set K is defined by all network flow rules and the KKT feasibility conditions for the driver's subproblem.

$$\sum_{k,w,p} \Bigg[\underbrace{\sum_{a \in A(p)} \beta_k t_a(v_a^*)}_{\text{Travel Time Cost}} + \underbrace{\sum_{a \in A(p)} (d_a \varpi) \kappa_{a,k}^{p*}}_{\text{Shadow Cost of Energy Consumed}} - \underbrace{\sum_{i \in N(p)} (B_k) \xi_{i,k}^{p*} + \sum_{i \in N(p)} (L_{min}) \beta_{i,k}^{p*}}_{\text{Shadow Cost of Battery Limits}}$$

$$- \underbrace{(L_{0,k}) \theta_{o(w),k}^{p*}}_{\text{Shadow Cost of Initial SOC}} - \underbrace{\sum_{a \in \tilde{A}(p)} (t_a(v_a)) \pi_{a,k}^{p*}}_{\text{Shadow Cost of Charging Time Upper Bound}} \Bigg] (f_{p,k}^w - f_{p,k}^{w*})$$

$$+ \sum_{k,w,p} \Bigg[- \sum_{a \in A(p)} (d_a \varpi) \cdot (\kappa_{a,k}^p - \kappa_{a,k}^{p*}) + \sum_{i \in N(p)} (B_k) \cdot (\xi_{i,k}^p - \xi_{i,k}^{p*})$$

$$- \sum_{i \in N(p)} L_{min} (\beta_{i,k}^p - \beta_{i,k}^{p*}) + \sum_{i \in N(p)} L_{0,k} (\theta_{o(w),k}^p - \theta_{o(w),k}^{p*})$$

$$+ \sum_{a \in A(p)} t_a(v_a^*) (\pi_{a,k}^p - \pi_{a,k}^{p*}) \Bigg] \geq 0 \tag{99}$$

3.4.4 Nonlinear Optimization for Solution

In this section, we solve NE-VI by reformulating it to be the following nonlinear optimization problem via a technique proposed by Aghassi et al. (2006):

NE-NLP:

$$\min_{f,v,L,g,h,\mu,\kappa,\xi,\beta,\theta,\pi} \quad \sum_{k,w,p} \Bigg[\sum_{a \in A(p)} \beta_k t_a(v_a) + \sum_{a \in A(p)} d_a \varpi \kappa_{a,k}^p - \sum_{i \in N(p)} B_k \xi_{i,k}^p + \sum_{i \in N(p)} L_{min} \beta_{i,k}^p$$

$$- \sum_{i \in N(p)} L_{0,k} \theta_{o(w),k}^p - \sum_{a \in A(p)} t_a(v_a^*) \pi_{a,k}^p \Bigg] f_{p,k}^w$$

$$+\sum_{k,w,p}\Bigg[-\sum_{a\in A(p)} d_a\varpi\kappa^p_{a,k}+\sum_{i\in N(p)} B_k\xi^p_{i,k}-\sum_{i\in N(p)} L_{min}\beta^p_{i,k}$$

$$+\sum_{i\in N(p)} L_{0,k}\theta^p_{o(w),k}+\sum_{a\in A(p)} t_a(v^*_a)\pi^p_{a,k}\Bigg]$$

$$-\sum_{k,w} q^w_k\mu^w_k+\sum_{p,k,w,a}(e_aP^l)g^p_{a,k}+\sum_{p,k,w,i}(\beta_k+s_iP^s)h^p_{i,k} \tag{100}$$

subject to:

$$\sum_{a\in A(p)}\beta_k t_a(v_a)+\sum_{a\in A(p)\cap\tilde{A}} g^p_{a,k}e_ap^l+\sum_{i\in N(p)\cap\tilde{N}} h^p_{i,k}(\beta_k+s_ip^s)\geq\mu^w_k \quad \forall p\in\hat{P}^w, w\in W \tag{101}$$

$$\sum_{p\in\hat{P}^w} f^w_{p,k}=q^w_k \qquad \forall w,k \tag{102}$$

$$v_a=\sum_{k,w,p} f^w_{p,k}\delta_{a,p} \qquad \forall a \tag{103}$$

$$f^w_{p,k}\geq 0 \qquad \forall p\in\hat{P}^w, w, k \tag{104}$$

$$L^p_{o(w),k}=L_{0,k} \tag{105}$$

$$L^p_{j,k}-(L^p_{i,k}+h^p_{i,k}s_i)+d_a\varpi-g^p_{a,k}e_a=0 \qquad \forall a=(i,j)\in A(p) \tag{106}$$

$$L^p_{i,k}+h^p_{i,k}s_i\leq B_k \qquad \forall i\in N(p) \tag{107}$$

$$L^p_{i,k}\geq L_{min} \qquad \forall i\in N(p) \tag{108}$$

$$g^p_{a,k}=0 \qquad \forall a\notin\tilde{A} \tag{109}$$

$$0\leq g^p_{a,k}\leq t_a(\tilde{v}_a) \qquad \forall a\in A(p)\cap\tilde{A} \tag{110}$$

$$h^p_{i,k}=0 \qquad \forall i\notin\tilde{N}; \tag{111}$$

$$h^p_{i,k}\geq 0 \qquad \forall i\in N(p)\cap\tilde{N} \tag{112}$$

$$\kappa^p_{qi,k}-\kappa^p_{ij,k}+\xi^p_{i,k}-\beta^p_{i,k}=0 \qquad \forall p\in\hat{P}^w, k, w, (q,i), (i,j)\in A(p), \; i\notin\{o(w), d(w)\} \tag{113}$$

$$-\kappa^p_{o(w)j,k}+\xi^p_{o(w),k}+\theta^p_{o(w)}-\beta^p_{o(w),k}=0 \qquad \forall p\in\hat{P}^w, k, w, (o(w),j)\in A(p) \tag{114}$$

$$\kappa^p_{qd(w),k}+\xi^p_{d(w),k}-\beta^p_{d(w),k}=0 \qquad \forall p\in\hat{P}^w, k, w, (q,d(w))\in A(p) \tag{115}$$

$$e_ap^l-e_a\kappa^p_{a,k}+\pi^p_{a,k}\geq 0 \qquad \forall p\in\hat{P}^w, k, w, a\in\tilde{A} \tag{116}$$

$$(\beta_k+s_ip^s)-s_i\kappa^p_{a_{out},k}+s_i\xi^p_{i,k}\geq 0 \qquad \forall p\in\hat{P}^w, k, w, i\in\tilde{N} \tag{117}$$

$$\xi^p_{i,k}, \beta^p_{i,k}\pi^p_{a,k} \geq 0 \tag{118}$$

3.4.5 Charging Lane Location (CLL) Problem

Finally, the overall WCL deployment problem is formulated as:

$$\min \sum_{k\in K}\sum_{w\in W} \mu^w_k q^w_k \tag{119}$$

$$\text{S.t.:} \sum_{a\in A} c_a d_a y_a \leq I \tag{120}$$

$$y_a \in \{0,1\} \qquad \forall a \in A \tag{121}$$

$$\sum_{p\in \hat{P}^w} f^w_{p,k} = q^w_k \qquad \forall w \in W, k \in K \tag{122}$$

$$v_a = \sum_{k,w,p} f^w_{p,k}\delta_{a,p} \qquad \forall a \in A \tag{123}$$

$$f^w_{p,k} \geq 0 \qquad \forall p, w, k \tag{124}$$

$$L^p_{o(w),k} = L_{0,k} \qquad \forall p \in \hat{P}^w, k, w \tag{125}$$

$$L^p_{i,k} + h^p_{i,k}s_i \leq B_k \qquad \forall p \in \hat{P}^w, k, w, i \tag{126}$$

$$L^p_{i,k} \geq L_{min} \qquad \forall p \in \hat{P}^w, k, w, i \tag{127}$$

$$h^p_{i,k} \geq 0 \qquad \forall p \in \hat{P}^w, k, w, i \in \tilde{N} \tag{128}$$

$$h^p_{i,k} = 0 \qquad \forall p \in \hat{P}^w, k, w, i \notin \tilde{N} \tag{129}$$

$$g^p_{a,k} \leq y_a \cdot t_a(v_a) \qquad \forall p \in \hat{P}^w, k, w, a \in A \tag{130}$$

$$g^p_{a,k} \geq 0 \qquad \forall p \in \hat{P}^w, k, w, a \in A \tag{131}$$

$$L^p_{j,k} - (L^p_{i,k} + h^p_{i,k}s_i) + d_a\varpi - y_a g^p_{a,k} e_a = 0 \qquad \forall p \in \hat{P}^w, k, w, a = (i,j) \tag{132}$$

$$\kappa^p_{qi,k} - \kappa^p_{ij,k} + \xi^p_{i,k} - \beta^p_{i,k} = 0 \qquad \forall p \in \hat{P}^w, k, w, (q,i), (i,j) \in A(p), \; i \notin \{o(w), d(w)\} \tag{133}$$

$$-\kappa^p_{o(w)j,k} + \xi^p_{o(w),k} - \beta^p_{o(w),k} = 0 \qquad \forall p \in \hat{P}^w, k, w, (o(w),j) \in A(p) \tag{134}$$

$$\kappa^p_{qd(w),k} + \xi^p_{d(w),k} - \beta^p_{d(w),k} = 0 \qquad \forall p \in \hat{P}^w, k, w, (q,d(w)) \in A(p) \tag{135}$$

$$(\beta_k + s_i p^s) - \kappa^p_{a_{out},k}s_i + \xi^p_{i,k}s_i \geq 0 \qquad \forall p \in \hat{P}^w, k, w, i \in \tilde{N} \tag{136}$$

$$y_a(e_a p^l - \kappa^p_{a,k}e_a + \pi^p_{a,k}) \geq 0 \qquad \forall p \in \hat{P}^w, k, w, a \in A \tag{137}$$

$$\xi^p_{i,k}(L^p_{i,k} + h^p_{i,k}s_i - B_k) = 0 \qquad \forall p \in \hat{P}^w, k, w, i \tag{138}$$

$$\beta^p_{i,k}(L_{min} - L^p_{i,k}) = 0 \qquad \forall p \in \hat{P}^w, k, w, i \tag{139}$$

$$((\beta_k + s_i p^s) - \kappa^p_{a_{out},k}s_i + \xi^p_{i,k}s_i)h^p_{i,k} = 0 \qquad \forall p \in \hat{P}^w, k, w, i \in \tilde{N} \tag{140}$$

$$\pi^p_{a,k}(g^p_{a,k} - y_a \cdot t_a(v_a)) = 0 \qquad \forall p \in \hat{P}^w, k, w, a \in A \tag{141}$$

$$y_a \cdot (e_a p^l - \kappa^p_{a,k} e_a + \pi^p_{a,k}) g^p_{a,k} = 0 \qquad \forall p \in \hat{P}^w, k, w, a \in A \tag{142}$$

$$\xi^p_{i,k} \geq 0 \qquad \forall p \in \hat{P}^w, k, w, i \tag{143}$$

$$\beta^p_{i,k} \geq 0 \qquad \forall p \in \hat{P}^w, k, w, i \tag{144}$$

$$\pi^p_{a,k} \geq 0 \qquad \forall p \in \hat{P}^w, k, w, a \in A \tag{145}$$

$$(C^w_{p,k} - \mu^w_k) f^w_{p,k} = 0 \qquad \forall p \in \hat{P}^w, k, w \tag{146}$$

$$C^w_{p,k} \geq \mu^w_k \qquad \forall p \in \hat{P}^w, k, w \tag{147}$$

$$C^w_{p,k} = \sum_{a \in A(p)} \beta_k t_a(v_a) + \sum_{a \in A(p)} y_a (g^p_{a,k} e_a p^l) + \sum_{i \in N(p) \cap \tilde{N}} h^p_{i,k} (\beta_k + s_i p^s) \tag{148}$$

where c_a is the cost of constructing WCL on link a per unit distance, I is the total available budget, and y_a is a binary decision variable equal to 1 if link a is selected to be WCL, and 0 otherwise.

3.4.6 Solution Methodology

The proposed CLL model represents a mathematical program with equilibrium constraints. Solving such problems is computationally challenging due to the non-convex nature of complementarity constraints. To address this, we adopt an iterative active-set framework, originally established by Zhang et al. (2009).

The core principle of this approach is to decompose the problem into manageable stages. First, we solve a restricted version of the model by fixing the binary deployment variables, thereby treating the charger locations as constant. This yields Lagrangian multipliers that represent the sensitivity or marginal value of adding or removing a charger on specific links. Second, these multipliers define the parameters of a binary Knapsack problem. Solving the Knapsack problem generates a candidate move, a set of links to switch from uncharged to charged (or vice-versa) to lower the objective value. This process repeats iteratively until convergence is achieved.

Restricted CLL Problem Formulation

To facilitate the active-set method, we partition the set of all candidate links A into two disjoint, exhaustive subsets for any given iteration: $\Omega_0 = \{a : y_a = 0\}$ (links without charging) and $\Omega_1 = \{a : y_a = 1\}$ (links with charging).

By fixing the binary decision variables y_a based on these sets, we formulate the restricted CLL as follows:

$$\min_{\pi,\eta,\phi,\kappa,\xi,\theta,\sigma,\beta,\gamma,\lambda,f,v,\rho,y} \sum_k \sum_{w\in W} \rho_k^w q_k^w + \sum_a y_a c_a d_a \tag{149}$$

$$\text{S. t.:} y_a = 0, \quad \forall a \in \Omega_0 \tag{150}$$

$$y_a = 1, \quad \forall a \in \Omega_1 \tag{151}$$

Restricted CLL is also subject to all network equilibrium conditions. Although the restricted CLL retains complementarity constraints, it essentially reduces to a standard Network Equilibrium Non-Linear Program (NE-NLP) because the integer constraints are fixed. The optimal solution and the associated dual variables for constraints (150) and (151) can be retrieved efficiently.

Algorithmic Procedure

The solution search proceeds through the following steps. Convergence properties of this method are detailed in Zhang et al. (2009).

Step 0: Initialization

Initialize the iteration counter $\tau = 1$. Define the initial active sets as $\Omega_0^1 = A$ and $\Omega_1^1 = \emptyset$, implying a baseline network with no wireless charging. Solve the NE-NLP under this configuration. To ensure robustness, if the NE-NLP solution is non-unique, multiple initial points may be evaluated to select the solution yielding the minimum social cost.

Step 1: Multiplier Estimation

Using the equilibrium flow obtained in the previous step, construct the full primal solution vector $(\pi, \eta, \ldots, y)$ for the restricted CLL. Solve the restricted CLL to extract the Lagrangian multipliers λ_a^k and μ_a^h corresponding to the active set constraints (150) and (151). Calculate the current total system cost $TT^\tau = \sum_w p^w g^w$ and proceed to Step 2.

Step 2: Iterative Improvement Loop

Initialize a bounding parameter $Q = -\infty$. Update the deployment plan via the following sub-routine:

(a) Knapsack Sub-problem: Solve for binary decision variables k and h to identify the optimal set of links to swap:

$$\min_{a\in\Omega_0^\tau} \sum \lambda_a^k k_a - \sum_{a\in\Omega_1^\tau} \mu_a^h h_a \tag{152}$$

$$\text{s.t.:} \sum_{a\in\Omega_0^\tau} c_a d_a k_a - \sum_{a\in\Omega_1^\tau} c_a d_a h_a \le I - \sum_{a\in\Omega_1^\tau} c_a d_a \tag{153}$$

$$\sum_{a\in\Omega_0^\tau} \lambda_a^k k_a - \sum_{a\in\Omega_1^\tau} \mu_a^h h_a \ge Q \tag{154}$$

$$k_a, h_a \in \{0,1\} \qquad \forall a \in A \tag{155}$$

where $k_a = 1$ indicates moving link a from Ω_0 to Ω_1, while $h_a = 1$ indicates removing a charger. If the optimal objective is zero, the algorithm terminates; the current plan is locally optimal. Otherwise, proceed to (b).

(b) Candidate Set Generation: Calculate the estimated improvement D and define tentative active sets $\tilde{\Omega}_0$ and $\tilde{\Omega}_1$:

$$D = \sum_{a\in\Omega_0^\tau} \lambda_a^k \hat{k}_a - \sum_{a\in\Omega_1^\tau} \mu_a^h \hat{h}_a \tag{156}$$

$$\tilde{\Omega}_0 = (\Omega_0^\tau \setminus \{a : \hat{k}_a = 1\}) \cup \{a : \hat{h}_a = 1\} \tag{157}$$

$$\tilde{\Omega}_1 = (\Omega_1^\tau \setminus \{a : \hat{h}_a = 1\}) \cup \{a : \hat{k}_a = 1\} \tag{158}$$

(c) Verification: Solve the NE-NLP using the candidate deployment $\hat{y}$ derived from $\tilde{\Omega}_0$ and $\tilde{\Omega}_1$. If the resulting social cost $TT < TT^\tau$, the move is successful. Proceed to Step 2d. If the cost does not decrease, reject the candidate plan. Update the lower bound $Q = D + \varepsilon$ (where ε is a small positive constant) and return to Step 2a to find the next best adjustment.

(d) Update: Accept the new configuration: set $\Omega_0^{\tau+1} = \tilde{\Omega}_0$, $\Omega_1^{\tau+1} = \tilde{\Omega}_1$, increment $\tau = \tau + 1$, and return to Step 1.

3.5 Key Takeaways

This section fills critical gaps in EV infrastructure planning by establishing comprehensive frameworks to evaluate and compare the established conductive charging station approach with the emerging wireless approach. The key takeaways from our methodological framework are as follows:

We developed a general cost-competitiveness model to strategically compare CS and WCL systems by analyzing the fundamental trade-offs between infrastructure investment and vehicle battery costs across various operational domains. A major strategic finding of this analysis is the identification of a scale-independent design principle for both charging

systems. This principle dictates that the optimal infrastructure density, such as the optimal fraction of a roadway to electrify for WCLs, is determined by local traffic characteristics, including traffic density and fleet utilization, rather than the overall physical size of the road network or total miles traveled.

Recognizing that the battery ranges of current EVs often far exceed typical daily travel needs, we developed a mathematical model specifically to evaluate charging strategies for single long-distance trips. This model assesses how mandatory or recommended driver rest breaks can be strategically utilized for charging, allowing for a structured comparison between WCL and CS technologies during extended travel.

Finally, we formulated mathematical optimization models to identify the optimal deployment locations for wireless and static charging infrastructure in two distinct operational contexts. We developed a model to find the optimal types and locations of chargers required to electrify a transit agency's fleet without requiring any alterations to their existing schedules, routes, or fleet size. Also, we formulated a charging lane location problem to optimize the placement of WCLs in a transportation network. This model explicitly accounts for the presence of existing static charging stations and the route choices of drivers who aim to minimize their individual generalized travel costs.

4 Findings

4.1 Economic Comparison

In this section, we conduct a series of numerical studies to provide concrete insights into the model's behavior and demonstrate its practical application. We begin by establishing the baseline parameters for our analysis. Then, we use these parameters to identify the optimal solution and benchmark the system's performance. Building on this, we explore the sensitivity of the optimal design with respect to key system features. Finally, we apply the complete framework to real-world bus rapid transit (BRT) systems in different cities to validate our findings and identify practical use cases.

4.1.1 Numerical Settings

We analyze an urban network with a total road length (l) of 500 miles and a total hourly vehicle-miles traveled (m) of 315,000 miles. The EV fleet is modeled with a utilization factor (u) of 0.1. Key vehicle parameters include an energy consumption rate (β) of 0.3 kWh/mile, a usable battery fraction (θ) of 0.8, and a WCL power transfer efficiency (γ)

of 0.9. System design parameters include a WCL segment length (d_w) of 1 mile and a maximum CS network occupancy (ρ_{max}) of 80%. In sections 4.1.2 and 4.1.3, we adopt a fundamental speed-density relationship, whereas section 4.1.4 is a steady-state speed scenario. Given a free-flow speed (v_f) of 35 mph and a jam density (λ_j) of 200 veh/mile, we select the uncongested equilibrium from the two possible solutions, resulting in an average density (λ) of 20 veh/mile. Additional calibration parameters include $\tau_a = 0.01$ and $\omega = 0.001$.

The initial capital cost assumptions and the resulting amortized hourly costs are listed in Table 5. The relevant conversion is performed using the Capital Recovery Factor (CRF) method, assuming a uniform annual discount rate of 5%. The formula for the CRF is:

$$\text{CRF} = \frac{i(1+i)^n}{(1+i)^n - 1} \tag{159}$$

where i is the annual discount rate and n is the asset's lifetime in years.

For the two regimes, to cover the most general case, we use the coupled situation to conduct most of the cases. The BRT system is more of a schedule system that can be addressed by the uncoupled analysis.

Table 5: Summary of economic parameter derivation.

Component	**Symbol**	**Upfront Capital Cost**	**Lifetime (n)**
WCL Infrastructure			
Fixed Cost	c_1^w	\$3,000,000 / mile	12 years
Variable Cost	c_2^w	\$10,000 / kW-mile	12 years
CS Infrastructure			
Fixed Cost	c_1^s	\$100,000 / station	10 years
Variable Cost	c_2^s	\$1,000 / kW-station	10 years
Battery Technology			
Battery Cost	c_b	\$250 / kWh	10 years

4.1.2 Charging Infrastructure Optimization

Figure 2 compares the fundamental cost structures of the WCL and CS paradigms. Figure 2a illustrates that for any given charging power (P_w), the total cost of the WCL system increases linearly with the number of charging segments (N_w), under optimized battery size (E_w). This reflects a system where the total cost is dominated by the marginal expense of infrastructure, with the y-intercept determined by the aggregate battery cost of

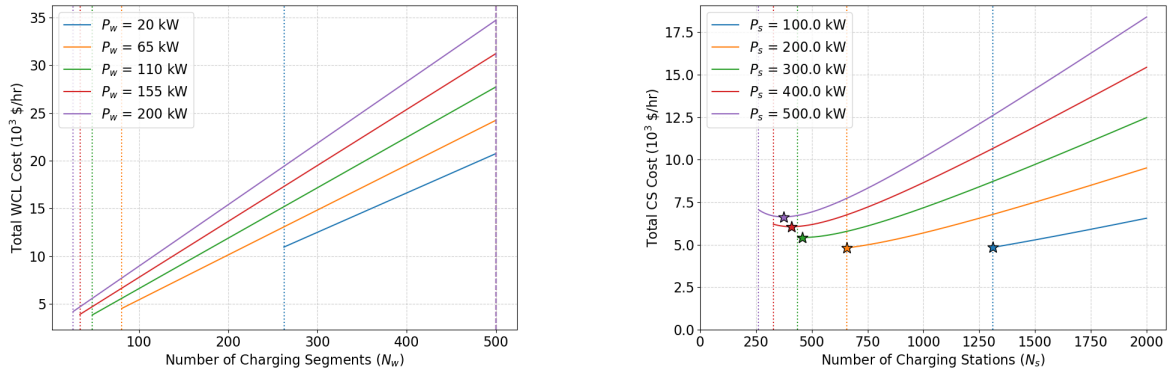

(a) (b)

Figure 2: Comparison of cost structures for (a) WCL and (b) CS systems.

the fleet. The analysis validates that for wireless charging; the optimal design is always the minimum number of segments required to meet the energy sufficiency constraint.

In contrast, Figure 2b shows the classic U-shaped cost curves of the CS system (For this visualization, we adopt a higher battery cost scenario to clearly highlight the convex trade-off). This convex relationship highlights a core economic trade-off: a low number of stations (N_s) requires the vehicle fleet to have large, expensive batteries to cover the distance between them. Conversely, a high number of stations increases the total infrastructure cost. The optimal point for each power level (P_s), represents the ideal balance that minimizes the total societal cost by perfectly trading off the investment in stations against the investment in vehicle batteries.

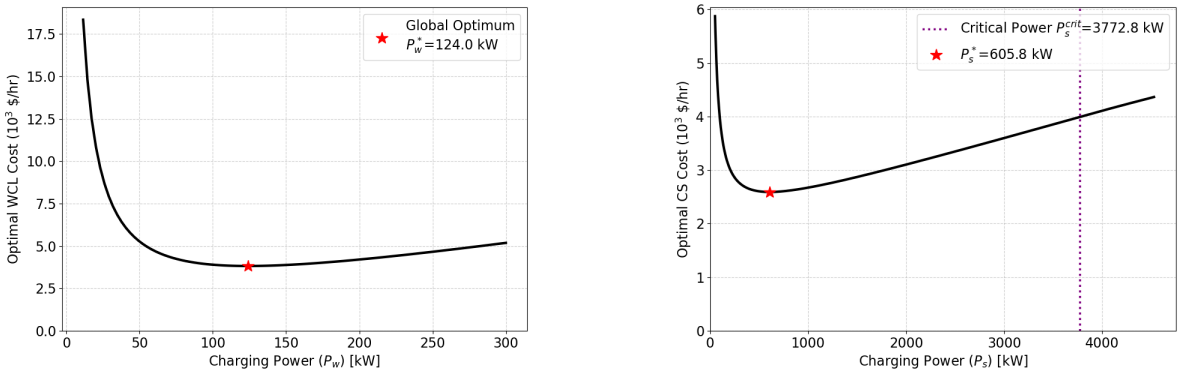

(a) (b)

Figure 3: Comparison of optimal charging power for (a) WCL and (b) CS systems.

Figure 3 compares the total societal cost as a function of the selected charging power

for the fully optimized WCL and CS systems. Figure 3a displays a smooth, convex cost curve for the WCL system. This U-shape illustrates a direct trade-off: at low power levels, the cost is high due to the large number of charging segments required for energy sufficiency and the high aggregate battery cost. At high power levels, the per-unit infrastructure cost (the c_2^w term) begins to dominate. The optimal power, P_w^* represents the ideal technological point that perfectly balances these competing costs. In contrast, Figure 3b reveals the more complex, piecewise nature of the CS system's cost. The curve follows the U-shaped, performance-driven cost function up to the critical power threshold ($P_{s,\text{crit}}$) and then transitions to the steadily increasing, economics-driven cost function. The global optimum, P_s^*, is the lowest point on this entire composite curve, representing the best possible design that considers both the economic trade-offs and the binding performance constraints of the network.

4.1.3 Sensitivity Analysis

Figure 4 visualizes how the optimal charging system design changes under different operational conditions. As traffic density increases (Figure 4a), the optimal static station power P_s^* exhibits a concave, inverted U-shape that mirrors the network's macroscopic flow rate. At lower densities, power scales up driven by the rising traffic volume to handle increasing vehicle arrivals and minimize access delays; however, as density further increases, the power requirement collapses because the congestion-induced speed reduction suppresses the effective arrival rate and service demand. In contrast, the wireless lane power P_w^* decreases monotonically, driven by the time-gain effect where vehicles spend more time over charging segments due to lower speeds. The system exploits this extended contact duration by reducing the power transfer rate, effectively substituting time intensity for power intensity. Simultaneously, the infrastructure density profiles reveal a shift in capital allocation where the CS system combats density by adding more discrete stations (δ_s^*), while the WCL system responds by expanding continuous network coverage (α^*), allowing for the substantial reduction in vehicle battery size (E_w^*). As fleet utilization increases (Figure 4b), the strategies diverge to prioritize efficiency. The CS system consolidates into fewer but exponentially more powerful stations (P_s^*) to minimize service downtime, a strategy which requires a modest increase in vehicle battery size (E_s^*). The WCL system, however, shifts the economic burden to the vehicle. The model prescribes significantly less road infrastructure (α^* drops from $\sim$28% to under 4%) in favor of much larger on-board batteries (E_w^*) to maintain high uptime.

The analysis reveals two fundamentally different infrastructure philosophies. The CS

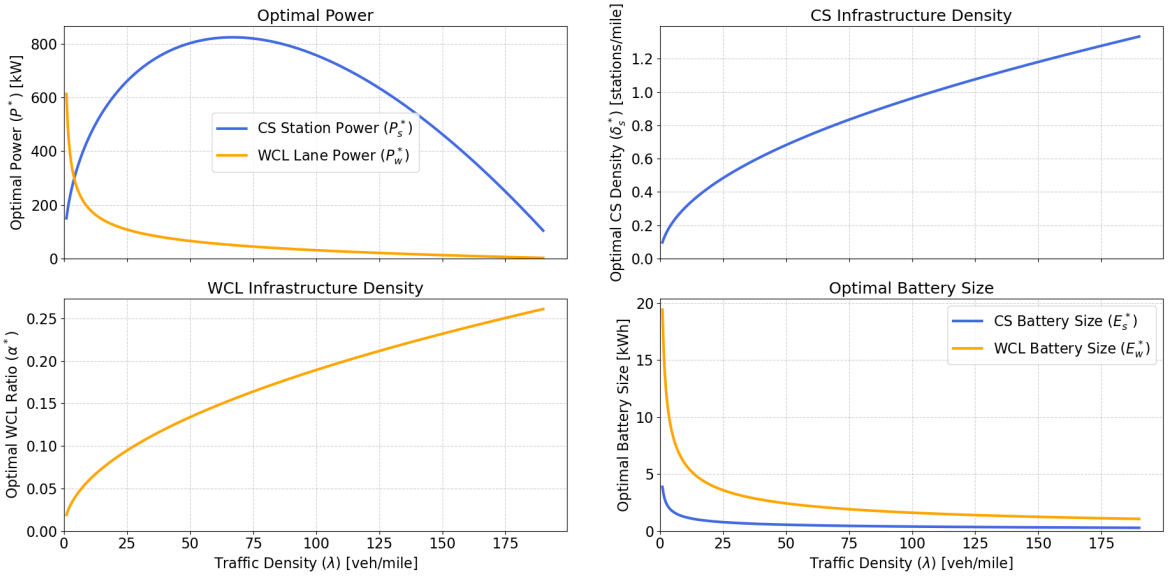

(a)

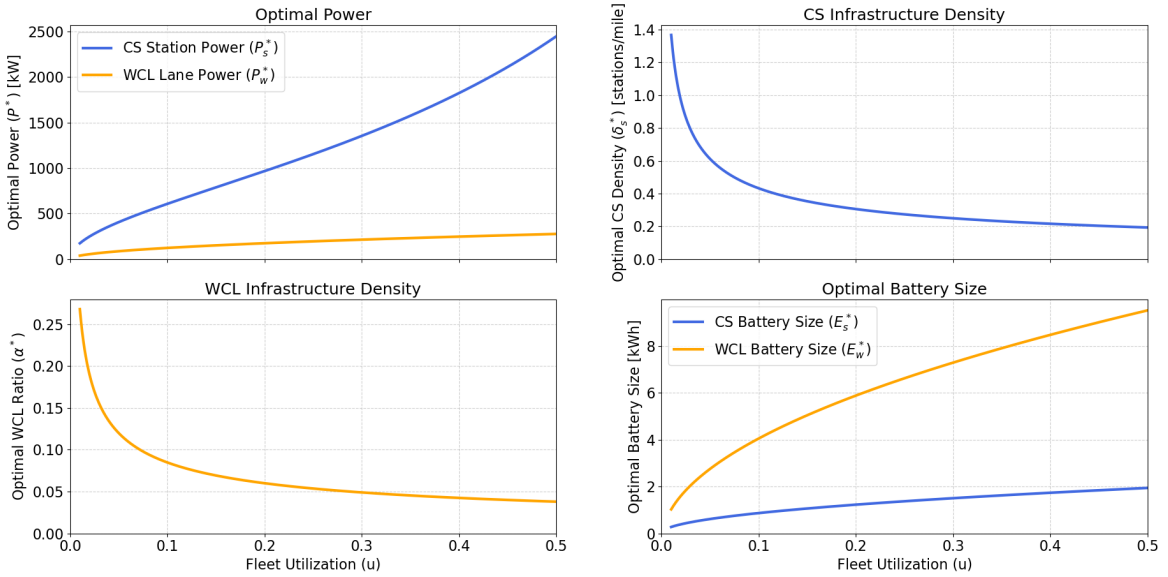

(b)

Figure 4: Impact of (a) traffic density and (b) fleet utilization on the optimal design parameters of CS and WCL systems.

system is a point-based infrastructure that responds to operational pressures by enhancing the capability of its charging points. The WCL system is a line-based infrastructure whose design is governed by the core trade-off between the extent of its network coverage and the size of the batteries on the vehicles it serves.

Figure 5 visualizes the magnitude of the cost difference ($C_s^* - C_w^*$), where brighter col-

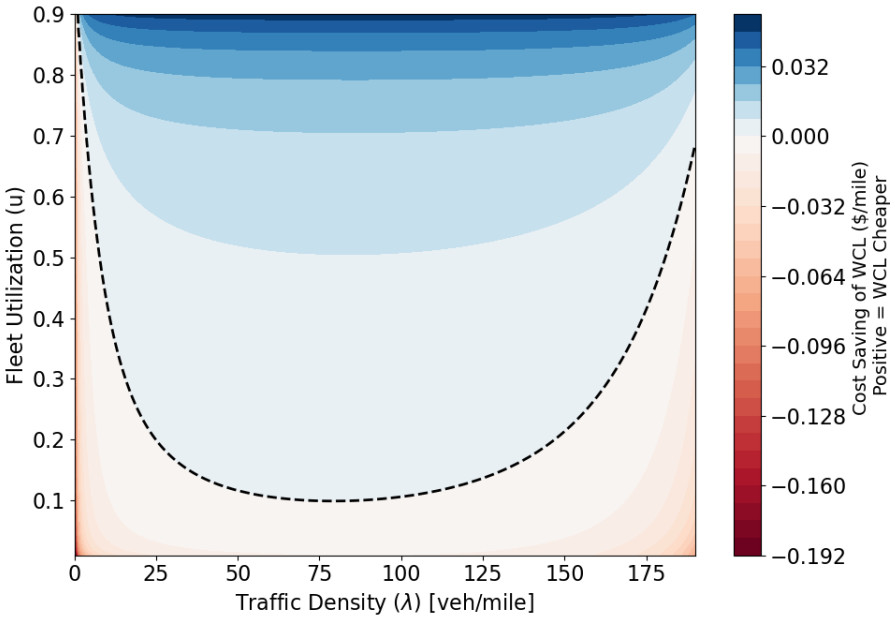

Figure 5: Cost difference of WCL system over CS system across a range of traffic densities and fleet utilizations.

ors indicate a greater economic advantage for the WCL system. The analysis reveals a non-monotonic, convex relationship with traffic density. While the WCL advantage initially grows with density (transitioning from red to deep blue) due to infrastructure amortization, this benefit is not infinite. At extremely high densities ($\lambda > 150$ veh/mile), the advantage begins to diminish as the system approaches the physical jam limit. In contrast, the advantage with respect to fleet utilization is monotonic; as fleets operate closer to $24/7$ ($u \to 1$), the utilization barrier of the CS system widens the performance gap, solidifying WCL as the superior paradigm for high-uptime operations.

In Figure 6, the indifference frontier represents the breakeven curve where the costs of the two systems are equal. This boundary divides the parameter space into distinct regions: the WCL-favored domain (green, top) and the CS-favored domain (blue, bottom). The sensitivity analysis reveals divergent responses to technological improvements:

- Battery Cost Reduction (c_b): A 50% reduction in battery cost shifts the boundary down, significantly expanding the WCL-favored region. This implies that WCL is better positioned to capitalize on cheaper energy storage, likely because it shifts the system optimal design toward larger, cheaper buffers to maximize power transfer efficiency, whereas CS benefits are capped by station constraints.

- Vehicle Efficiency Improvement (β): Conversely, enhancing vehicle efficiency (low-

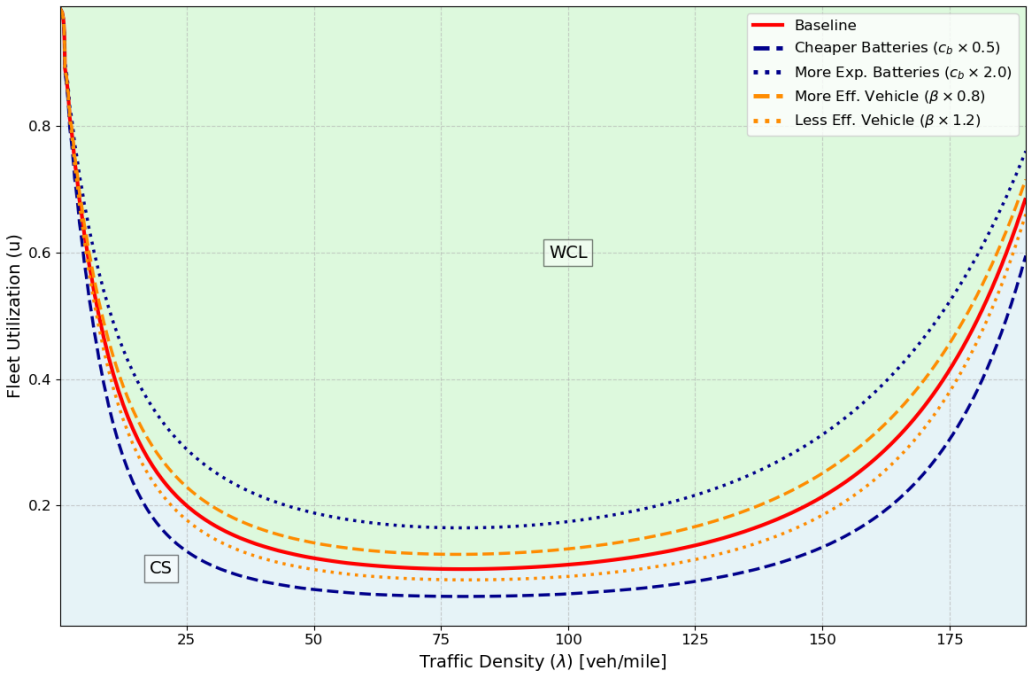

Figure 6: Regions of economic preference for WCL and CS systems as a function of traffic density and fleet utilization, under different battery cost or vehicle energy efficiency.

ering energy consumption β by 20%) shifts the boundary up, shrinking the WCL domain. This indicates that highly efficient vehicles favor the CS model. The logic is straightforward: if a vehicle consumes very little energy, the range constraints of the CS system become less harsh, allowing it to remain viable even in higher-intensity operations. Symmetrically, a 20% increase in energy consumption shifts the boundary down, favoring WCL. As vehicle efficiency degrades, the stop-and-charge penalty of CS becomes unmanageable, making the continuous energy delivery of WCL the superior choice.

Figure 7 provides an analysis of the cost scalability of the two systems, identifying the critical points at which one technology becomes more cost-effective than the other. The analysis is presented in two panels, examining the impact of traffic density (λ) and fleet utilization (u) on the cost per Vehicle Mile Traveled (VMT).

Figure 7a illustrates the cost comparison as a function of traffic density, holding fleet utilization constant at $u = 0.1$. The WCL system exhibits a U-shaped cost profile: costs are high in sparse traffic due to infrastructure capitalization, decrease as density rises, but rise sharply again at high densities ($\lambda > 150$). The CS system remains relatively stable across the density spectrum. Consequently, the WCL system is only cost-effective within a specific density window defined by two crossover points at $\lambda = 72.1$ and $\lambda = 85.8$ veh/mile.

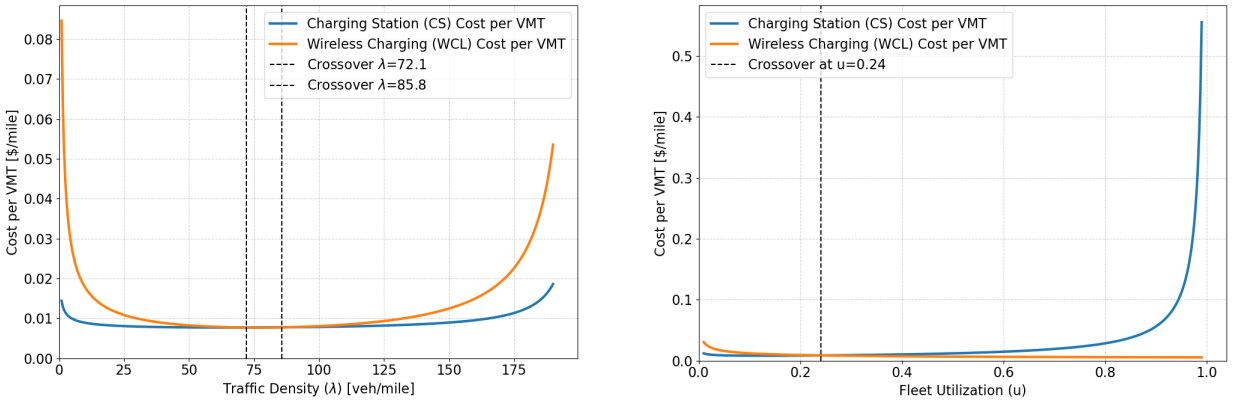

(a) (b)

Figure 7: Critical cost crossover points between CS and WCL systems for (a) $u = 0.1$ and (b) $\lambda = 10\, veh/mile$

Outside this interval, whether in low-density scenarios or highly congested environments, the CS system proves to be the more economical choice.

Figure 7b examines cost scalability with respect to fleet utilization, holding traffic density constant at $\lambda = 10$ veh/mile. Here, the WCL system demonstrates superior scalability, with its average cost remaining low and stable even as utilization approaches 100%. In contrast, the CS system exhibits severe diseconomies of scale at high utilization. As u increases, the cost of the CS system rises exponentially, driven by queuing delays and capacity constraints. The critical crossover point occurs at $u = 0.24$. For fleets with low utilization ($u < 0.24$), CS is the cheaper option. However, for fleets operating above this threshold, the WCL system is substantially more cost-effective due to its resilience to high-throughput demands.

4.1.4 Real-world Charging Comparison

To demonstrate our framework's utility as a practical decision-making tool, we apply our theoretical model to the real-world BRT data from BRTdata (2025). We first process the raw operational metrics $\{l, f, v, n\}$ to derive the necessary intensive parameters in Table 6. Given the total circulation length of a route (l), the average operating speed (v), and the service frequency (f), we first determine the number of active buses (n_a) required to service that route at any given moment. This is found by multiplying the round-trip time (l/v) by the dispatch frequency (f):

$$n_a = \left(\frac{l}{v}\right) f \tag{160}$$

The traffic density (λ), defined as the number of active buses per unit length (n/l), can then be calculated. By substituting the expression for n, the circulation length (l) cancels out, yielding a simple and powerful expression for density that is independent of the route's total length:

$$\lambda = \frac{f}{v} \tag{161}$$

Table 6: BRT corridors and calculated traffic parameters.

City	**Length (l)** (mi)	**Frequency (f)** (veh/h)	**Speed (v)** (mph)	**Total Fleet (n)**	**Active (n_a)** (veh)	**Density (λ)** (veh/mi)	**Utilization (u)**
Amsterdam	56.7	10	35.0	80	16.20	0.29	0.20
Bangkok	15.3	15	26.0	20	8.83	0.58	0.44
Beijing	74.5	60	26.0	187	171.92	2.31	0.92
Bogota	114.4	320	27.2	2363	1345.88	11.76	0.57
Brisbane	28.4	295	37.5	475	223.25	7.87	0.47
Chengdu	28.8	40	26.0	300	44.31	1.54	0.15
Dalian	13.7	75	24.0	64	42.81	3.13	0.67
Guangzhou	22.9	350	24.8	989	323.99	14.11	0.33
Istanbul	52.0	156	35.0	415	232.11	4.46	0.56
Jakarta	251.2	40	19.0	1460	528.84	2.11	0.36
Lima	26.0	117	25.5	487	119.53	4.59	0.25
New York	102.3	17	16.4	398	105.90	1.04	0.27
Cleveland	11.4	8	17.7	21	5.15	0.45	0.24
Nagoya	6.8	15	30.0	25	3.40	0.50	0.14
Paris	41.2	17	23.5	71	29.80	0.72	0.42
Xiamen	48.9	104	27.0	220	188.76	3.85	0.86
Zhengzhou	30.5	52	18.4	290	85.76	2.83	0.30

Figure 8 illustrates the two distinct economic regimes bounded by the WCL indifference frontier. The analysis reveals that WCL is the superior choice in environments characterized by either high traffic density or high fleet utilization. A significant number of high-performing Asian and South American systems fall into this category. Notably, Beijing and Xiamen are identified as prime candidates for WCL due to their extremely high fleet utilization ($u > 0.8$), while Bogota and Guangzhou are favored for WCL due to their high traffic densities ($\lambda > 10$ veh/mile). Systems like Istanbul, Dalian, and Brisbane lie close to the boundary, representing marginal cases where the choice is less clear-cut.

Conversely, the model confirms that CS remains the more economical solution for systems operating with a combination of low traffic density and low-to-moderate fleet utilization. This group includes most of the European and North American BRT systems in the dataset, such as those in Amsterdam, New York, Paris, and Cleveland, as well as other systems like Chengdu and Nagoya. For these operational profiles, the high capital cost of WCL is not justified.

This application to real-world data serves as a powerful demonstration of our theoretical framework. The indifference frontier is not a simple line but a curve that captures the

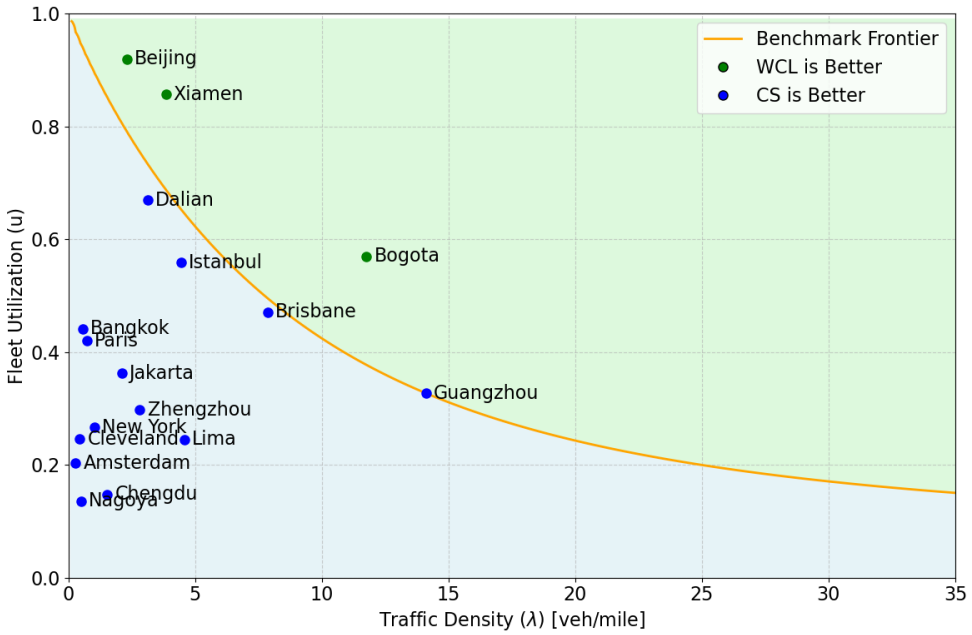

Figure 8: cost-effectiveness regimes for various BRT systems.

complex trade-off between traffic density and fleet utilization. It provides a practical, data-driven tool for transit agencies to quickly assess which charging paradigm represents the most economically sound investment for their specific operational context.

The analyses address a critical gap in electric vehicle infrastructure planning: the lack of a general framework to strategically evaluate the conventional CS paradigm against the emerging WCL paradigm. By developing a macroscopic cost-competitiveness model for each technology, we analyzed the fundamental trade-off between infrastructure investment and vehicle battery costs to determine the optimal system design under diverse conditions. Our analysis revealed several key findings with significant strategic implications. Most notably, we uncovered a scale-independent design principle from both charging systems, showing that the optimal fraction of roadway to electrify is an intensive property determined by local traffic characteristics, remarkably independent of the network's overall size.

Furthermore, we identified a fundamental divergence in the asymptotic properties of the two paradigms regarding fleet utilization and traffic density. In the utilization domain, the technologies exhibit contrasting limits: while CS costs diverge at high utilization due to mandatory downtime, WCL demonstrates asymptotic stability, maintaining finite costs even as fleet intensity maximizes. Conversely, in the density domain, the cost profile is regime-dependent: while WCL capitalizes on monotonic economies of scale under free-

flow conditions, the coupled traffic dynamics reveal a convex trade-off where these amortization benefits are eventually eroded by congestion. The intersection of these distinct asymptotic behaviors gives rise to an indifference frontier, a multidimensional decision boundary determined by the interplay of endogenous traffic physics and techno-economic parameters. This boundary delineates the specific operational window where the high fixed costs of WCL are justified by its superior throughput efficiency, separating it from regimes of sparse demand or extreme congestion where the CS paradigm remains economically superior.

Our findings indicate that while in-motion charging offers only modest time and distance savings for single trips made by light-duty vehicles, these benefits become substantial for heavy-duty vehicles that make such trips regularly. The aggregate effect is even greater as the fleet size increases, providing significant advantages for fleet owners. In-motion charging can also help fleets meet service demands with electric vehicles without expanding the fleet, as it minimizes downtime from stationary charging. Consequently, two promising applications for IVC technology include intercity highway networks and transit agencies that operate fixed intracity routes.

4.2 Single Trip

In this section, we present two types of numerical analyses: (i) we conduct a sensitivity analysis on variables like trip distance and driving range to evaluate their effect on trip time using the model presented in Section 3.2.1, and (ii) we relax assumptions, such as the availability of fast charging at each stop, to assess potential trip time savings for real-world origin-destination routes.

First, we perform numerical examples to investigate the benefits of in motion wireless charging for light-duty EV users. The model was implemented using Python and solved with the Gurobi optimization software. We consider trip lengths of up to 3,690 miles, the longest driving distance in the U.S., stretching from Cape Flattery, Washington, to Key West, Florida. We conduct a sensitivity analysis on EV battery capacity (E) and the wireless and charging power (p_w). Table 7 shows the default values employed throughout this section.

Figure 9a shows the total trip time, including mandatory stops, while Figure 9b displays differences in total trip times with and without wireless charging. The maximum trip time difference is 1.5 hours for trips longer than 3,600 miles. On average, trips without wireless charging are 0.65 hours longer due to recharging time. The downward steps in Figure 9b result from rest stops after reaching the maximum driving period. For instance, with an EV

Table 7: Default parameter values.

Parameter	Value [unit]
E	100 [kWh]
α_w	0.9
α_p	0.9
β	0.25 [kWh/mi]
θ	1.0
p_p	350 [kW]
p_w	50 [kW]
T	8.0 [hr]
t^r	0.5 [hr]
v	70 [mph]

range of 400 miles ($E = 100[kWh]$ and $\beta = 0.25[kWh/mi]$), trips up to 400 miles do not require stopping, taking under 8 hours with or without wireless charging. For trips between 400 to 560 miles, the maximum traversable distance in 8 hours at 70 mph, the EV must stop to recharge if not using wireless charging, creating a half-hour gap in total trip times. For trips from 560 to 800 miles, one stop is necessary as the trip exceeds maximum driving hours without rest, regardless of wireless charging usage, decreasing the total trip time difference to zero.

Figure 10 shows the impact of battery size on the travel time difference with and without in-motion wireless charging. As expected, the difference decreases as battery size increases, and a battery size of 140 kWh, or a range of 560 miles, completely eliminates the time difference.

Figure 11 illustrates the length of wireless charging lanes required for various charging power levels. As charging power increases, the necessary length decreases significantly. Similar to trip time difference (Figure 9b), reductions in the required length occur when vehicles reach their maximum driving time without resting.

Then, we consider 9 cities across the state of Michigan, as displayed in Figure 12. For each pair of cities, we calculated the shortest path based on distance within Michigan, and estimated their travel times. Table 8 shows travel distances in miles, which are placed above the diagonal, and their corresponding estimated travel times, presented below the main diagonal.

We consider an electric vehicle with a battery capacity of 70 kWh and an energy usage rate of 0.25 kWh per mile, which provides a driving range of 280 miles on a full charge. For the 17 origin-destination (OD) pairs with travel distances under 285 miles, the EV can complete the journey without additional charging, so in-motion wireless charging offers no time savings. For the remaining 19 OD pairs, we determine the necessary stops at existing

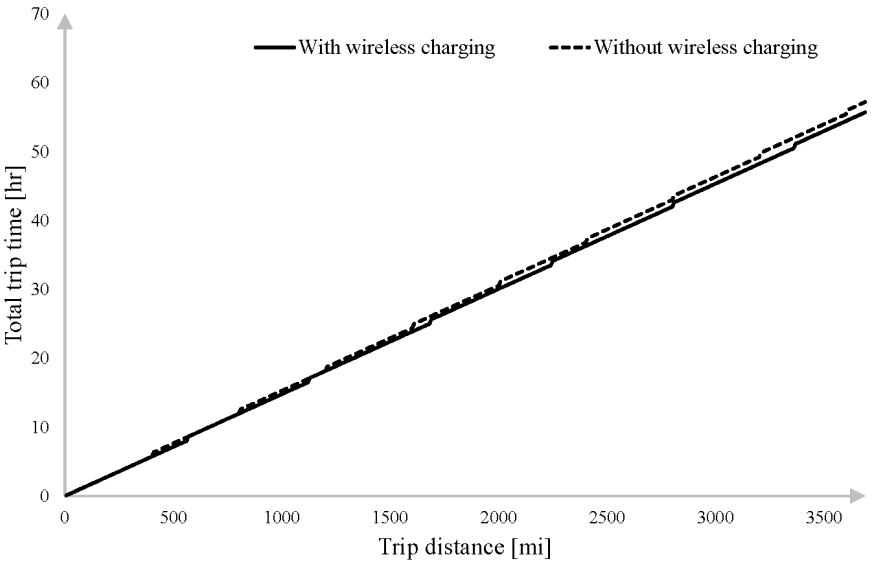

(a)

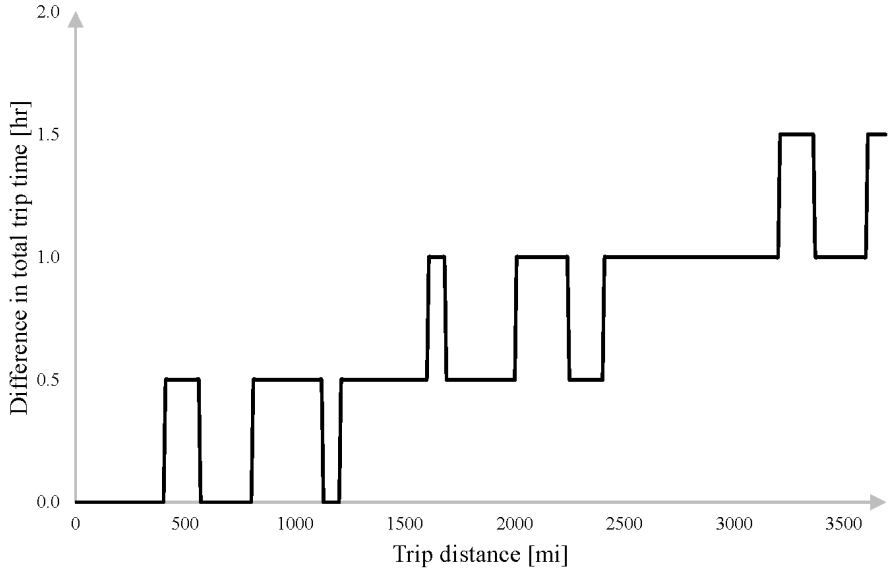

(b)

Figure 9: (a) Total trip time and (b) differences in total trip time for various trip lengths with and without wireless charging.

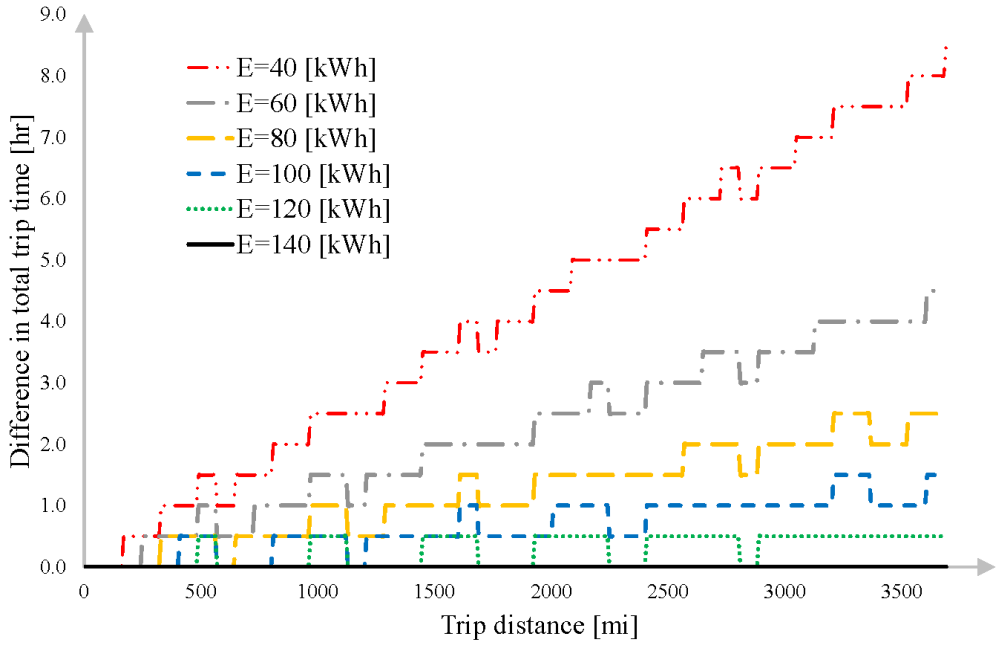

Figure 10: Differences in total trip time for various battery capacity and trip lengths with and without wireless charging.

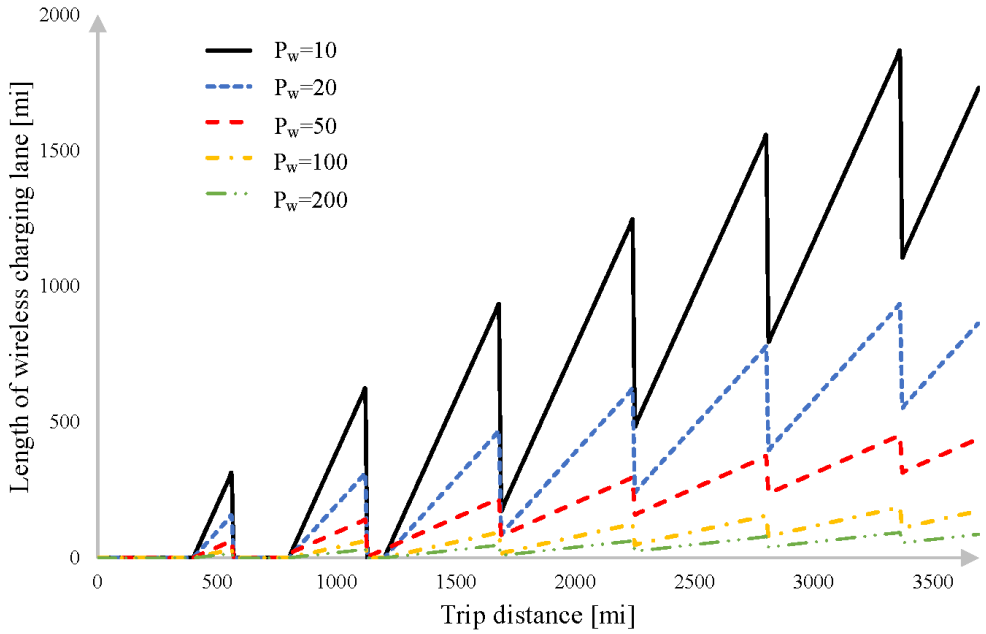

Figure 11: Length of wireless charging lane.

Figure 12: Location of selected cities.

charging stations to complete the trip. Table 9 presents the charging time at each stop, and both travel time and distance savings if in-motion wireless charging allowed the trip to be completed without stopping for charging. When calculating the travel time savings, if the total trip time based on Table 8 is longer than 8 hours, we add a 30-minute rest stop. Travel distance savings occur when the EV must diverge from its route to access charging stations. We can see that if in-motion wireless charging were available, the average travel time saving for all 36 OD pairs would be 18.4 minutes, with the highest saving being 56 minutes. Moreover, the additional travel distance required to access existing charging

Table 8: Travel distances in miles (shown above the diagonal) and corresponding estimated travel times (shown below the main diagonal) for selected cities in Michigan.

	Copper Harbor	Detroit	Grand Rapids	Ironwood	Kalamazoo	Mackinaw City	Marquette	New Buffalo	Traverse City
Copper Harbor		602	548	156	598	313	147	656	414
Detroit	9:27		157	599	140	289	455	214	255
Grand Rapids	8:51	2:21		548	52	228	403	110	143
Ironwood	2:59	9:14	8:46		655	311	146	655	412
Kalamazoo	9:37	2:07	0:51	10:08		286	453	79	193
Mackinaw City	5:33	4:00	3:43	5:16	4:15		167	345	102
Marquette	2:51	6:40	6:12	2:34	6:57	2:52		510	268
New Buffalo	10:26	3:04	1:44	10:08	1:16	4:53	7:33		245
Traverse City	7:32	3:56	2:21	7:15	3:06	2:09	4:46	4:25	

Table 9: Charging times and saved travel time and distance if in-motion charging were available.

OD pair	Charging times [min]	Travel time saving [min]	Travel distance saving [mi]
Copper Harbor, Detroit	23, 30, 18	41	1
Copper Harbor, Grand Rapids	14, 31, 18	33	1
Copper Harbor, Kalamazoo	23, 31, 18	42	2
Copper Harbor, Mackinaw City	13	13	0
Copper Harbor, New Buffalo	23, 18, 30, 15	56	7
Copper Harbor, Traverse City	23, 15	38	17
Detroit, Ironwood	24, 31, 20	45	3
Detroit, Mackinaw City	13	13	2
Detroit, Marquette	19, 28	47	4
Grand Rapids, Ironwood	7, 30, 24	31	0
Grand Rapids, Marquette	5, 30	35	1
Ironwood, Kalamazoo	32, 24, 15	41	3
Ironwood, Mackinaw City	13	13	0
Ironwood, New Buffalo	15, 17, 27 ,20	49	6
Ironwood, Traverse City	15, 19	34	17
Kalamazoo, Mackinaw City	12	12	1
Kalamazoo, Marquette	14, 31	45	2
Mackinaw City, New Buffalo	5, 16	21	0
Marquette, New Buffalo	5, 27, 20	52	6
Sum		661	73

facilities is up to 17 miles, with an average of 2 miles, because many are strategically located along major roads.

4.3 Transit Systems

To help transit agencies and policymakers evaluate the transition to an electric fleet with the model discussed in the previous section, we have developed a web app available at https://transit-electrification.streamlit.app/. Users can choose a transit agency from a list that features most urban transit agencies in Michigan and enter parameters like electric bus range, bus energy consumption, stationary and in-motion charging powers, and stationary charging setup duration. The app determines the number and optimal placement of stationary chargers, along with the location and required length of in-motion chargers, displaying these results on a map. Figure 13 presents a screenshot of the developed web app. The web application produces a report summarizing the analysis details, such as block distances and the bus ranges for routes traversing each block, among other findings. A sample report can be found in Appendix 8.7. Furthermore, the web application is fully open-access, allowing users to copy the project and modify the underlying GTFS data. This flexibility is highly valuable for accommodating recent schedule changes or comparing multiple operational schedules. For additional support or inquiries, users can

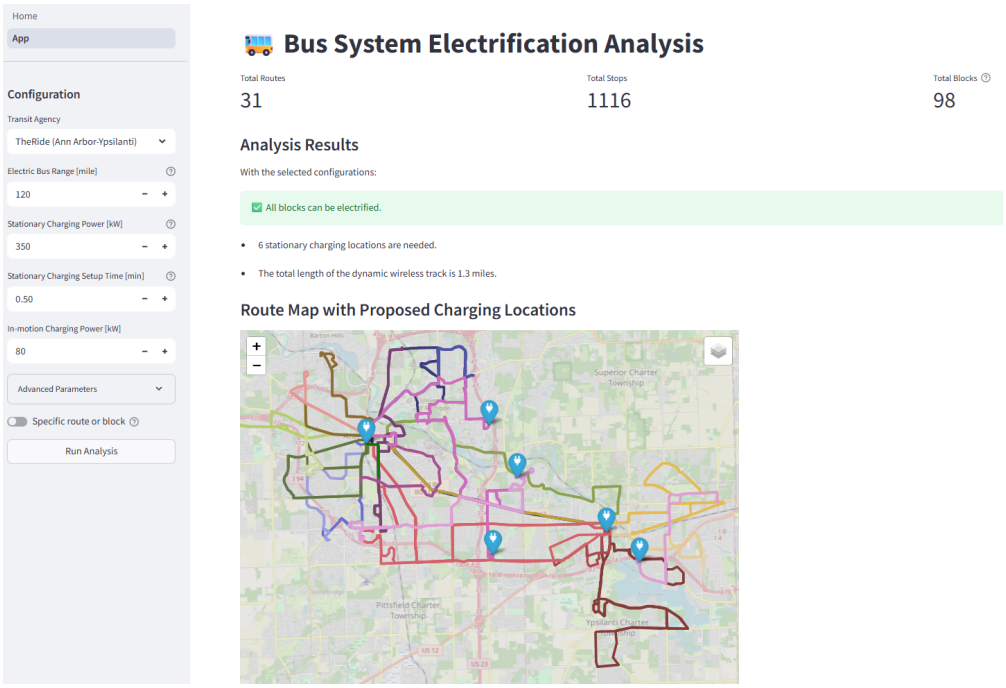

Figure 13: Screenshot of developed web app available at https://transit-electrification.streamlit.app/.

reach out to the research team via the contact information provided on the application's home page.

In solving the model, we use GTFS data from transit agencies, which are freely available on their websites. Given that buses are larger than light-duty vehicles, they have bigger batteries but consume more electricity. We consider a battery capacity of 250 kWh and energy consumption of 2.5 kWh/mi, resulting in a 100-mile electric bus range. Similarly, buses can have multiple charging pads, so we assume a wireless stationary charging power of 250 kW and an in-motion charging power of 80 kW. The plug-in stationary charging power is assumed to be 350 kW. We also assume the setup time for stationary chargers is 3.5 minutes for plug-in and 0.5 minutes for wireless. We assume that the buses have access to chargers at the depot for overnight charging and, therefore, start their service with a fully charged battery.

The cost of building stationary or wireless chargers in various locations can depend on factors such as grid network properties and pavement repair schedules. In the absence of access to this information, we assume that the cost of building stationary chargers is uniform across all stops and is considerably lower than that of building in-motion chargers. Additionally, we assume that the cost of building in-motion chargers is the same across all segments.

Table 10: Feasible blocks and charger configurations for different transit agencies.

Transit agency	City	Number of blocks	No charger	Stationary plug-in charger only		Stationary wireless charger only		Stationary and in-motion wireless chargers		
			Number of feasible blocks	Number of feasible blocks	Number of chargers	Number of feasible blocks	Number of chargers	Number of feasible blocks	Number of stationary chargers	Length of in-motion charger [mi]
BATA	Traverse City	28	13	28	10	28	11	28	11	0
CATA	Lansing	88	23	78	6	85	8	88	9	40.6
DDOT	Detroit	329	205	322	18	323	22	329	22	31.6
MAX	Holland	8	0	8	1	8	1	8	1	0
METRO	Kalama-zoo	26	3	22	3	22	4	26	9	7.6
Smart	Detroit	332	130	331	27	331	31	332	31	1.7
The Rapid	Grand Rapids	112	21	110	7	112	9	112	9	0
The Ride	Ann Arbor-Ypsilanti	98	33	43	2	75	8	98	15	14.6

Since the web app is publicly accessible, we did not perform a sensitivity analysis but considered a relaxed model version where some blocks cannot be electrified without in-motion wireless chargers. To achieve this, we relax constraints (59) by defining a new binary decision variable u_b, which equals 1 if the constraints are violated, and include it as a penalty term in the objective function. Hence, the modified objective function and constraints are:

$$min\, Z = \sum_i c_i \cdot x_i + \sum_k c_k \cdot y_k + \sum_b M \cdot u_b \tag{52.a}$$

$$s^k_{b,r} \geq -M \cdot u_b \qquad \forall b \in \mathcal{B}, r \in \mathcal{R}_b, k \in \mathcal{K}_r \tag{59.a}$$

where M is a sufficiently large number. Table 10 shows the results for 8 major urban transit agencies in Michigan.

The third column presents the total number of blocks operated by each transit agency. Generally, the agency's fleet size matches the number of blocks, along with a few extra vehicles reserved for maintenance and training purposes. The fourth column presents the number of blocks with distances shorter than the bus range, allowing them to be covered by electric buses without needing to charge during their schedule. The fifth and sixth columns present results for scenarios with only plug-in stationary chargers. Due to the penalty for infeasible blocks being much higher than the cost of adding plug-in chargers at stops, the model finds the minimum number of stops needed to enable most blocks, taking into consideration the blocks schedules and charger properties. This means buses need to wait at a stop longer than the plug-in charger setup time of 3.5 minutes, and the recharged energy must make at least one block feasible for selection. The seventh and eighth columns show results for when only stationary wireless chargers are used, which have a shorter setup time and lower power output. Finally, the last three columns

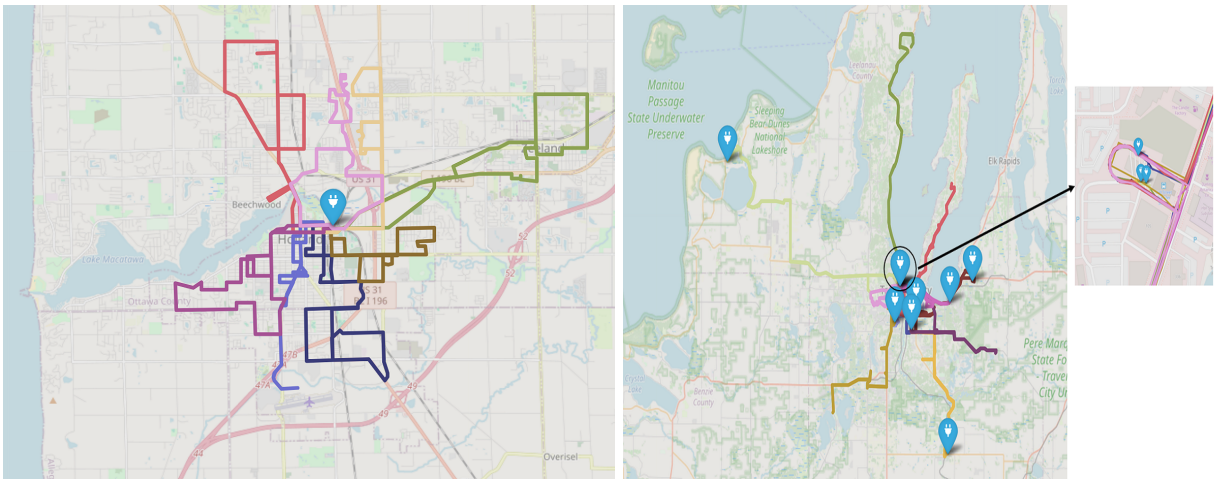

(a) MAX transit agency. (b) BATA tranist agency.

Figure 14: The optimal location of stationary plug-in chargers.

illustrate the results from using both stationary and in-motion wireless chargers. Here, all blocks become feasible by implementing in-motion wireless chargers, and the last column provides the length of the necessary in-motion wireless track in miles.

The selected transit agencies encompass a variety of scenarios, from smaller agencies like MAX in Holland, which has 8 blocks, to larger ones like DDOT and SMART in Detroit and the surrounding metropolitan area, with over 300 blocks. None of the chosen agencies can fully electrify their fleets without additional chargers, as indicated in the fourth column. The number of blocks with distances less than 100 miles ranges from 0 out of 8 blocks in Holland to 205 out of 329 blocks for DDOT in Detroit. We can see that all 8 blocks of the MAX transit agency can be electrified by adding a stationary plug-in charger at a single location, as shown in Figure 14a. Similarly, all 28 blocks of BATA in Traverse City can be electrified with plug-in chargers installed at 10 locations, as shown in Figure 14b. For other agencies, using only plug-in chargers can enhance the number of feasible blocks. For instance, in SMART, only 1 out of 332 blocks remain infeasible with installing plug-in chargers in 27 locations.

Similarly, different scenarios emerge among the agencies when we consider only stationary wireless chargers. For the MAX transit agency, the number and placement of chargers remain unchanged in comparison to plug-in charger. However, BATA and SMART require more chargers to achieve the same number of feasible blocks compared to using plug-in chargers, due to the lower charging power of wireless chargers. In other agencies, stationary wireless chargers can increase the number of feasible blocks. For example, The Rapid can electrify all blocks by installing stationary wireless chargers at

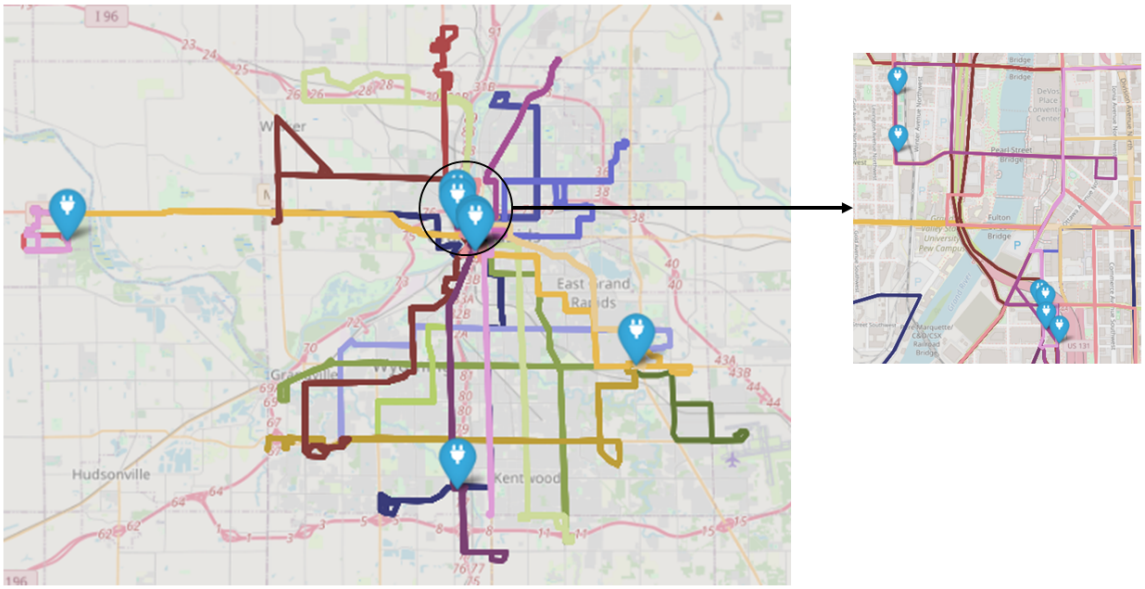

Figure 15: The optimal location of stationary wireless chargers for The Rapid transit agency.

9 locations, as shown in Figure 15, due to the reduced setup time of wireless chargers compared to plug-in chargers.

Finally, with a combination of stationary and in-motion wireless chargers, all agencies are able to electrify their blocks using 100-mile range buses without modifying their operations. For instance, the SMART agency, which could electrify 331 blocks with either 27 stationary plug-in chargers or 31 stationary wireless chargers, requires 1.7 miles of in-motion wireless track to accommodate the remaining 1 block. The CATA and DDOT agencies require in-motion wireless tracks of 40.6 miles and 31.6 miles, respectively. These agencies have blocks characterized by long routes and tight schedules, necessitating the installation of in-motion wireless tracks along nearly the entire length of these routes. Figures 16a and 16b shows the location of stationary and in-motion wireless chargers for these agencies.

4.4 Intercity Highway Network

We received the roadway network and OD demand matrices for automobiles, single-unit trucks, and multi-unit trucks from the Michigan Department of Transportation (MDOT). The provided network is highly detailed within Michigan, including lower-class facilities (e.g., local roads), whereas the representation outside Michigan is intentionally sparse

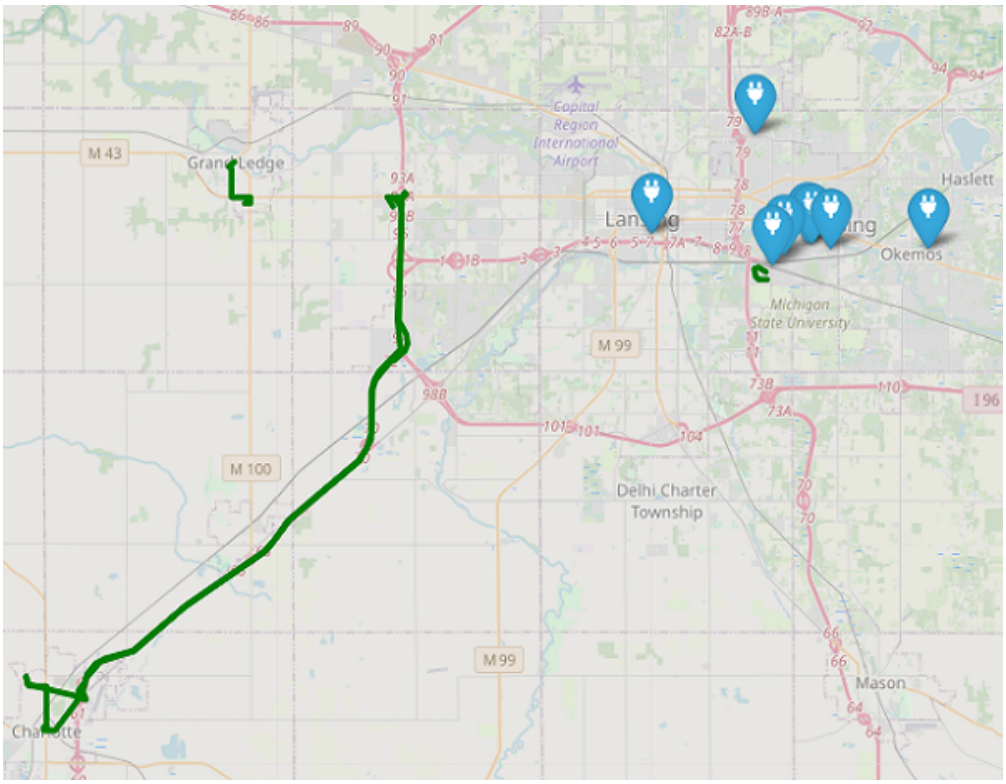

(a) CATA transit agency.

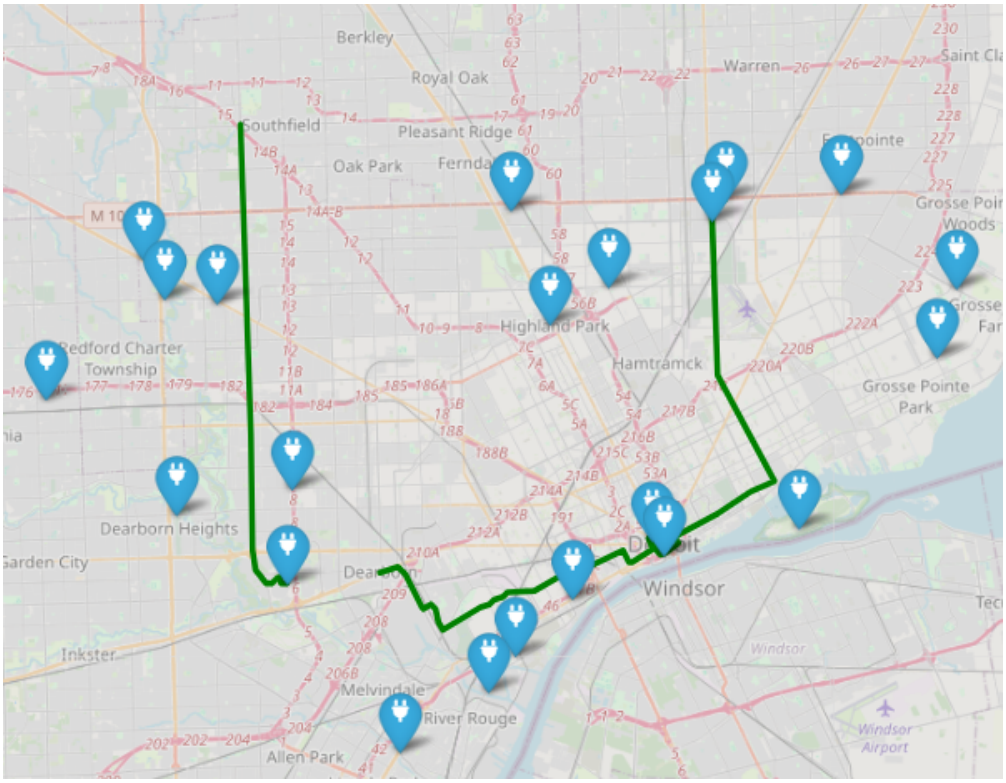

(b) DDOT transit agency.

Figure 16: The optimal location of stationary and in-motion wireless chargers.

and largely limited to major arterials that connect Michigan to the rest of US and Canada. Figures 17 illustrates this contrast: Michigan appears as a dense mesh, while the out-of-state network primarily preserves long-distance connectivity. In addition, Figure 18 shows the zoomed view of all links inside Michigan.

Figure 17: Full network.

Because the objective of this study is to evaluate charging-related infrastructure on corridors most relevant to intercity travel, we restrict the scope to the state of Michigan and retain only major arterial links. This filtering step substantially improves computational tractability. The resulting analysis network is shown in Figure 19; the retained links form a statewide backbone that connects major activity centers and principal corridors in both peninsulas.

In the original MDOT OD dataset, origins and destinations may be placed on any roadway class, including links that are removed during filtering. To ensure that every OD pair remains connected on the analysis network, we aggregate demand to the county level and represent each county by a node that lies on the modified network and is chosen to be representative of the county's spatial center. Practically, this is implemented by mapping each county to a feasible analysis-network node (e.g., the node closest to the county

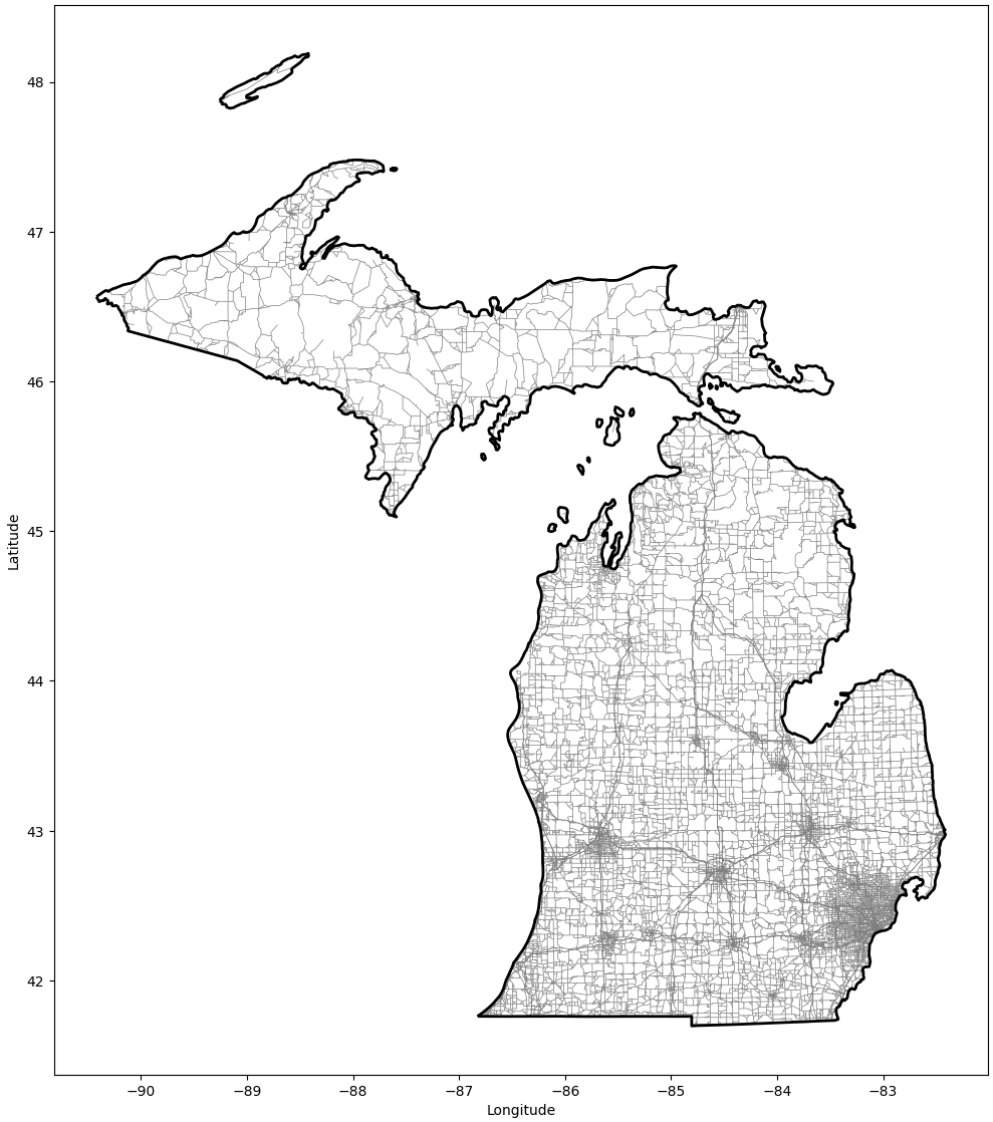

Figure 18: Zoomed view over Michigan.

centroid) and then summing OD flows by county-to-county pair and vehicle class.

During aggregation, OD pairs shorter than 20 miles (measured on the original network) are excluded. The rationale is that short trips are more likely to be served by local roads that were removed from the analysis network and are also less likely to require en-route fast charging or in-motion charging to complete the trip. For the remaining trips, we assume vehicles begin with an initial state of charge equal to 85 percent of battery capacity to account for access travel from the original OD location to the county representative node. We further enforce a minimum reserve range of 10 miles to avoid solutions that rely on complete battery depletion. Figure 20 visualizes the resulting county-level OD structure. The straight lines are plotted for visualization only to show the spatial distribution of OD

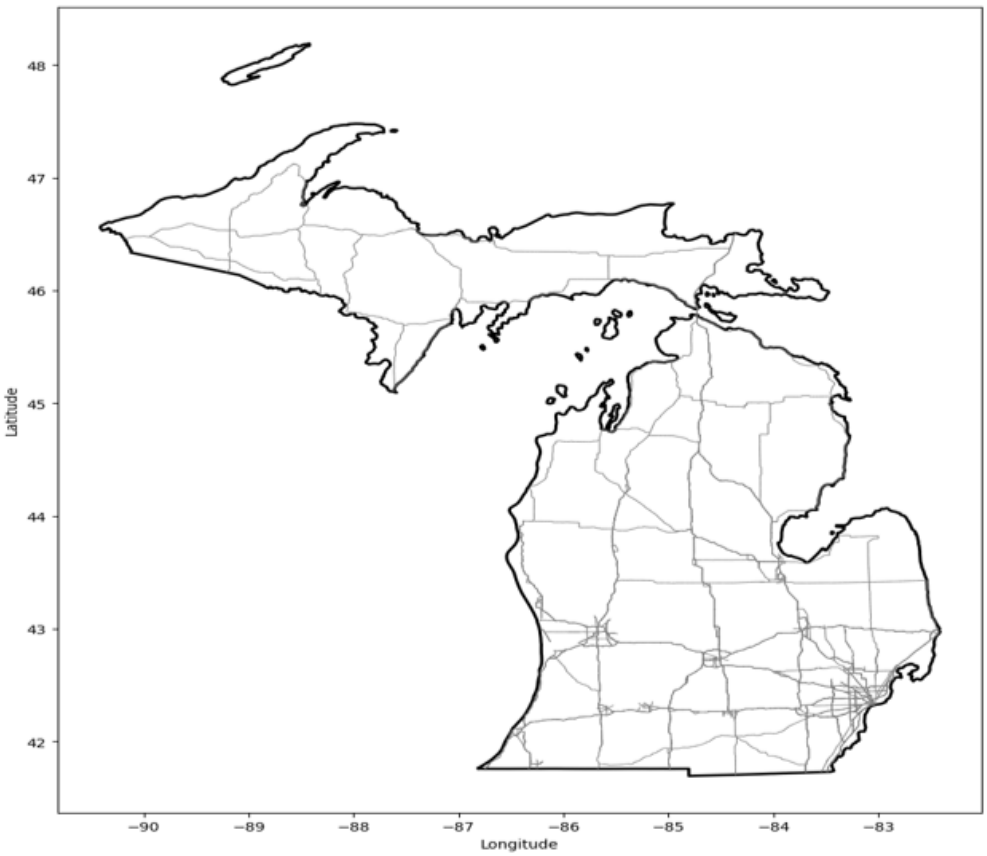

Figure 19: Modified Michigan network used for assignment and infrastructure optimization .

connections and do not count for routing and costs which will be computed along network paths.

To verify that the reduced network and aggregated OD set provide a reasonable representation of system usage patterns, we computed a user equilibrium (UE) traffic assignment on the modified network without taking into account the driving range of the vehicles. The resulting UE conditions provide a consistency check that major corridors attract flow in expected ways under the reduced representation. Figures 21a and 21b report the UE link speeds and volume-to-capacity (V/C) ratios, respectively. Broadly, the results exhibit higher speeds on uncongested links and lower speeds (with correspondingly higher V/C ratios) on major commuter/freight corridors, consistent with expected travel patterns on Michigan's arterial backbone.

We incorporate existing public DC fast-charging stations (Level 3) obtained from the U.S. Department of Energy's Alternative Fuels Data Center. Each station is mapped to the analysis network by adding connector links as needed so that chargers are reachable from the retained arterial links. Level 1 and Level 2 chargers are excluded because their

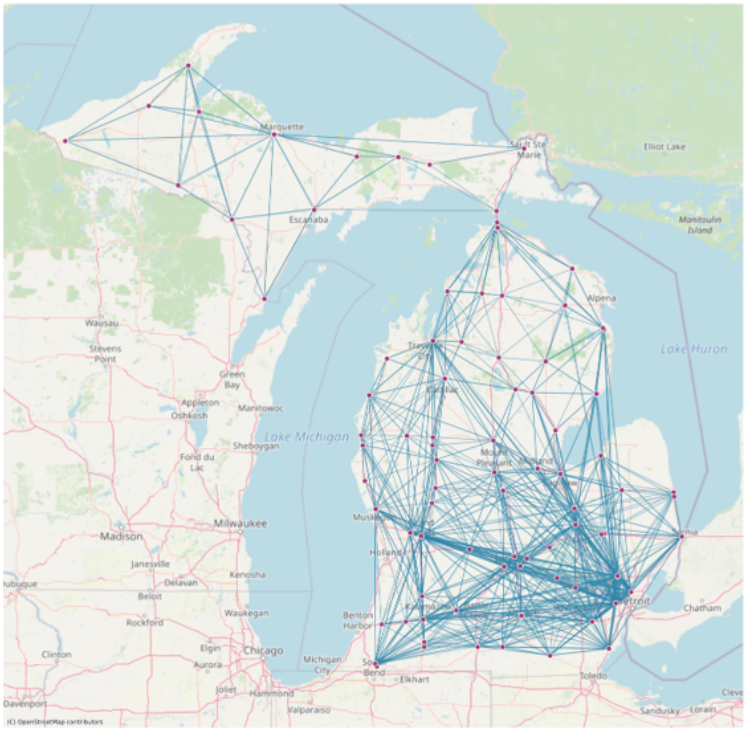

Figure 20: County-level OD representation after aggregation and exclusion of short trips. Straight lines indicate OD connections for visualization.

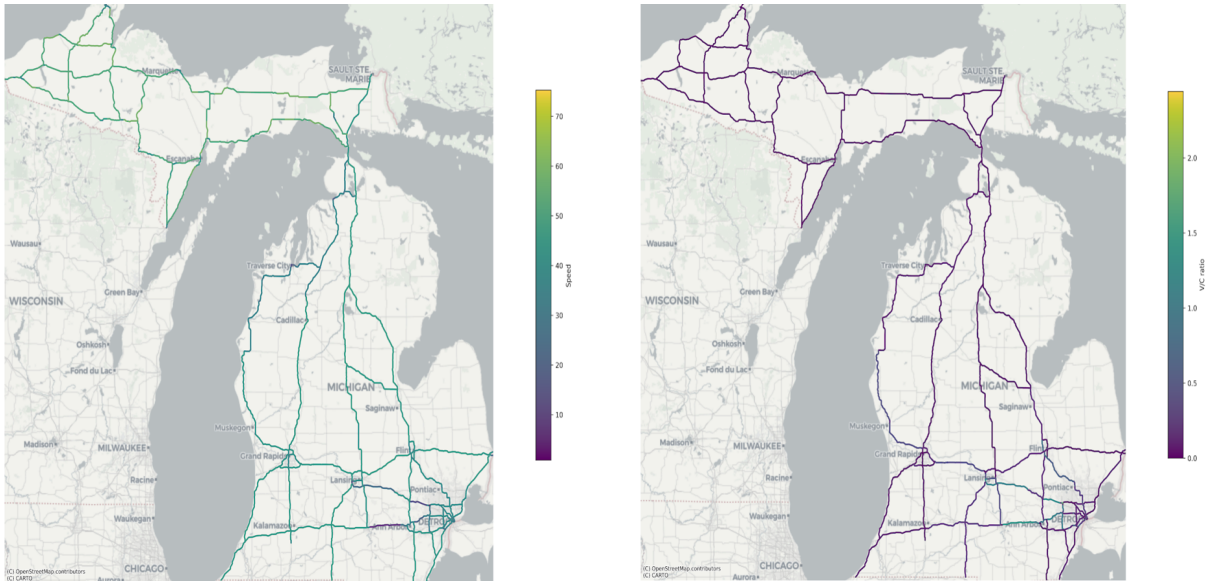

(a) (b)

Figure 21: User equilibrium (a) speed and (b) V/C ratio conditions on the modified network.

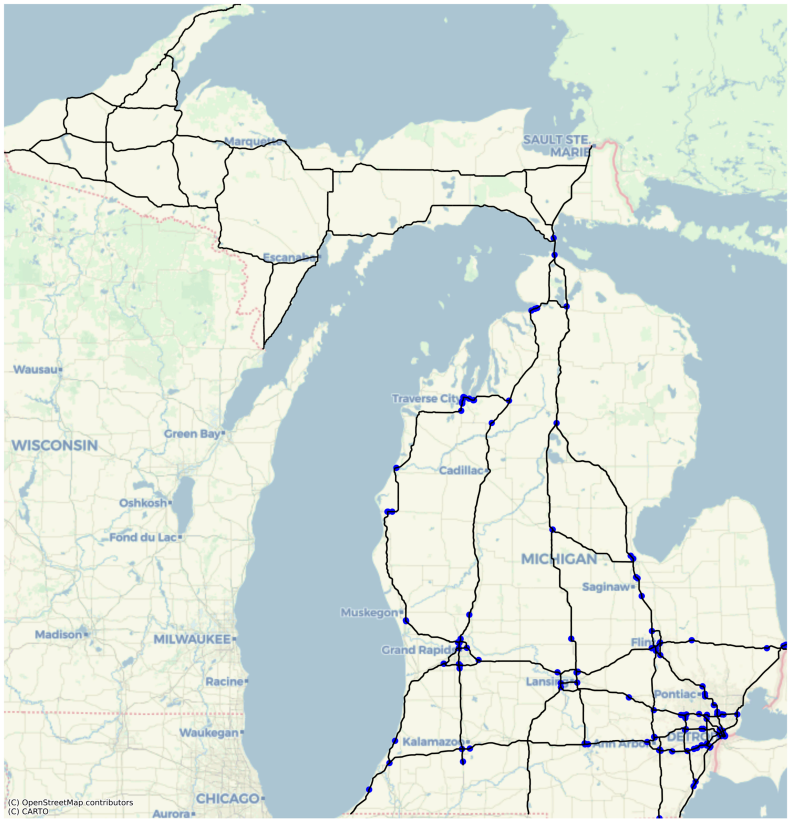

Figure 22: Public DC fast chargers (blue dots) mapped to the modified network (black links).

charging rates are not intended for typical en-route recharging over intercity travel. Figure 22 shows the resulting DC fast charger set overlaid on the modified network. The spatial distribution is non-uniform, with substantial clustering in urbanized areas and along major corridors, which is important for interpreting when wireless charging complements versus substitutes for stationary charging.

Finally, we solve the optimization model in Section 3.4.5 under three budget levels ($50M, $100M, and $200M) and three in-motion wireless charging power levels (25, 50, and 100 kW). In the following figures, regular arterial links are shown in black, selected IVC lane segments are highlighted in green, and existing DC fast chargers are shown as blue points.

For power levels of 25 kW and 50 kW, the optimal IVC investment under $50M and $100M budgets is identical, and the model uses only $5.2M. As shown in Figures 23a and 23b, the selected infrastructure is a short segment near the Grand Rapids area. This outcome indicates that, under low charging power, many candidate IVC investments yield limited marginal reductions in generalized user cost; therefore, the model concentrates

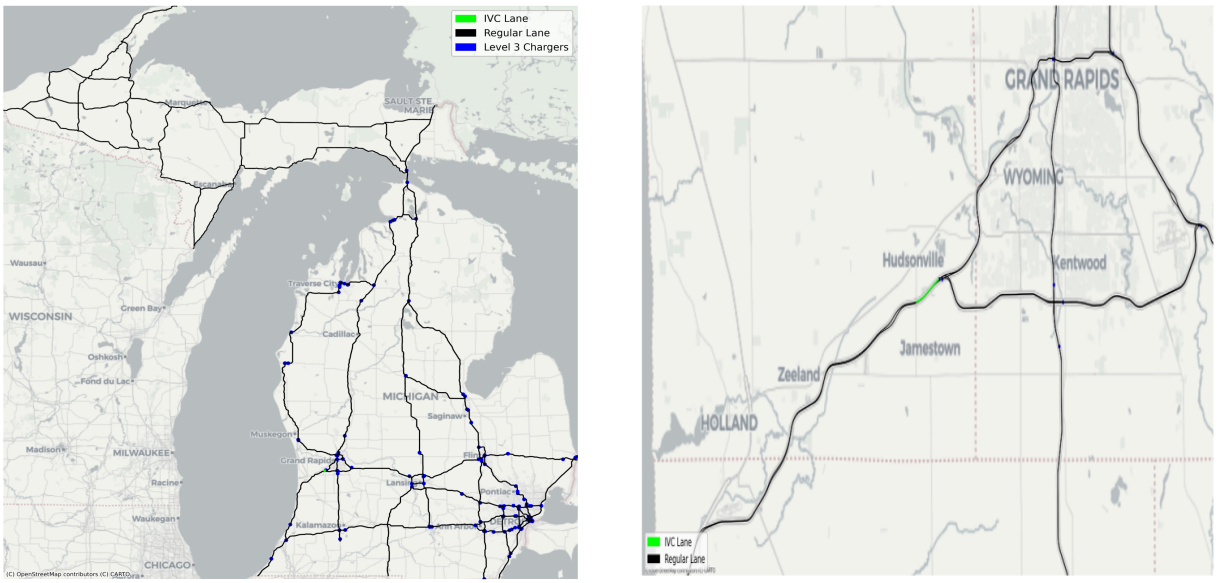

(a) Statewide view.

(b) Zoom view.

Figure 23: Optimal IVC lane placement under low-power charging (25 and 50 kW) and moderate budgets ($50M and $100M).

on a location where even a short electrified segment can extend effective range for some itineraries and reduce the need for an additional stationary charging stop.

When the available budget increases to $200M (still at 25 kW or 50 kW), the model selects substantially more IVC links, concentrated in Wayne County (Figure 24), and uses approximately $175M. This shift is consistent with the high density of demand to/from the Detroit metropolitan area. IVC segments on heavily used corridors can provide meaningful time and inconvenience savings by enabling additional energy intake without stopping, even in a region that already has many fast chargers.

At 100 kW, the model finds cost-effective IVC investments even at $50M and $100M budgets, using approximately $43M. Figures 25a and 25b show that selected links again appear near Grand Rapids, indicating that higher power increases the per-mile energy benefit of IVC segments and makes deployment attractive on fewer, shorter corridors. These IVC segments complement the existing fast-charging network by reducing reliance on dwell-time-intensive stops for some trips.

When the budget increases to $200M, the 100 kW solution shifts toward the same southeast Michigan (Wayne County) investment pattern observed under low-power charging with $200M, reflecting that high-demand corridors dominate the marginal benefits once sufficient funds are available to electrify multiple links.

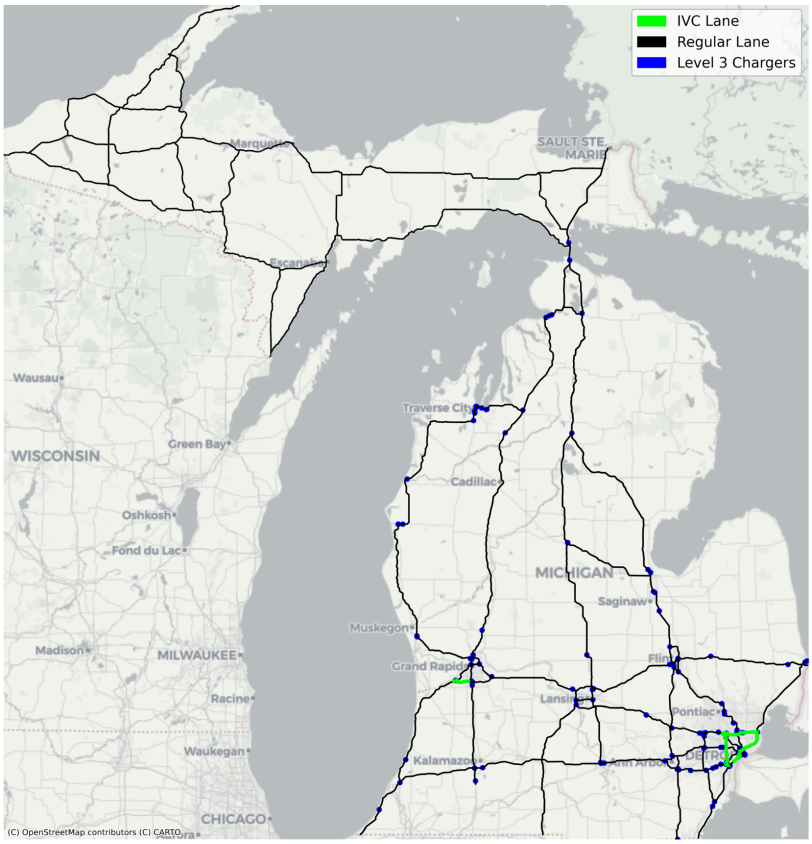

Figure 24: Optimal IVC lane placement for 25, 50, and 100 kW under the $200M budget.

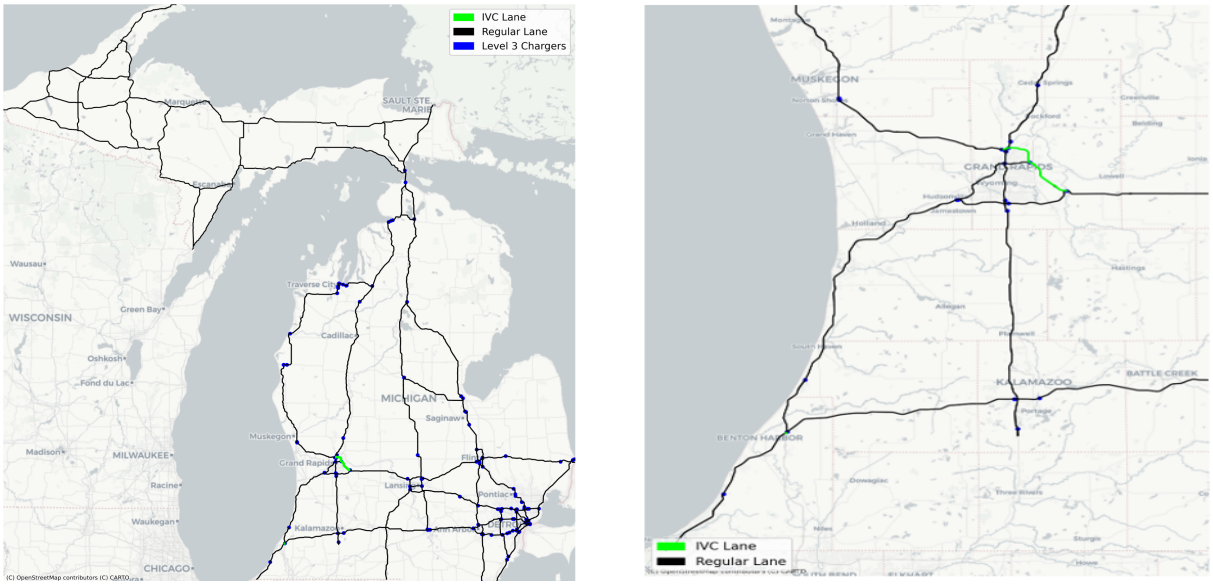

(a) Statewide view. (b) Zoom view.

Figure 25: Optimal IVC lane placement under higher-power charging (100 kW) and moderate budgets.

4.5 Key Takeaways

This section applies the methodological frameworks established earlier to conduct concrete numerical studies and real-world validations, yielding critical insights into the comparative performance of conductive and inductive charging technologies. The key takeaways from our findings are as follows:

Our numerical studies reveal distinct, boundary-defining operational domains for each charging infrastructure. Most importantly, WCL is substantially more cost-effective in environments characterized by high traffic density and high fleet utilization (such as commercial or autonomous operations), while CS remains economically superior for low-density and low-utilization networks.

For single, long-distance trips utilizing light-duty EVs, numerical evaluations show that in-motion charging yields relatively modest time savings averaging just 18.4 minutes across the evaluated regional routes in Michigan. This limited temporal benefit occurs because the required charging periods frequently overlap with natural driver rest breaks, effectively neutralizing the time-saving advantage of continuous charging for casual passenger travel.

To bridge the gap between theory and implementation, we developed a publicly accessible web application that uses real-world GTFS data to optimize infrastructure for transit agencies. The tool allows policymakers to determine the optimal number and placement of varying technologies, evaluating the trade-offs between stationary and in-motion wireless segments across transit routes. Our analyses of major Michigan urban transit agencies indicate that even stationary wireless chargers allow buses to recharge during brief stops for passenger boarding and alighting, enabling the electrification of transit buses without requiring schedule changes or fleet size increases.

The State of Michigan road network analysis demonstrated how in-motion charging can complement existing fast chargers. We found that optimal deployment is highly sensitive to wireless power capacity and available budget; for example, under a $200 million budget at 100 kW charging power, investments optimally shift to high-demand corridors (e.g., Southeast Michigan) to maximize the per-mile energy benefit and reduce travel time due to stationary charging stops.

5 Discussion

The results presented in this study offer a multi-faceted evaluation of IVC technology, clarifying its role within the broader ecosystem of transportation electrification. By analyzing

both transit and intercity highway use cases, we identified distinct mechanisms through which IVC generates value, validating our initial hypotheses regarding range anxiety mitigation (H1) and the existence of high impact locations (H3).

In the context of public transit, the analysis confirms that while stationary plug-in chargers are sufficient for smaller agencies with shorter blocks, they fail to support the full electrification of larger, more complex systems without disrupting existing schedules. For agencies such as DDOT and SMART, the dwell time required for plug-in charging often exceeds the available operational windows. In contrast, IVC, particularly in-motion charging, decouples energy transfer from vehicle dwell time. This finding supports Hypothesis 2 (H2), demonstrating that current or near-future IVC specifications (e.g., 80–100 kW dynamic transfer) are technically sufficient to enable operations that are otherwise infeasible under stationary (both plug-in and wireless) strategy. The trade-off, however, lies in capital investment; while in-motion infrastructure ensures 100% block feasibility, it requires significantly higher upfront costs compared to stationary solutions. This suggests that a hybrid approach, prioritizing stationary wireless chargers at high-frequency stops and reserving in-motion segments for the most demanding routes, may offer the optimal balance between cost and operational continuity.

For the intercity highway network, our macroscopic models reveal that IVC optimal placement is a complement to, rather than a replacement for the DC fast-charging network. The sensitivity analysis indicates that the value of IVC is highly dependent on power transfer levels and available budget. At lower budget levels, deployment is scattered and less effective at offsetting the time costs of stopping. However, at higher investment budget, the optimal deployment shifts decisively toward high-density corridors, such as those surrounding Wayne County. This shift occurs because of higher budget levels, allowing longer wireless lane segments which provides meaningful range extension. This also validates the high impact locations (H3), showing that targeted investments in specific high-volume links can yield disproportionate benefits in reducing network-wide travel time and range anxiety.

Furthermore, the economic comparison emphasizes that IVC's competitiveness is intrinsically linked to EV utilization and traffic density. Unlike personal EVs, which may sit idle for long periods, commercial and transit fleets with high utilization rates amortize the infrastructure cost more effectively. Consequently, the immediate pathway for IVC adoption in Michigan appears to be through shared, high-utilization assets such as transit systems where the technology's ability to minimize downtime translates directly into economic value.

6 Conclusions

This project sets out to evaluate the efficacy, optimal placement, and economic viability of IVC technology within the State of Michigan. Through a combination of literature review, stakeholder engagement, and rigorous mathematical modeling, we have developed a comprehensive framework for identifying high-impact use cases for this emerging technology.

The findings of this study position IVC not as a universal solution, but as a specific tool within a rapidly evolving electrification landscape. Public transit represents the most immediate and viable use case for IVC because buses operate on fixed routes, allowing for consistent utilization of installed infrastructure. Our analysis of Michigan major urban transit agencies reveals a clear operational divide. Smaller agencies can typically electrify their entire systems using plug-in charging or stationary IVC at terminals and stops without disrupting operations. However, for larger urban agencies (e.g., DDOT, SMART), current schedules often exceed the range and dwell-time capabilities of standard electric buses. For these larger networks, agencies must choose between: (1) increasing fleet size to allow for rotation and charging downtime, (2) altering service schedules to accommodate longer dwell times, or (3) deploying in-motion IVC to charge while driving for full electrification of their system. The optimal decision is strictly economic, balancing the capital cost of IVC construction against the recurring labor and capital costs of expanding the fleet, or changing the service. To assist in this complex decision-making process, this project developed a web-based application that allows agencies to simulate these scenarios and identify the most cost-effective strategy for their specific routes.

For intercity travel, the benefits of IVC are more constrained. With the increasing range of modern EVs and the necessity for drivers to rest during long trips, the time and distance savings provided by IVC for any single individual trip are limited. However, our optimal placement model indicates that the optimal implementation for dynamic charging is on major arterials with high traffic flow. These corridors offer two distinct advantages: first, the high volume of vehicles extends the infrastructure's benefit to a larger user base; second, the characteristically lower speeds on these arterials result in longer travel times over the charging segments. This increases the total energy transferred per vehicle pass, maximizing the utility of the wireless charging.

Finally, it is critical to contextualize these findings within the broader scope of ongoing battery research and development. Significant effort is currently focused on improving battery chemistry to increase charging speeds to match the refueling time of internal combustion vehicles (Liu et al., 2025; Pan et al., 2025). If ultra-fast charging becomes ubiq-

uitous and comparable to gas station refueling, the necessity for charging while driving would largely diminish. Therefore, IVC should be viewed as a bridging technology or a specialized solution for high-utilization fleets, rather than a permanent requirement for all electric mobility.

Based on our findings, we recommend a targeted deployment strategy for wireless charging in the State of Michigan that initially prioritizes Southeast Michigan to support transit agencies like DDOT. Embedding this infrastructure into public roadways guarantees immediate and consistent utilization by transit fleets. Crucially, this transit-first approach lays the groundwork for broader adoption, allowing commercial and private vehicle owners the time to gradually integrate wireless charging receivers into their vehicles. Furthermore, focusing on Southeast Michigan aligns with the optimal deployment locations identified in our statewide network analysis.

7 References

Aghassi, M., Bertsimas, D., Perakis, G., 2006. Solving asymmetric variational inequalities via convex optimization. Operations Research Letters 34, 481–490.

Ahmad, A., Alam, M.S., Chabaan, R., 2017. A comprehensive review of wireless charging technologies for electric vehicles. IEEE transactions on transportation electrification 4, 38–63.

Alternative Fuels Data Center, 2023. Alternative Fueling Station Counts by State. URL: https://afdc.energy.gov/stations/states.

Bahrami, S., Aashtiani, H.Z., Nourinejad, M., Roorda, M.J., 2017. A complementarity equilibrium model for electric vehicles with charging. International Journal of Transportation Science and Technology 6, 255–271.

Bahrami, S., Nourinejad, M., Amirjamshidi, G., Roorda, M.J., 2020. The plugin hybrid electric vehicle routing problem: A power-management strategy model. Transportation Research Part C: Emerging Technologies 111, 318–333.

Bosshard, R., Kolar, J.W., 2016. Inductive power transfer for electric vehicle charging: Technical challenges and tradeoffs. IEEE Power Electronics Magazine 3, 22–30.

BRTdata, ., 2025. The global brt data database. https://brtdata.org/. Accessed: 2025-10-01.

Charge up Michigan Program, 2023. Available online at: https://www.michigan.gov/egle/about/organization/materials-management/energy/rfps-loans/charge-up-michigan-program.

Chen, Z., He, F., Yin, Y., 2016. Optimal deployment of charging lanes for electric vehicles in transportation networks. Transportation Research Part B: Methodological 91, 344–365.

Chen, Z., Liu, W., Yin, Y., 2017a. Deployment of stationary and dynamic charging infrastructure for electric vehicles along traffic corridors. Transportation Research Part C: Emerging Technologies 77, 185–206.

Chen, Z., Liu, W., Yin, Y., 2017b. Deployment of stationary and dynamic charging infrastructure for electric vehicles along traffic corridors. Transportation Research Part C: Emerging Technologies 77, 185–206.

Chen, Z., Yin, Y., Song, Z., 2018. A cost-competitiveness analysis of charging infrastructure for electric bus operations. Transportation Research Part C: Emerging Technologies 93, 351–366.

Deflorio, F., Castello, L., 2017. Dynamic charging-while-driving systems for freight delivery services with electric vehicles: Traffic and energy modelling. Transportation Research Part C: Emerging Technologies 81, 342–362.

Federal Motor Carrier Safety Administration, 2024. 49 CFR Part 395, Department of Transportation. URL: https://www.ecfr.gov/current/title-49/part-395.

Fuel Economy, 2024. US Department of Energy and US Environmental Protection Agency. URL: https://www.energy.gov/eere/vehicles/articles/fotw-1375-december-30-2024-median-ev-range-model-year-2024-reached-record.

Fuller, M., 2016. Wireless charging in california: Range, recharge, and vehicle electrification. Transportation Research Part C: Emerging Technologies 67, 343–356.

He, F., Yin, Y., Zhou, J., 2013a. Integrated pricing of roads and electricity enabled by wireless power transfer. Transportation Research Part C: Emerging Technologies 34, 1–15.

He, F., Yin, Y., Zhou, J., 2013b. Integrated pricing of roads and electricity enabled by wireless power transfer. Transportation Research Part C: Emerging Technologies 34, 1–15.

He, J., Yang, H., Tang, T.Q., Huang, H.J., 2020. Optimal deployment of wireless charging lanes considering their adverse effect on road capacity. Transportation Research Part C: Emerging Technologies 111, 171–184.

He, M., Wang, S., Zhuge, C., 2023. A data-driven large-scale micro-simulation approach to deploying and operating wireless charging lanes. Transportation Research Part D: Transport and Environment 121.

Hossain, M., Pokhrel, S., Vu, H., 2023. Efficient and private scheduling of wireless electric vehicles charging using reinforcement learning. IEEE Transactions on Intelligent Transportation Systems 24, 4089–4102.

Hwang, I., Jang, Y., Ko, Y., Lee, M., 2018. System optimization for dynamic wireless charging electric vehicles operating in a multiple-route environment. IEEE Transactions on Intelligent Transportation Systems 19, 1709–1726.

Hybrid - EV Committee, 2022. Wireless power transfer for heavy-duty electric vehicles. Technical Report. SAE International.

Hybrid - EV Committee, 2024. Wireless power transfer for light-duty plug-in/electric vehicles and alignment methodology. Technical Report. SAE International.

Iliopoulou, C., Kepaptsoglou, K., 2019. Integrated transit route network design and infrastructure planning for on-line electric vehicles. Transportation Research Part D: Transport and Environment 77, 178–197.

Jang, Y.J., 2018. Survey of the operation and system study on wireless charging electric vehicle systems. Transportation Research Part C: Emerging Technologies 95, 844–866.

Jang, Y.J., Jeong, S., Ko, Y.D., 2015. System optimization of the on-line electric vehicle operating in a closed environment. Computers & Industrial Engineering 80, 222–235.

Jeong, S., Jang, Y.J., Kum, D., 2015. Economic analysis of the dynamic charging electric vehicle. IEEE Transactions on Power Electronics 30, 6368–6377.

Ko, Y.D., Jang, Y.J., 2013. The optimal system design of the online electric vehicle utilizing wireless power transmission technology. IEEE Transactions on intelligent transportation systems 14, 1255–1265.

Ko, Y.D., Jang, Y.J., Lee, M.S., 2015. The optimal economic design of the wireless powered intelligent transportation system using genetic algorithm considering nonlinear cost function. Computers & Industrial Engineering 89, 67–79.

Lai, S., Dong, Z.Y., Qiu, J., Tao, Y., Zhao, J., Wang, G., 2024. Competitive pricing strategy for the wireless charging lane operator considering range anxiety of electric vehicle users. IEEE Transactions on Intelligent Transportation Systems .

Lee, S., Huh, J., Park, C., Choi, N.S., Cho, G.H., Rim, C.T., 2010. On-line electric vehicle using inductive power transfer system, in: 2010 IEEE Energy Conversion Congress and Exposition, IEEE. pp. 1598–1601.

Li, M.K., Yu, J.J., Ma, L., Zhang, W., 2019. Modeling and mitigating fatigue-related accident risk of taxi drivers. Accident Analysis & Prevention 123, 79–87.

Liao, X., Saeednia, M., Nogal, M., Tavasszy, L., 2024. Scaling up dynamic charging infrastructure: Significant battery cost savings. Transportation Research Part D: Transport and Environment 129, 104128.

Liu, H., Wang, D., 2017. Locating multiple types of charging facilities for battery electric vehicles. Transportation Research Part B: Methodological 103, 30–55.

Liu, H., Zou, Y., Chen, Y., Long, J., 2021. Optimal locations and electricity prices for dynamic wireless charging links of electric vehicles for sustainable transportation. Transportation Research Part E: Logistics and Transportation Review 152.

Liu, J., Pei, Y., Dong, C., He, Q., Wang, Z., 2024a. Optimizing electric bus charging infrastructure deployment under two charging modes considering seasonal differences. Transportation Letters 16, 1126–1139.

Liu, S., Wang, D.Z., Tian, Q., Lin, Y.H., 2024b. Optimal configuration of dynamic wireless charging facilities considering electric vehicle battery capacity. Transportation Research Part E: Logistics and Transportation Review 181, 103376.

Liu, Y., Shi, H., Yang, M., Wang, H., Ma, Y., Li, X., Jin, D., Ma, C., Ren, Z., Shi, X., et al., 2025. Kilogram-scale production of ultrafast-charging micro-expanded graphite anode toward high-power and long-life ah-level pouch batteries. Advanced Materials 37, e06584.

Liu, Z., Song, Z., 2017. Robust planning of dynamic wireless charging infrastructure for battery electric buses. Transportation Research Part C: Emerging Technologies 83, 77–103.

Liu, Z., Song, Z., He, Y., 2017. Optimal deployment of dynamic wireless charging facilities for an electric bus system. Transportation Research Record 2647, 100–108.

Luo, X., Fan, W., 2023. Joint design of electric bus transit service and wireless charging facilities. Transportation Research Part E: Logistics and Transportation Review 174.

Morris, C., 2015. Utah state university builds a dynamic wireless charging test track. Charged-Electric Vehicles Magazine .

Morrow, W.R., Gallagher, K.S., Collantes, G., Lee, H., 2010. Analysis of policies to reduce oil consumption and greenhouse-gas emissions from the us transportation sector. Energy Policy 38, 1305–1320.

Mouhrim, N., El Hilali Alaoui, A., Boukachour, J., 2019. Pareto efficient allocation of an in-motion wireless charging infrastructure for electric vehicles in a multipath network. International Journal of Sustainable Transportation 13, 419–432.

Mubarak, M., Üster, H., Abdelghany, K., Khodayar, M., 2021. Strategic network design and analysis for in-motion wireless charging of electric vehicles. Transportation Research Part E: Logistics and Transportation Review 145.

Nasr Esfahani, H., Liu, Z., Song, Z., 2022. Optimal pricing for bidirectional wireless charging lanes in coupled transportation and power networks. Transportation Research Part C: Emerging Technologies 135.

Ngo, H., Kumar, A., Mishra, S., 2020. Optimal positioning of dynamic wireless charging infrastructure in a road network for battery electric vehicles. Transportation Research Part D: Transport and Environment 85.

Nie, Y.M., Ghamami, M., 2013. A corridor-centric approach to planning electric vehicle charging infrastructure. Transportation Research Part B: Methodological 57, 172–190.

Niroumand, R., Bahrami, S., Aashtiani, H.Z., Hajbabaie, A., 2023. Battery electric vehicles network equilibrium with flow-dependent energy consumption. Transportation Research Record 2677, 444–462.

Ouyang, K., Wang, D., 2025. Optimal operation strategies for freight transport with electric vehicles considering wireless charging lanes. Transportation Research Part E: Logistics and Transportation Review 193.

Pan, J., Sun, Z., Wu, X., Liu, T., Xing, Y., Chen, J., Xue, Z., Tang, D., Dong, X., Zhang, H., et al., 2025. Mechanically robust bismuth-embedded carbon microspheres for ultrafast charging and ultrastable sodium-ion batteries. Journal of the American Chemical Society 147, 3047–3061.

Riemann, R., Wang, D., Busch, F., 2015. Optimal location of wireless charging facilities for electric vehicles: Flow capturing location model with stochastic user equilibrium. Transportation Research Part C: Emerging Technologies 58, 1–12.

Shladover, S.E., 1992. Highway electrification and automation. UC Berkeley: California Partners for Advanced Transportation Technology .

Smart Road Gotland, 2023. Available online at: https://www.smartroadgotland.com.

State of Michigan, 2022. Whitmer announces first-in-the-u.s. wireless electric vehicle charging road system contract awarded by mdot. Available online at: https://www.michigan.gov/whitmer/news/press-releases/2022/02/01/announces-first-in-the-u-s--wireless-electric-vehicle-charging-road-system-contract-a

Suh, N.P., Cho, D.H., 2017. The on-line electric vehicle: wireless electric ground transportation systems. Springer.

Sun, X., Chen, Z., Yin, Y., 2020. Integrated planning of static and dynamic charging infrastructure for electric vehicles. Transportation Research Part D: Transport and Environment 83.

Tavakoli, R., Dede, E.M., Chou, C., Pantic, Z., 2021. Cost-efficiency optimization of ground assemblies for dynamic wireless charging of electric vehicles. IEEE Transactions on Transportation Electrification 8, 734–751.

Tran, C.Q., Keyvan-Ekbatani, M., Ngoduy, D., Watling, D., 2022. Dynamic wireless charging lanes location model in urban networks considering route choices. Transportation Research Part C: Emerging Technologies 139, 103652.

Wang, S., Li, Y., Chen, A., Zhuge, C., 2023. Electrification of a citywide bus network: A data-driven micro-simulation approach. Transportation Research Part D: Transport and Environment 116.

Wang, Y., Ma, M., Liang, S., Wang, Y., Liu, N., 2024. Optimal control strategy for electric vehicle platoons in dynamic wireless charging lane considering charge demand differences. Physica A: Statistical Mechanics and its Applications 655, 130190.

Williamson, A., Lombardi, D.A., Folkard, S., Stutts, J., Courtney, T.K., Connor, J.L., 2011. The link between fatigue and safety. Accident Analysis & Prevention 43, 498–515.

Yang, C., Lou, W., Yao, J., Xie, S., 2018. On charging scheduling optimization for a wirelessly charged electric bus system. IEEE Transactions on Intelligent Transportation Systems 19, 1814–1826.

Ye, Z., Bragin, M.A., Yu, N., Wei, R., 2024. Joint planning of dynamic wireless charging lanes and power delivery infrastructure for heavy-duty drayage trucks. Applied Energy 375, 124029.

Zhang, L., Lawphongpanich, S., Yin, Y., 2009. An active-set algorithm for discrete network design problems. Transportation and Traffic Theory 2009: Papers selected for presentation at ISTTT18 , 283–300.

8 Appendices

8.1 List of Acronyms

Acronym	Definition
BPR	Bureau of Public Roads
BRT	Bus Rapid Transit
CLL	Charging Lane Location
CS	Charging Station
DC	Direct Current
EV	Electric Vehicle
GHG	Greenhouse Gas
GTFS	General Transit Feed Specification
IIJA	Infrastructure Investment and Jobs Act
IVC	Inductive Vehicle Charging
KAIST	Korea Advanced Institute of Science and Technology
KKT	Karush-Kuhn-Tucker
MCNE	Multi-class Network Equilibrium
MDOT	Michigan Department of Transportation
NE-NLP	Network Equilibrium Non-Linear Program
NE-VI	Network Equilibrium with Variational Inequality
O-D	Origin-Destination
SAE	Society of Automotive Engineers
SOC	State of Charge
SP	Shortest Path
UE	User Equilibrium
V/C	Volume to Capacity
VMT	Vehicle Miles Traveled
WCL	Wireless Charging Lane

8.2 Proof of Proposition 1

Proof. The total minimized cost $C_s^*(P_s)$ is a piecewise function based on the two regimes defined by the critical power threshold $P_{s,\text{crit}}$ (from (24) in the main text):

$$C_s^*(P_s) = \begin{cases} C_{s,\text{perf}}(P_s) & \text{if } P_s \leq P_{s,\text{crit}} \\ C_{s,\text{econ}}(P_s) & \text{if } P_s > P_{s,\text{crit}} \end{cases} \tag{162}$$

where $C_{s,\text{perf}}(P_s) = (\hat{c}_1^s + c_2^s P_s)\left(\frac{m\beta}{P_s \rho_{\max}(1-u)}\right) + c_b n \left(\frac{l P_s \rho_{\max}(1-u)}{\theta m}\right)$ and $C_{s,\text{econ}}(P_s) = 2\sqrt{\frac{c_b n l \beta}{\theta}(\hat{c}_1^s + c_2^s P_s)}$. We analyze each piece to find the global minimum.

(1) Analysis of the Economics-Driven Regime ($P_s > P_{s,\text{crit}}$)

The cost function in this regime, $C_{s,\text{econ}}(P_s)$, is strictly increasing with respect to P_s since its derivative is always positive. Therefore, its minimum value on the domain $(P_{s,\text{crit}}, \infty)$ occurs at the boundary point, $P_{s,\text{crit}}$.

(2) Analysis of the Performance-Driven Regime ($P_s \leq P_{s,\text{crit}}$)

The cost function in this regime, $C_{s,\text{perf}}(P_s)$, is a convex function. To find its unconstrained minimum, we take the derivative with respect to P_s and set it to zero:

$$\frac{dC_{s,\text{perf}}}{dP_s} = -\frac{\hat{c}_1^s m \beta}{P_s^2 \rho_{\max}(1-u)} + \frac{c_b n l \rho_{\max}(1-u)}{\theta m} = 0 \tag{163}$$

Solving for P_s gives the unconstrained minimum for this piece, which we denote $P_{s,\text{perf}}^*$:

$$P_{s,\text{perf}}^* = \sqrt{\frac{\hat{c}_1^s m^2 \beta \theta}{c_b n l \rho_{\max}^2 (1-u)^2}} \tag{164}$$

(3) Consistency Check

Next, we must prove that this solution is always consistent, meaning it falls within its valid domain ($P_{s,\text{perf}}^* \leq P_{s,\text{crit}}$). This is equivalent to showing that the condition for being in the performance-driven regime, $N_{s,\text{perf}}^* \geq N_{s,\text{econ}}^*$, holds true when evaluated at $P_{s,\text{perf}}^*$. After

squaring both sides, the condition is:

$$\frac{m^2\beta^2}{(P_s^*)^2\rho_{\max}^2(1-u)^2} \geq \frac{c_b nl\beta}{(\hat{c}_1^s + c_2^s P_s^*)\theta} \tag{165}$$

Substituting the expression for $(P_{s,\text{perf}}^*)^2$ from (164) into the left-hand side gives:

$$\frac{m^2\beta^2}{\left(\frac{\hat{c}_1^s m^2\beta\theta}{c_b nl\rho_{\max}^2(1-u)^2}\right)\rho_{\max}^2(1-u)^2} = \frac{c_b nl\beta}{\hat{c}_1^s\theta} \tag{166}$$

The inequality becomes:

$$\frac{c_b nl\beta}{\hat{c}_1^s\theta} \geq \frac{c_b nl\beta}{(\hat{c}_1^s + c_2^s P_s^*)\theta} \tag{167}$$

Since all parameters are positive, we can cancel the common term $\frac{c_b nl\beta}{\theta}$, leaving:

$$\frac{1}{\hat{c}_1^s} \geq \frac{1}{\hat{c}_1^s + c_2^s P_s^*} \quad \Longrightarrow \quad \hat{c}_1^s + c_2^s P_s^* \geq \hat{c}_1^s \quad \Longrightarrow \quad c_2^s P_s^* \geq 0 \tag{168}$$

This condition is always true, confirming that $P_{s,\text{perf}}^*$ is always a valid solution within the performance-driven regime (or on its boundary).

(4) Conclusion

Since the minimum of the performance-driven regime, $P_{s,\text{perf}}^*$, is always a valid solution within its domain, and the cost in the economics-driven regime, $C_{s,\text{econ}}(P_s)$, only increases as power moves away from the boundary point $P_{s,\text{crit}}$, the global minimum of the entire piecewise cost function $C_s^*(P_s)$ must occur at $P_{s,\text{perf}}^*$. Therefore, $P_s^* = P_{s,\text{perf}}^*$. □

8.3 Proof of Corollary 1.1

Proof. From the fully optimized static charging (CS) model, the optimal number of stations is:

$$N_s^* = \sqrt{\frac{c_b nl\beta}{\hat{c}_1^s\theta}} \tag{169}$$

The optimal station density, δ_s^*, is found by dividing by the total road length, l:

$$\delta_s^* = \frac{N_s^*}{l} = \frac{1}{l}\sqrt{\frac{c_b nl\beta}{\hat{c}_1^s\theta}} = \sqrt{\frac{c_b\beta}{\hat{c}_1^s\theta}\cdot\frac{n}{l}} \tag{170}$$

The fleet density n/l can be expressed in terms of the model's system characteristics:

$$\frac{n}{l} = \frac{(n_a/u)}{l} = \frac{(\lambda l/u)}{l} = \frac{\lambda}{u} \tag{171}$$

Substituting this back into the expression for station density yields the final, scale-independent form:

$$\delta_s^* = \sqrt{\frac{c_b \beta \lambda}{\hat{c}_1^s \theta u}} \tag{172}$$

The resulting expression for δ_s^* is independent of the parameters L and m. □

8.4 Proof of Proposition 4

Proof. We differentiate the cost functions with respect to λ:

1. Amortization Rate (Low Density): For WCL, the marginal savings from density are driven by the linear decay of the track cost:

$$\frac{\partial J_w}{\partial \lambda} \approx -\frac{c_2^w \beta}{\gamma \lambda^2} \quad \text{(Rapid Decay)} \tag{173}$$

For CS, the marginal savings come only from the square-root battery term, as the variable charger cost is constant:

$$\frac{\partial J_s}{\partial \lambda} \approx -\frac{1}{2}\lambda^{-3/2} \quad \text{(Slower Decay)} \tag{174}$$

Thus, WCL gains efficiency faster than CS as traffic grows.

2. Congestion Sensitivity (High Density): As $\lambda \to \lambda_{jam}$, speed $v \to 0$. WCL costs diverge proportionally to $\frac{1}{v}$ (affecting both infrastructure and time). CS costs also diverge, but the infrastructure component remains unaffected by speed, making the total sensitivity to congestion lower than that of WCL. □

8.5 Proof of Proposition 5

Proof. We examine the limit as utilization approaches unity ($u \to 1^-$):

1. Static System: The variable infrastructure term depends on the charging power $P_{req} \propto \frac{1}{1-u}$.

$$\lim_{u \to 1^-} J_s(u) = \text{Constant} + \lim_{u \to 1^-} \frac{c_2^s \beta}{\rho_{\max}(1-u)} = +\infty \tag{175}$$

This divergence confirms that static charging is structurally incompatible with continuous operations.

2. Wireless System: The WCL infrastructure terms depend on utilization only via fleet size scaling ($N_w \propto u^{-1/2}$ or u^{-1}), not dwell time constraints.

$$\lim_{u \to 1^-} J_w(u) = \frac{K_1(1)}{v\sqrt{\lambda}} + \cdots = \text{Finite Value} \tag{176}$$

Since the limit exists and is finite, WCL acts as an operational stabilizer for high-uptime fleets. □

8.6 Proof of Proposition 6

Proof. The indifference frontier is the set of points (λ, u) where the cost difference function $F(\lambda, u) = \bar{C}^*_{s,m} - \bar{C}^*_{w,m} = 0$. The proof proceeds in two parts: first, we prove the existence of this boundary, and second, we analyze its sensitivity to key parameters.

Part 1: Existence of the boundary

We prove the existence of the boundary by analyzing the asymptotic behavior of the continuous function $F(\lambda, u)$ at the boundaries of the operational domain.

- Behavior with respect to Traffic Density (λ):
  - As $\lambda \to 0$, the WCL cost grows faster ($O(1/\lambda)$) than the CS cost ($O(1/\sqrt{\lambda})$), thus $F \to -\infty$.
  - As $\lambda \to \lambda^-_{jam}$, the CS cost converges to a higher positive constant than the WCL cost, thus $F > 0$.

  Since F transitions from negative to positive along the λ axis for any fixed u, the Intermediate Value Theorem (IVT) guarantees a root $\lambda_{\text{crit}}(u)$ exists.

- Behavior with respect to Fleet Utilization (u):
  - As $u \to 0$, the WCL cost grows faster ($O(1/u)$) than the CS cost ($O(1/\sqrt{u})$), thus $F \to -\infty$.
  - As $u \to 1$, the CS cost approaches infinity while the WCL cost remains finite, thus $F \to +\infty$.

Since F transitions from negative to positive along the u axis for any fixed λ, the IVT guarantees a root $u_{\text{crit}}(\lambda)$ exists.

The existence of these roots for any given λ or u confirms that a continuous boundary must exist.

Part 2: Sensitivity of the boundary

By the Implicit Function Theorem, the sensitivity of a critical point (e.g., λ_{crit}) to a change in any parameter p_i is given by:

$$\frac{\partial \lambda_{\text{crit}}}{\partial p_i} = -\frac{\partial F/\partial p_i}{\partial F/\partial \lambda} \tag{177}$$

A detailed analysis shows that at the crossover point, the denominator $\partial F/\partial \lambda$ is positive. Therefore, the sign of the sensitivity is the opposite of the sign of the numerator, $\partial F/\partial p_i$. We analyze the numerator for each parameter:

- WCL Costs (c_1^w, c_2^w): An increase in WCL costs decreases F. Thus, $\partial F/\partial c^w < 0$. The sensitivity is $\frac{\partial \lambda_{\text{crit}}}{\partial c^w} = -\frac{(-)}{(+)} > 0$, so λ_{crit} is an increasing function.
- CS Costs ($\hat{c}_1^s, c_2^s$): An increase in CS costs increases F. Thus, $\partial F/\partial c^s > 0$. The sensitivity is $\frac{\partial \lambda_{\text{crit}}}{\partial c^s} = -\frac{(+)}{(+)} < 0$, so λ_{crit} is a decreasing function.
- CS Throughput (ρ_{max}): An increase in ρ_{max} decreases C_s and therefore decreases F. Thus, $\partial F/\partial \rho_{max} < 0$. The sensitivity is $\frac{\partial \lambda_{\text{crit}}}{\partial \rho_{max}} = -\frac{(-)}{(+)} > 0$, so λ_{crit} is an increasing function.
- WCL Parameter (γ): An increase in γ decreases C_w and therefore increases F. Thus, $\partial F/\partial \gamma > 0$. The sensitivity is $\frac{\partial \lambda_{\text{crit}}}{\partial \gamma} = -\frac{(+)}{(+)} < 0$, so λ_{crit} is a decreasing function.
- Travel Time Coefficient (ω): An increase in ω increases C_s and therefore increases F. Thus, $\partial F/\partial \omega > 0$. The sensitivity is $\frac{\partial \lambda_{\text{crit}}}{\partial \omega} = -\frac{(+)}{(+)} < 0$, so λ_{crit} is a decreasing function.

A symmetrical proof using $\frac{\partial u_{\text{crit}}}{\partial p_i} = -\frac{\partial F/\partial p_i}{\partial F/\partial u}$ confirms the sensitivity trends for u_{crit}.

Part 3: Extension to the Exogenous Speed Regime (MFD Dynamics)

In the endogenous speed regime, traffic speed v is a decreasing function of density ($v'(\lambda) < 0$). This introduces non-monotonicity in the cost difference function $F(\lambda, u)$, creating a potential second root (the congestion threshold $\bar{\lambda}$) where WCL viability ends.

At this upper intersection, the cost difference curve F crosses zero from positive (viable) to negative (non-viable) as density increases. Consequently, the partial derivative of F with respect to λ generally flips sign compared to the lower bound: $\left.\frac{\partial F}{\partial \lambda}\right|_{\bar{\lambda}} < 0$.

In contrast, at the lower bound $\underline{\lambda}$, the slope is positive ($\partial F/\partial \lambda > 0$). Applying the Implicit Function Theorem to this upper bound yields:

$$\frac{\partial \bar{\lambda}}{\partial p_i} = -\frac{\partial F/\partial p_i}{\partial F/\partial \lambda} = -\frac{\partial F/\partial p_i}{(-)} \tag{178}$$

Since the denominator is now negative, the sign of the sensitivity $\frac{\partial \bar{\lambda}}{\partial p_i}$ is the *same* as the sign of the numerator $\partial F/\partial p_i$. This leads to inverse properties compared to the lower bound. For example, WCL Costs (c^w): Since $\partial F/\partial c^w < 0$, the sensitivity is $\frac{\partial \bar{\lambda}}{\partial c^w} < 0$. Thus, an increase in cost lowers the upper congestion limit ($\bar{\lambda} \downarrow$), contracting the viability region.

Conclusion: In the MFD regime, parameters that improve WCL viability expand the solution interval $[\underline{\lambda}, \bar{\lambda}]$ bilaterally: they decrease the necessary adoption threshold ($\underline{\lambda}$) while simultaneously increasing the system's resilience to congestion ($\bar{\lambda}$). □

8.7 Transit Web App Sample Report

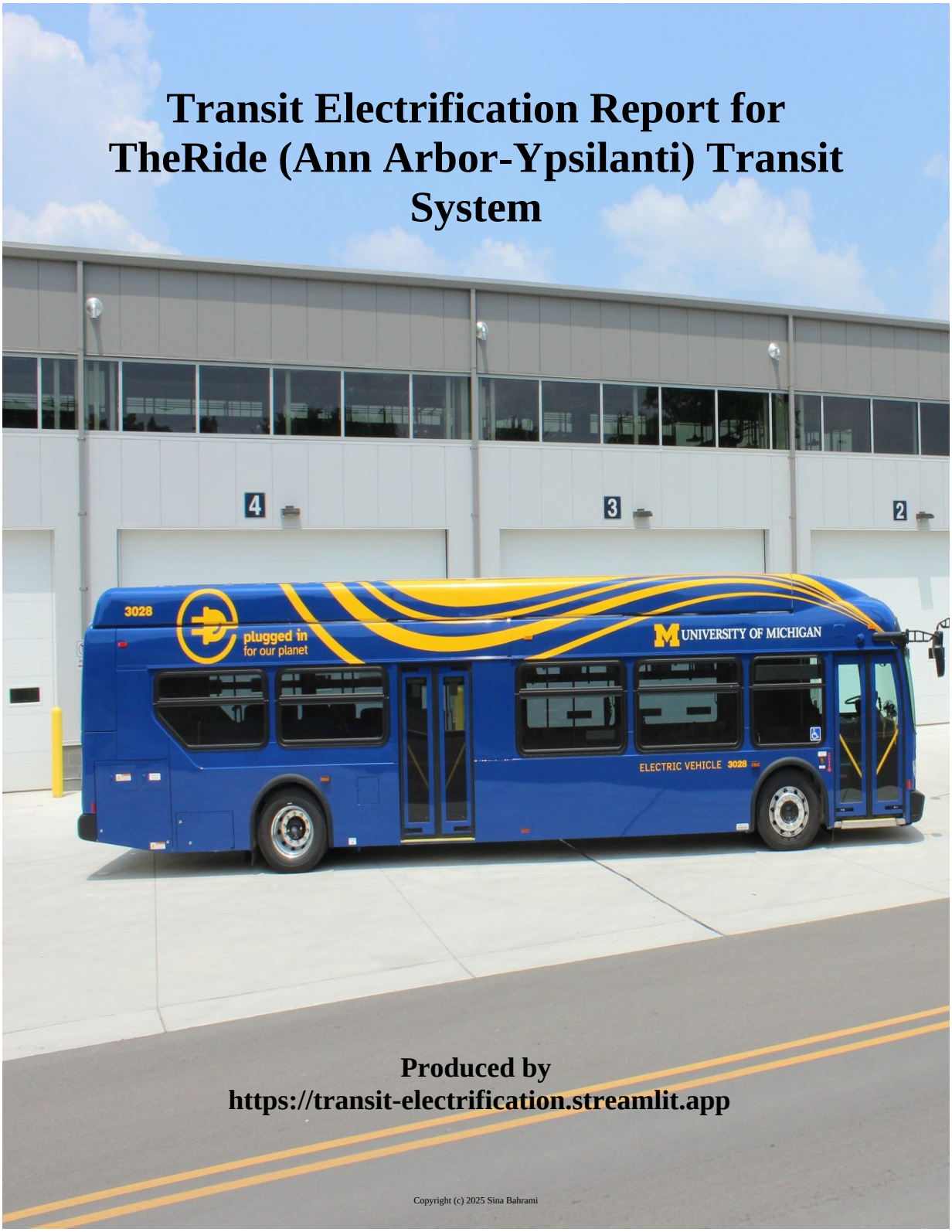

Introduction

This report provides a detailed summary of the transit electrification study for the TheRide (Ann Arbor-Ypsilanti) transit system. The system includes 31 routes, and 1116 stops. Figure 1 shows the map of the routes.

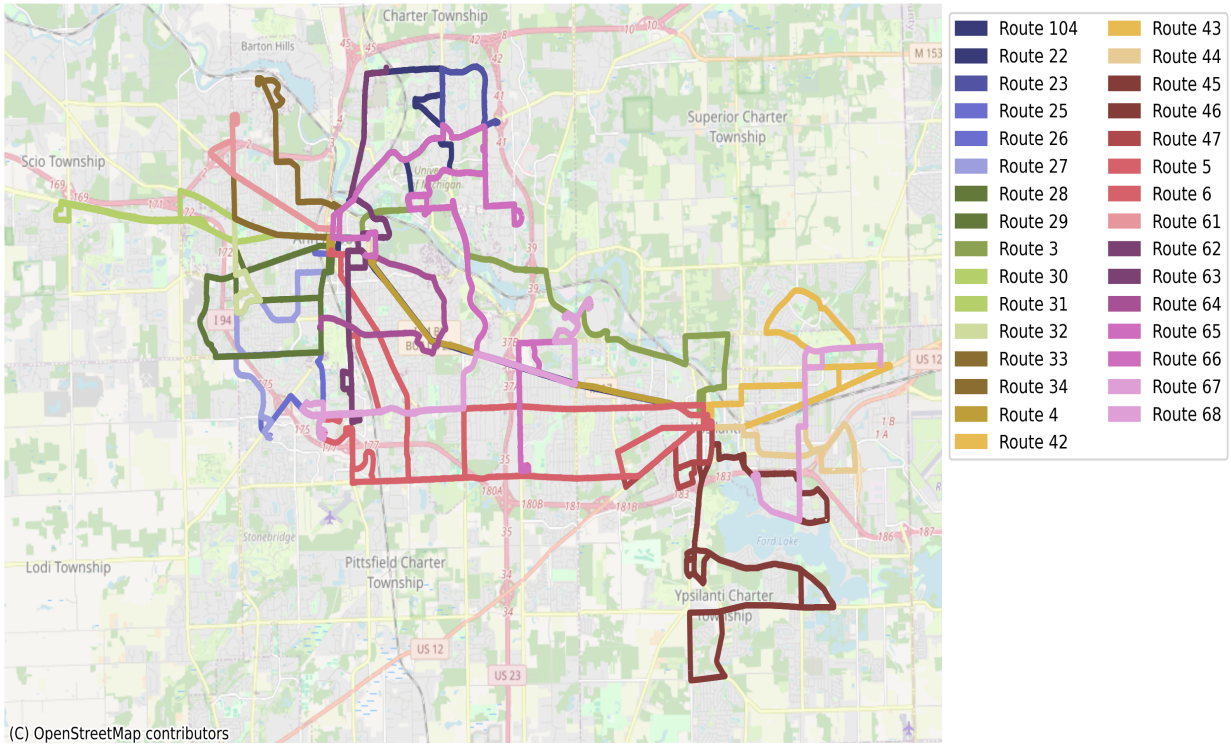

Figure 1: Map of the transit service.

The agency operates 98 blocks, each defined as a sequence of consecutive routes assigned to a single vehicle for daily operations. Table 1 provides a detailed overview of these blocks, including their total driving distances and the routes serviced within each block.

Table 1: Summary of blocks.

Block ID	Total Distance (miles)	Routes in the Block
630363	23.7	64, 63
630263	23.7	64, 63
4144	25.8	4
4164	25.8	4
270927	27.8	28, 23
630563	27.9	64, 63
630663	28.7	64, 63
270727	29.6	23, 28
271027	29.6	23, 28

Block ID	Total Distance (miles)	Routes in the Block
340134	31.3	34
260826	34.2	31, 32
4094	34.3	4
4114	34.3	4
4124	34.3	4
4134	34.3	4
630163	37.2	64, 63
630463	37.2	64, 63
340234	37.6	34
421142	38.9	44, 42, 45, 46
4044	42.8	4
4064	42.8	4
260726	43.4	26, 29
270227	43.4	28, 23
300630	46.4	30, 22, 33
421042	47.2	44, 42, 45, 46
620362	48.4	62
4024	51.5	4
300730	54.2	33, 30, 22
260426	65.1	29, 26
271427	81.3	28, 23
260926	83.9	31, 32
4174	85.8	4
4154	94.4	4
260226	103.0	31, 32
260126	115.0	32, 31
620462	115.2	62
260326	116.3	32, 31
260626	117.3	31, 32, 26
620262	121.8	62
270427	126.1	23, 28
1042104	129.0	104
1043104	129.0	104
1041104	129.0	104

Block ID	Total Distance (miles)	Routes in the Block
4074	137.3	4
4034	137.3	4
4054	137.3	4
4014	137.3	4
6016	139.9	67, 6
6066	139.9	67, 6
6056	139.9	6, 67
6096	139.9	6, 67
270327	140.0	28, 23
270627	141.7	23, 28
270127	143.3	28, 23
610461	145.8	61, 65
4084	145.9	4
300530	147.5	33, 30, 22
5025	152.5	5, 66
5015	153.5	5, 66
5075	155.3	66, 5
610261	156.0	65, 61
420342	157.7	42, 45, 46, 44
420942	161.1	3
420742	161.3	3
5055	162.4	5, 66
5095	166.8	5, 66
610161	167.0	61, 65
610361	167.0	61, 65
420142	172.8	46, 44, 42, 45
300130	174.7	30, 22, 33
6036	177.3	6
271227	178.0	27, 25
260526	180.8	26, 29
620162	182.8	62
4104	197.4	4
430143	203.1	47, 43, 68
300330	204.9	22, 33, 30

Block ID	Total Distance (miles)	Routes in the Block
270527	207.4	23, 28
270827	208.1	23, 28
6046	209.2	67, 6
300430	212.7	22, 33, 30
420642	214.5	3, 45
420842	214.5	3, 45
5045	226.3	66, 5
300230	226.9	30, 22, 33
5035	233.4	5, 66
5085	233.8	5, 66
271327	233.8	25, 27, 28
271127	235.7	27, 25, 28
6026	238.2	6, 67
5065	239.7	66, 5
6076	245.1	6
6086	245.1	6
420542	252.3	45, 46, 44, 42, 3
430243	270.8	43, 68, 47
420442	275.2	44, 42, 45, 46
430343	276.1	68, 43, 47
420242	285.6	42, 45, 46, 44

Selected Electrification Characteristics

The selected electric bus range is 120.0 miles, and buses consume 2.50 kWh per mile of travel. The selected stationary charging system is wireless, with a power output of 350 kW. Buses require 30 seconds to start charging after stopping. In addition, dynamic in-motion wireless charging is available, providing 80.0 kW of charging power.

Results

With the selected bus and charger configuration, a total of 98 blocks can be successfully electrified. To achieve the electrification of the feasible blocks, it will be necessary to install 12 stationary charging stations. In addition to the stationary chargers, 1.30 miles of dynamic wireless charging track will be required. The spatial distribution of these chargers is presented in Figure 2. Furthermore, Figure 3 illustrates the arrangement of chargers along the transit routes.

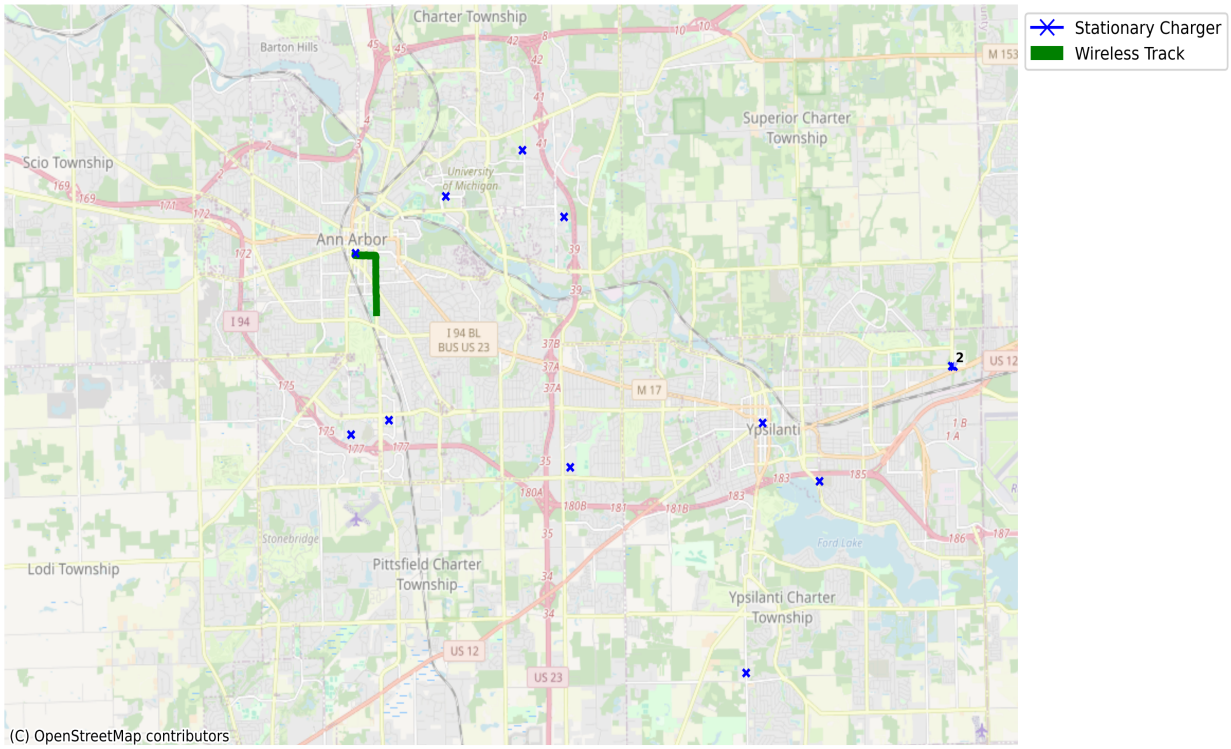

Figure 2: Spatial distribution of chargers.

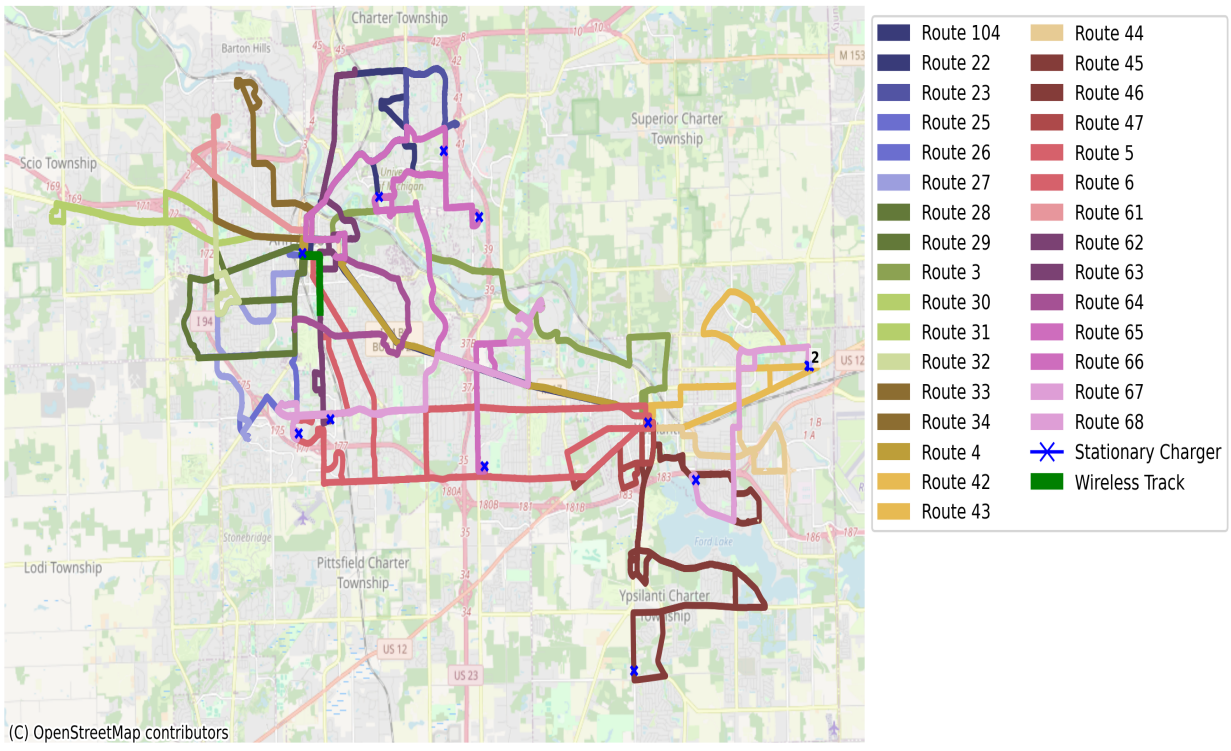

Figure 3: Arrangement of chargers along transit routes.

For each block, Table 2 presents the sequential travel distances of its routes, the time gaps between consecutive routes, and the bus range both before and after traversing each route.

Table 2: Detailed block information.

Block ID	Information	Values
630363	Route travel distances [mile]	5.0, 5.1, 4.2, 4.3, 5.0
	Stop time [min]	3.0, 0.0, 3.0, 0.0
	Bus remaining range [mile]	120.0, 115.0, 115.0, 109.9, 109.9, 105.7, 105.7, 101.4, 101.4, 96.3
630263	Route travel distances [mile]	5.1, 4.2, 4.3, 5.0, 5.1
	Stop time [min]	0.0, 3.0, 0.0, 3.0
	Bus remaining range [mile]	120.0, 114.9, 114.9, 110.7, 110.7, 106.4, 106.4, 101.4, 101.4, 96.3
4144	Route travel distances [mile]	8.6, 8.5, 8.6
	Stop time [min]	2.0, 4.0
	Bus remaining range [mile]	120.0, 111.4, 116.0, 107.5, 116.8, 108.2
4164	Route travel distances [mile]	8.6, 8.5, 8.6
	Stop time [min]	2.0, 4.0
	Bus remaining range [mile]	120.0, 111.4, 116.0, 107.5, 116.8, 108.2
270927	Route travel distances [mile]	2.7, 3.4, 7.8, 7.8, 2.7, 3.4
	Stop time [min]	0.0, 3.0, 3.0, 3.0, 0.0
	Bus remaining range [mile]	120.0, 117.3, 117.3, 113.9, 120.0, 112.2, 112.2, 104.5, 111.5, 108.9, 108.9, 105.5
630563	Route travel distances [mile]	5.1, 4.2, 4.3, 5.0, 5.1, 4.2
	Stop time [min]	0.0, 3.0, 0.0, 3.0, 0.0
	Bus remaining range [mile]	120.0, 114.9, 114.9, 110.7, 110.7, 106.4, 106.4, 101.4, 101.4, 96.3, 96.3, 92.1
630663	Route travel distances [mile]	5.0, 5.1, 4.2, 4.3, 5.0, 5.1
	Stop time [min]	3.0, 0.0, 3.0, 0.0, 3.0
	Bus remaining range [mile]	120.0, 115.0, 115.0, 109.9, 109.9, 105.7, 105.7, 101.4, 101.4, 96.3, 96.3, 91.3

Block ID	Information	Values
270727	Route travel distances [mile]	7.8, 2.7, 3.4, 7.8, 7.8
	Stop time [min]	3.0, 0.0, 3.0, 3.0
	Bus remaining range [mile]	120.0, 112.4, 119.4, 116.7, 116.7, 113.3, 120.0, 112.2, 112.2, 104.5
271027	Route travel distances [mile]	7.8, 7.8, 2.7, 3.4, 7.8
	Stop time [min]	3.0, 3.0, 0.0, 3.0
	Bus remaining range [mile]	120.0, 112.2, 112.2, 104.5, 111.5, 108.9, 108.9, 105.5, 112.5, 104.6
340134	Route travel distances [mile]	3.3, 3.0, 3.3, 3.0, 3.3, 3.0, 3.3, 3.0, 3.3, 3.0
	Stop time [min]	3.0, 0.0, 3.0, 0.0, 3.0, 0.0, 3.0, 0.0, 3.0
	Bus remaining range [mile]	120.0, 116.7, 120.0, 117.0, 117.0, 113.7, 120.0, 117.0, 117.0, 113.7, 120.0, 117.0, 117.0, 113.7, 120.0, 117.0, 117.0, 113.7, 120.0, 117.0
260826	Route travel distances [mile]	3.4, 3.7, 5.2, 4.7, 3.4, 3.7, 5.2, 4.7
	Stop time [min]	0.0, 3.0, 0.0, 3.0, 0.0, 3.0, 0.0
	Bus remaining range [mile]	120.0, 116.6, 116.6, 112.9, 119.9, 114.7, 114.7, 109.9, 116.9, 113.5, 113.5, 109.8, 116.8, 111.6, 111.6, 106.8
4094	Route travel distances [mile]	8.5, 8.6, 8.5, 8.6
	Stop time [min]	2.0, 4.0, 2.0
	Bus remaining range [mile]	120.0, 111.5, 116.1, 107.5, 116.8, 108.3, 113.0, 104.4
4114	Route travel distances [mile]	8.5, 8.6, 8.5, 8.6
	Stop time [min]	2.0, 4.0, 2.0
	Bus remaining range [mile]	120.0, 111.5, 116.1, 107.5, 116.8, 108.3, 113.0, 104.4
4124	Route travel distances [mile]	8.6, 8.5, 8.6, 8.5
	Stop time [min]	2.0, 4.0, 2.0
	Bus remaining range [mile]	120.0, 111.4, 116.0, 107.5, 116.8, 108.2, 112.9, 104.4
4134	Route travel distances [mile]	8.6, 8.5, 8.6, 8.5
	Stop time [min]	2.0, 4.0, 2.0
	Bus remaining range [mile]	120.0, 111.4, 116.0, 107.5, 116.8, 108.2, 112.9, 104.4

Block ID	Information	Values
630163	Route travel distances [mile]	5.1, 4.2, 4.3, 5.0, 5.1, 4.2, 4.3, 5.0
	Stop time [min]	0.0, 3.0, 0.0, 3.0, 0.0, 3.0, 0.0
	Bus remaining range [mile]	120.0, 114.9, 114.9, 110.7, 110.7, 106.4, 106.4, 101.4, 101.4, 96.3, 96.3, 92.1, 92.1, 87.8, 87.8, 82.8
630463	Route travel distances [mile]	5.1, 4.2, 4.3, 5.0, 5.1, 4.2, 4.3, 5.0
	Stop time [min]	0.0, 3.0, 0.0, 3.0, 0.0, 3.0, 0.0
	Bus remaining range [mile]	120.0, 114.9, 114.9, 110.7, 110.7, 106.4, 106.4, 101.4, 101.4, 96.3, 96.3, 92.1, 92.1, 87.8, 87.8, 82.8
340234	Route travel distances [mile]	3.0, 3.3, 3.0, 3.3, 3.0, 3.3, 3.0, 3.3, 3.0, 3.3, 3.0, 3.3
	Stop time [min]	0.0, 3.0, 0.0, 3.0, 0.0, 3.0, 0.0, 3.0, 0.0, 3.0, 0.0
	Bus remaining range [mile]	120.0, 117.0, 117.0, 113.7, 120.0, 117.0, 117.0, 113.7, 120.0, 117.0, 117.0, 113.7, 120.0, 117.0, 117.0, 113.7, 120.0, 117.0, 117.0, 113.7, 120.0, 117.0, 117.0, 113.7
421142	Route travel distances [mile]	4.4, 3.9, 4.6, 6.1, 4.2, 3.9, 6.2, 5.8
	Stop time [min]	0.0, 3.0, 0.0, 3.0, 0.0, 3.0, 0.0
	Bus remaining range [mile]	120.0, 115.6, 115.6, 111.8, 118.8, 114.2, 114.2, 108.1, 115.1, 111.0, 111.0, 107.1, 114.1, 107.9, 107.9, 102.1
4044	Route travel distances [mile]	8.5, 8.6, 8.5, 8.6, 8.5
	Stop time [min]	2.0, 4.0, 2.0, 4.0
	Bus remaining range [mile]	120.0, 111.5, 116.1, 107.5, 116.8, 108.3, 113.0, 104.4, 113.7, 105.2
4064	Route travel distances [mile]	8.5, 8.6, 8.5, 8.6, 8.5
	Stop time [min]	2.0, 4.0, 2.0, 4.0
	Bus remaining range [mile]	120.0, 111.5, 116.1, 107.5, 116.8, 108.3, 113.0, 104.4, 113.7, 105.2
260726	Route travel distances [mile]	4.3, 3.0, 3.1, 4.2, 4.3, 3.0, 3.1, 4.2, 4.3, 3.0, 3.1, 4.2
	Stop time [min]	0.0, 3.0, 0.0, 3.0, 0.0, 3.0, 0.0, 3.0, 0.0, 3.0, 0.0
	Bus remaining range [mile]	120.0, 115.7, 115.7, 112.9, 119.9, 116.8, 116.8, 112.6, 119.6, 115.4, 115.4, 112.5, 119.5, 116.4, 116.4, 112.2, 119.2, 115.0, 115.0, 112.1, 119.1, 116.1, 116.1, 111.9
270227	Route travel distances [mile]	2.7, 3.4, 7.8, 7.8, 2.7, 3.4, 7.8, 7.8
	Stop time [min]	0.0, 3.0, 3.0, 3.0, 0.0, 3.0, 3.0
	Bus remaining range [mile]	120.0, 117.3, 117.3, 113.9, 120.0, 112.2, 112.2, 104.5, 111.5, 108.9, 108.9, 105.5, 112.5, 104.6, 104.6, 97.0

Block ID	Information	Values
300630	Route travel distances [mile]	5.9, 5.8, 7.7, 7.5, 3.4, 4.5, 5.9, 5.8
	Stop time [min]	0.0, 3.0, 2.0, 3.0, 0.0, 3.0, 0.0
	Bus remaining range [mile]	120.0, 114.1, 114.1, 108.5, 115.5, 107.8, 112.4, 105.2, 112.2, 108.8, 108.8, 104.3, 111.3, 105.4, 105.4, 99.8
421042	Route travel distances [mile]	4.4, 3.9, 4.6, 6.1, 4.2, 3.9, 6.2, 5.8, 4.4, 3.9
	Stop time [min]	0.0, 3.0, 0.0, 3.0, 0.0, 3.0, 0.0, 3.0, 0.0
	Bus remaining range [mile]	120.0, 115.6, 115.6, 111.8, 118.8, 114.2, 114.2, 108.1, 115.1, 111.0, 111.0, 107.1, 114.1, 107.9, 107.9, 102.1, 109.1, 104.7, 104.7, 100.8
620362	Route travel distances [mile]	3.4, 3.5, 3.4, 3.5, 3.4, 3.5, 3.4, 3.5, 3.4, 3.5, 3.4, 3.5, 3.4, 3.5
	Stop time [min]	0.0, 3.0, 0.0, 3.0, 0.0, 3.0, 0.0, 3.0, 0.0, 3.0, 0.0, 3.0, 0.0
	Bus remaining range [mile]	120.0, 119.2, 119.2, 115.7, 120.0, 119.2, 119.2, 115.7, 120.0, 119.2, 119.2, 115.7, 120.0, 119.2, 119.2, 115.7, 120.0, 119.2, 119.2, 115.7, 120.0, 119.2, 119.2, 115.7, 120.0, 119.2, 119.2, 115.7
4024	Route travel distances [mile]	8.5, 8.6, 8.5, 8.6, 8.5, 8.6
	Stop time [min]	2.0, 4.0, 2.0, 4.0, 2.0
	Bus remaining range [mile]	120.0, 111.5, 116.1, 107.5, 116.8, 108.3, 113.0, 104.4, 113.7, 105.2, 109.8, 101.2
300730	Route travel distances [mile]	3.4, 4.5, 5.9, 5.8, 7.7, 7.5, 3.4, 4.5, 5.9, 5.8
	Stop time [min]	0.0, 3.0, 0.0, 3.0, 2.0, 3.0, 0.0, 3.0, 0.0
	Bus remaining range [mile]	120.0, 116.6, 116.6, 112.1, 119.1, 113.3, 113.3, 107.6, 114.6, 106.9, 111.6, 104.3, 111.3, 107.9, 107.9, 103.4, 110.4, 104.6, 104.6, 98.9
260426	Route travel distances [mile]	3.1, 4.2, 4.3, 3.0, 3.1, 4.2, 4.3, 3.0, 3.1, 4.2, 4.3, 3.0, 3.1, 4.2, 4.3, 3.0, 3.1, 4.2
	Stop time [min]	0.0, 3.0, 0.0, 3.0, 0.0, 3.0, 0.0, 3.0, 0.0, 3.0, 0.0, 3.0, 0.0, 3.0, 0.0, 3.0, 0.0
	Bus remaining range [mile]	120.0, 116.9, 116.9, 112.7, 119.7, 115.5, 115.5, 112.6, 119.6, 116.6, 116.6, 112.4, 119.4, 115.1, 115.1, 112.2, 119.2, 116.2, 116.2, 112.0, 119.0, 114.7, 114.7, 111.9, 118.9, 115.8, 115.8, 111.6, 118.6, 114.3, 114.3, 111.5, 118.5, 115.4, 115.4, 111.2
271427	Route travel distances [mile]	2.7, 3.4, 7.8, 7.8, 8.5, 8.5, 8.5, 8.5, 8.5, 8.5, 8.5
	Stop time [min]	0.0, 3.0, 3.0, 3.0, 3.0, 3.0, 3.0, 3.0, 3.0, 3.0
	Bus remaining range [mile]	120.0, 117.3, 117.3, 113.9, 120.0, 112.2, 112.2, 104.5, 111.5, 103.0, 110.0, 101.7, 108.7, 100.2, 107.2, 98.8, 105.8, 97.3, 104.3, 95.9, 102.9, 94.5

Block ID	Information	Values
260926	Route travel distances [mile]	3.4, 3.7, 5.2, 4.7, 3.4, 3.7, 5.2, 4.7, 5.2, 4.7, 5.2, 4.7, 5.2, 4.7, 5.2, 4.7
	Stop time [min]	0.0, 3.0, 0.0, 3.0, 0.0, 3.0, 0.0, 3.0, 0.0, 3.0, 0.0, 3.0, 0.0, 3.0, 0.0, 3.0
	Bus remaining range [mile]	120.0, 116.6, 116.6, 112.9, 119.9, 114.7, 114.7, 109.9, 116.9, 113.5, 113.5, 109.8, 116.8, 111.6, 111.6, 106.8, 113.8, 108.6, 108.6, 103.9, 110.9, 105.7, 105.7, 100.9, 107.9, 102.7, 102.7, 98.0, 105.0, 99.8, 99.8, 95.0, 102.0, 96.8, 96.8, 92.1
4174	Route travel distances [mile]	8.6, 8.5, 8.6, 8.5, 8.6, 8.5, 8.6, 8.5, 8.6, 8.5
	Stop time [min]	2.0, 4.0, 6.0, 4.0, 4.0, 4.0, 4.0, 4.0, 4.0
	Bus remaining range [mile]	120.0, 111.4, 116.0, 107.5, 116.8, 108.2, 120.0, 111.5, 120.0, 111.4, 120.0, 111.5, 120.0, 111.4, 120.0, 111.5, 120.0, 111.4, 120.0, 111.5
4154	Route travel distances [mile]	8.6, 8.5, 8.6, 8.5, 8.6, 8.5, 8.6, 8.5, 8.6, 8.5, 8.6
	Stop time [min]	2.0, 4.0, 0.0, 4.0, 4.0, 4.0, 4.0, 4.0, 4.0, 4.0
	Bus remaining range [mile]	120.0, 111.4, 116.0, 107.5, 116.8, 108.2, 108.2, 99.7, 109.0, 100.4, 109.7, 101.2, 110.5, 101.9, 111.2, 102.7, 112.0, 103.4, 112.7, 104.2, 113.5, 104.9
260226	Route travel distances [mile]	3.7, 5.2, 6.7, 3.4, 3.7, 5.2, 4.7, 3.4, 3.7, 5.2, 4.7, 3.4, 3.7, 5.2, 4.7, 3.4, 3.7, 5.2, 4.7, 3.4, 3.7, 5.2, 6.7
	Stop time [min]	3.0, 0.0, 3.0, 0.0, 3.0, 0.0, 3.0, 0.0, 3.0, 0.0, 3.0, 0.0, 3.0, 0.0, 3.0, 0.0, 3.0, 0.0, 3.0, 0.0, 3.0, 0.0
	Bus remaining range [mile]	120.0, 116.3, 120.0, 114.8, 114.8, 108.1, 115.1, 111.7, 111.7, 108.0, 115.0, 109.8, 109.8, 105.0, 112.0, 108.6, 108.6, 104.9, 111.9, 106.7, 106.7, 101.9, 108.9, 105.5, 105.5, 101.8, 108.8, 103.6, 103.6, 98.9, 105.9, 102.4, 102.4, 98.7, 105.7, 100.5, 100.5, 95.8, 102.8, 99.4, 99.4, 95.6, 102.6, 97.4, 97.4, 90.8
260126	Route travel distances [mile]	4.7, 3.4, 3.7, 7.2, 6.7, 3.4, 3.7, 5.2, 4.7, 3.4, 3.7, 5.2, 4.7, 3.4, 3.7, 5.2, 4.7, 3.4, 3.7, 5.2, 4.7, 3.4, 3.7, 7.2, 6.7
	Stop time [min]	3.0, 0.0, 3.0, 0.0, 3.0, 0.0, 3.0, 0.0, 3.0, 0.0, 3.0, 0.0, 3.0, 0.0, 3.0, 0.0, 3.0, 0.0, 3.0, 0.0, 3.0, 0.0, 3.0, 0.0, 3.0, 0.0
	Bus remaining range [mile]	120.0, 115.3, 120.0, 116.6, 116.6, 112.9, 119.9, 112.7, 112.7, 106.0, 113.0, 109.6, 109.6, 105.9, 112.9, 107.7, 107.7, 103.0, 110.0, 106.5, 106.5, 102.8, 109.8, 104.6, 104.6, 99.9, 106.9, 103.5, 103.5, 99.7, 106.7, 101.5, 101.5, 96.8, 103.8, 100.4, 100.4, 96.7, 103.7, 98.4, 98.4, 93.7, 100.7, 97.3, 97.3, 93.6, 100.6, 93.4, 93.4, 86.8

Block ID	Information	Values
620462	Route travel distances [mile]	3.4, 3.5, 3.4, 3.5, 3.4, 3.5, 3.4, 3.5, 3.4, 3.5, 3.4, 3.5, 3.4, 3.5, 3.4, 3.5, 3.4, 3.5, 3.4, 3.5, 3.4, 3.5, 3.0, 3.5, 3.0, 3.5, 3.0, 3.5, 3.0, 3.5, 3.0, 3.5, 3.0, 3.5, 3.0, 3.5, 3.0, 3.5
	Stop time [min]	0.0, 3.0, 0.0, 3.0, 0.0, 3.0, 0.0, 3.0, 0.0, 8.0, 0.0, 3.0, 0.0, 3.0, 0.0, 3.0, 0.0, 3.0, 0.0, 3.0, 0.0, 3.0, 0.0, 4.0, 0.0, 3.0, 0.0, 3.0, 0.0, 3.0, 0.0, 3.0, 0.0
	Bus remaining range [mile]	120.0, 119.2, 119.2, 115.7, 120.0, 119.2, 119.2, 115.7, 120.0, 119.2, 119.2, 115.7, 120.0, 119.2, 119.2, 115.7, 120.0, 119.2, 119.2, 115.7, 120.0, 119.3, 119.3, 115.8, 120.0, 119.3, 119.3, 115.8, 120.0, 119.3, 119.3, 115.8, 120.0, 119.3, 119.3, 115.8, 120.0, 119.3, 119.3, 115.8, 120.0, 119.3, 119.3, 115.8, 120.0, 119.3, 119.3, 115.8, 120.0, 119.3, 119.3, 115.8, 120.0, 119.3, 119.3, 115.8, 120.0, 119.3, 119.3, 115.8, 120.0, 119.3, 119.3, 115.8
260326	Route travel distances [mile]	5.2, 4.7, 3.4, 3.7, 7.2, 4.7, 3.4, 3.7, 5.2, 4.7, 3.4, 3.7, 5.2, 4.7, 3.4, 3.7, 5.2, 4.7, 3.4, 3.7, 5.2, 4.7, 3.4, 3.7, 7.2, 4.7
	Stop time [min]	0.0, 3.0, 0.0, 3.0, 0.0, 3.0, 0.0, 3.0, 0.0, 3.0, 0.0, 3.0, 0.0, 3.0, 0.0, 3.0, 0.0, 3.0, 0.0, 3.0, 0.0, 3.0, 0.0, 3.0, 0.0, 3.0, 0.0, 3.0, 0.0, 3.0, 0.0
	Bus remaining range [mile]	120.0, 114.8, 114.8, 110.0, 117.0, 113.6, 113.6, 109.9, 116.9, 109.8, 109.8, 105.0, 112.0, 108.6, 108.6, 104.9, 111.9, 106.7, 106.7, 101.9, 108.9, 105.5, 105.5, 101.8, 108.8, 103.6, 103.6, 98.9, 105.9, 102.4, 102.4, 98.7, 105.7, 100.5, 100.5, 95.8, 102.8, 99.4, 99.4, 95.6, 102.6, 97.4, 97.4, 92.7, 99.7, 96.3, 96.3, 92.6, 99.6, 92.4, 92.4, 87.7
260626	Route travel distances [mile]	3.4, 3.7, 5.2, 4.7, 3.4, 3.7, 5.2, 4.7, 3.4, 3.7, 4.3, 3.0, 3.4, 3.7, 4.3, 3.0, 3.4, 3.7, 4.3, 3.0, 3.4, 3.7, 4.3, 3.0, 3.4, 3.7, 4.3, 3.0, 3.4, 3.7, 4.3
	Stop time [min]	0.0, 3.0, 0.0, 3.0, 0.0, 3.0, 0.0, 3.0, 0.0, 3.0, 0.0, 3.0, 0.0, 3.0, 0.0, 3.0, 0.0, 3.0, 0.0, 3.0, 0.0, 3.0, 0.0, 3.0, 0.0, 3.0, 0.0, 3.0, 0.0, 3.0, 0.0
	Bus remaining range [mile]	120.0, 116.6, 116.6, 112.9, 119.9, 114.7, 114.7, 109.9, 116.9, 113.5, 113.5, 109.8, 116.8, 111.6, 111.6, 106.8, 113.8, 110.4, 110.4, 106.7, 113.7, 109.4, 109.4, 106.6, 113.6, 110.2, 110.2, 106.4, 113.4, 109.2, 109.2, 106.3, 113.3, 109.9, 109.9, 106.2, 113.2, 108.9, 108.9, 106.1, 113.1, 109.7, 109.7, 105.9, 112.9, 108.7, 108.7, 105.8, 112.8, 109.4, 109.4, 105.7, 112.7, 108.4, 108.4, 105.6, 112.6, 109.1, 109.1, 105.4, 112.4, 108.2

Block ID	Information	Values
620262	Route travel distances [mile]	3.4, 3.5, 3.4, 3.5, 3.4, 3.5, 3.4, 3.5, 3.4, 3.5, 3.4, 3.5, 3.4, 3.5, 3.4, 3.5, 3.4, 3.5, 3.4, 3.5, 3.4, 3.5, 3.0, 3.5, 3.0, 3.5, 3.0, 3.5, 3.0, 3.5, 3.0, 3.5, 3.0, 3.5, 3.0, 3.5, 3.0, 3.5
	Stop time [min]	0.0, 3.0, 0.0, 3.0, 0.0, 3.0, 0.0, 3.0, 0.0, 3.0, 0.0, 13.0, 0.0, 3.0, 0.0, 3.0, 0.0, 3.0, 0.0, 3.0, 0.0, 3.0, 0.0, 5.0, 0.0, 3.0, 0.0, 3.0, 0.0, 3.0, 0.0, 3.0, 0.0, 3.0
	Bus remaining range [mile]	120.0, 119.2, 119.2, 115.7, 120.0, 119.2, 119.2, 115.7, 120.0, 119.2, 119.2, 115.7, 120.0, 119.2, 119.2, 115.7, 120.0, 119.2, 119.2, 115.7, 120.0, 119.2, 119.2, 115.7, 120.0, 119.3, 119.3, 115.8, 120.0, 119.3, 119.3, 115.8, 120.0, 119.3, 119.3, 115.8, 120.0, 119.3, 119.3, 115.8, 120.0, 119.3, 119.3, 115.8, 120.0, 119.3, 119.3, 115.8, 120.0, 119.3, 119.3, 115.8, 120.0, 119.3, 119.3, 115.8, 120.0, 119.3, 119.3, 115.8, 120.0, 119.3, 119.3, 115.8, 120.0, 119.3, 119.3, 115.8
270427	Route travel distances [mile]	7.8, 2.7, 3.4, 7.8, 7.8, 2.7, 3.4, 7.8, 7.8, 7.8, 7.8, 2.7, 3.4, 7.8, 7.8, 7.8, 7.8, 2.7, 3.4, 7.8, 7.8
	Stop time [min]	3.0, 0.0, 3.0, 3.0, 3.0, 0.0, 3.0, 3.0, 3.0, 3.0, 3.0, 0.0, 3.0, 3.0, 3.0, 3.0, 3.0, 0.0, 3.0, 3.0
	Bus remaining range [mile]	120.0, 112.4, 119.4, 116.7, 116.7, 113.3, 120.0, 112.2, 112.2, 104.5, 111.5, 108.9, 108.9, 105.5, 112.5, 104.6, 104.6, 97.0, 104.0, 96.1, 96.1, 88.4, 95.4, 92.8, 92.8, 89.4, 96.4, 88.5, 88.5, 80.9, 87.9, 80.0, 80.0, 72.4, 79.4, 76.7, 76.7, 73.3, 80.3, 72.5, 72.5, 64.8
1042104	Route travel distances [mile]	8.1, 8.0, 8.1, 8.0, 8.1, 8.0, 8.1, 8.0, 8.1, 8.0, 8.1, 8.0, 8.1, 8.0, 8.1, 8.0
	Stop time [min]	15.0, 14.0, 15.0, 14.0, 15.0, 14.0, 15.0, 14.0, 15.0, 14.0, 15.0, 14.0, 8.0, 11.0, 8.0
	Bus remaining range [mile]	120.0, 111.9, 120.0, 112.0, 112.0, 103.9, 120.0, 112.0, 112.0, 103.9, 120.0, 112.0, 112.0, 103.9, 120.0, 112.0, 112.0, 103.9, 120.0, 112.0, 112.0, 103.9, 120.0, 112.0, 112.0, 103.9, 120.0, 112.0, 112.0, 103.9, 120.0, 112.0
1043104	Route travel distances [mile]	8.0, 8.1, 8.0, 8.1, 8.0, 8.1, 8.0, 8.1, 8.0, 8.1, 8.0, 8.1, 8.0, 8.1, 8.0, 8.1
	Stop time [min]	14.0, 15.0, 14.0, 15.0, 14.0, 15.0, 14.0, 15.0, 14.0, 15.0, 14.0, 15.0, 11.0, 8.0, 11.0
	Bus remaining range [mile]	120.0, 112.0, 112.0, 103.9, 120.0, 112.0, 112.0, 103.9, 120.0, 112.0, 112.0, 103.9, 120.0, 112.0, 112.0, 103.9, 120.0, 112.0, 112.0, 103.9, 120.0, 112.0, 112.0, 103.9, 120.0, 112.0, 112.0, 103.9, 120.0, 112.0, 112.0, 103.9
1041104	Route travel distances [mile]	8.0, 8.1, 8.0, 8.1, 8.0, 8.1, 8.0, 8.1, 8.0, 8.1, 8.0, 8.1, 8.0, 8.1, 8.0, 8.1
	Stop time [min]	14.0, 15.0, 14.0, 15.0, 14.0, 15.0, 14.0, 15.0, 14.0, 15.0, 14.0, 15.0, 14.0, 8.0, 11.0
	Bus remaining range [mile]	120.0, 112.0, 112.0, 103.9, 120.0, 112.0, 112.0, 103.9, 120.0, 112.0, 112.0, 103.9, 120.0, 112.0, 112.0, 103.9, 120.0, 112.0, 112.0, 103.9, 120.0, 112.0, 112.0, 103.9, 120.0, 112.0, 112.0, 103.9, 120.0, 112.0, 112.0, 103.9

Block ID	Information	Values
4074	Route travel distances [mile]	8.5, 8.6, 8.5, 8.6, 8.5, 8.6, 8.5, 8.6, 8.5, 8.6, 8.5, 8.6, 8.5, 8.6, 8.5, 8.6
	Stop time [min]	2.0, 4.0, 2.0, 4.0, 2.0, 4.0, 4.0, 4.0, 4.0, 4.0, 4.0, 2.0, 4.0, 2.0, 4.0
	Bus remaining range [mile]	120.0, 111.5, 116.1, 107.5, 116.8, 108.3, 113.0, 104.4, 113.7, 105.2, 109.8, 101.2, 110.5, 102.0, 111.3, 102.7, 112.0, 103.5, 112.8, 104.2, 113.5, 105.0, 114.4, 105.7, 110.4, 101.9, 111.2, 102.6, 107.2, 98.7, 108.0, 99.4
4034	Route travel distances [mile]	8.5, 8.6, 8.5, 8.6, 8.5, 8.6, 8.5, 8.6, 8.5, 8.6, 8.5, 8.6, 8.5, 8.6, 8.5, 8.6
	Stop time [min]	2.0, 4.0, 2.0, 4.0, 4.0, 4.0, 4.0, 4.0, 4.0, 4.0, 4.0, 4.0, 1.0, 2.0, 4.0
	Bus remaining range [mile]	120.0, 111.5, 116.1, 107.5, 116.8, 108.3, 113.0, 104.4, 113.7, 105.2, 114.5, 105.9, 115.2, 106.7, 116.0, 107.4, 116.7, 108.2, 117.5, 108.9, 118.2, 109.7, 119.0, 110.4, 119.7, 111.2, 113.5, 104.9, 109.6, 101.0, 110.4, 101.7
4054	Route travel distances [mile]	8.5, 8.6, 8.5, 8.6, 8.5, 8.6, 8.5, 8.6, 8.5, 8.6, 8.5, 8.6, 8.5, 8.6, 8.5, 8.6
	Stop time [min]	2.0, 4.0, 2.0, 4.0, 3.0, 4.0, 4.0, 4.0, 4.0, 4.0, 4.0, 4.0, 2.0, 2.0, 4.0
	Bus remaining range [mile]	120.0, 111.5, 116.1, 107.5, 116.8, 108.3, 113.0, 104.4, 113.7, 105.2, 112.2, 103.5, 112.9, 104.3, 113.7, 105.0, 114.4, 105.8, 115.2, 106.5, 115.9, 107.4, 116.7, 108.1, 117.4, 108.9, 113.5, 104.9, 109.6, 101.0, 110.4, 101.7
4014	Route travel distances [mile]	8.5, 8.6, 8.5, 8.6, 8.5, 8.6, 8.5, 8.6, 8.5, 8.6, 8.5, 8.6, 8.5, 8.6, 8.5, 8.6
	Stop time [min]	2.0, 4.0, 2.0, 4.0, 2.0, 4.0, 8.0, 4.0, 4.0, 4.0, 4.0, 4.0, 0.0, 2.0, 4.0
	Bus remaining range [mile]	120.0, 111.5, 116.1, 107.5, 116.8, 108.3, 113.0, 104.4, 113.7, 105.2, 109.8, 101.2, 110.5, 102.0, 120.0, 111.4, 120.0, 111.5, 120.0, 111.4, 120.0, 111.5, 120.0, 111.4, 120.0, 111.5, 111.5, 102.8, 107.5, 99.0, 108.3, 99.7
6016	Route travel distances [mile]	9.6, 4.4, 4.5, 9.5, 9.6, 4.4, 4.5, 9.5, 9.6, 4.4, 4.5, 9.5, 9.6, 4.4, 4.5, 9.5, 9.6, 4.4, 4.5, 9.5
	Stop time [min]	3.0, 3.0, 0.0, 15.0, 3.0, 3.0, 0.0, 15.0, 3.0, 3.0, 0.0, 15.0, 3.0, 3.0, 0.0, 15.0, 3.0, 3.0, 0.0
	Bus remaining range [mile]	120.0, 110.4, 117.4, 116.4, 120.0, 115.5, 115.5, 106.0, 106.0, 96.4, 103.4, 102.4, 109.4, 104.9, 104.9, 95.4, 95.4, 85.8, 92.8, 91.8, 98.8, 94.2, 94.2, 84.8, 84.8, 75.2, 82.2, 81.2, 88.2, 83.6, 83.6, 74.1, 74.1, 64.6, 71.6, 70.5, 77.5, 73.0, 73.0, 63.5

Block ID	Information	Values
6066	Route travel distances [mile]	9.6, 4.4, 4.5, 9.5, 9.6, 4.4, 4.5, 9.5, 9.6, 4.4, 4.5, 9.5, 9.6, 4.4, 4.5, 9.5, 9.6, 4.4, 4.5, 9.5
	Stop time [min]	3.0, 3.0, 0.0, 15.0, 3.0, 3.0, 0.0, 15.0, 3.0, 3.0, 0.0, 15.0, 3.0, 3.0, 0.0, 15.0, 3.0, 3.0, 0.0
	Bus remaining range [mile]	120.0, 110.4, 117.4, 116.4, 120.0, 115.5, 115.5, 106.0, 106.0, 96.4, 103.4, 102.4, 109.4, 104.9, 104.9, 95.4, 95.4, 85.8, 92.8, 91.8, 98.8, 94.2, 94.2, 84.8, 84.8, 75.2, 82.2, 81.2, 88.2, 83.6, 83.6, 74.1, 74.1, 64.6, 71.6, 70.5, 77.5, 73.0, 73.0, 63.5
6056	Route travel distances [mile]	4.5, 9.5, 9.6, 4.4, 4.5, 9.5, 9.6, 4.4, 4.5, 9.5, 9.6, 4.4, 4.5, 9.5, 9.6, 4.4, 4.5, 9.5, 9.6, 4.4
	Stop time [min]	0.0, 15.0, 3.0, 3.0, 0.0, 15.0, 3.0, 3.0, 0.0, 15.0, 3.0, 3.0, 0.0, 15.0, 3.0, 3.0, 0.0, 15.0, 3.0
	Bus remaining range [mile]	120.0, 115.5, 115.5, 106.0, 106.0, 96.4, 103.4, 102.4, 109.4, 104.9, 104.9, 95.4, 95.4, 85.8, 92.8, 91.8, 98.8, 94.2, 94.2, 84.8, 84.8, 75.2, 82.2, 81.2, 88.2, 83.6, 83.6, 74.1, 74.1, 64.6, 71.6, 70.5, 77.5, 73.0, 73.0, 63.5, 63.5, 54.0, 61.0, 59.9
6096	Route travel distances [mile]	4.5, 9.5, 9.6, 4.4, 4.5, 9.5, 9.6, 4.4, 4.5, 9.5, 9.6, 4.4, 4.5, 9.5, 9.6, 4.4, 4.5, 9.5, 9.6, 4.4
	Stop time [min]	0.0, 15.0, 3.0, 3.0, 0.0, 15.0, 3.0, 3.0, 0.0, 15.0, 3.0, 3.0, 0.0, 15.0, 3.0, 3.0, 0.0, 15.0, 3.0
	Bus remaining range [mile]	120.0, 115.5, 115.5, 106.0, 106.0, 96.4, 103.4, 102.4, 109.4, 104.9, 104.9, 95.4, 95.4, 85.8, 92.8, 91.8, 98.8, 94.2, 94.2, 84.8, 84.8, 75.2, 82.2, 81.2, 88.2, 83.6, 83.6, 74.1, 74.1, 64.6, 71.6, 70.5, 77.5, 73.0, 73.0, 63.5, 63.5, 54.0, 61.0, 59.9
270327	Route travel distances [mile]	2.7, 3.4, 7.8, 7.8, 2.7, 3.4, 7.8, 7.8, 2.7, 3.4, 7.8, 7.8, 7.8, 7.8, 2.7, 3.4, 7.8, 7.8, 7.8, 7.8, 2.7, 3.4, 7.8, 7.8
	Stop time [min]	0.0, 3.0, 3.0, 3.0, 0.0, 3.0, 3.0, 3.0, 0.0, 3.0, 3.0, 3.0, 3.0, 3.0, 0.0, 3.0, 3.0, 3.0, 3.0, 3.0, 0.0, 3.0, 3.0
	Bus remaining range [mile]	120.0, 117.3, 117.3, 113.9, 120.0, 112.2, 112.2, 104.5, 111.5, 108.9, 108.9, 105.5, 112.5, 104.6, 104.6, 97.0, 104.0, 101.3, 101.3, 97.9, 104.9, 97.1, 97.1, 89.4, 96.4, 88.5, 88.5, 80.9, 87.9, 85.2, 85.2, 81.8, 88.8, 81.0, 81.0, 73.3, 80.3, 72.5, 72.5, 64.8, 71.8, 69.2, 69.2, 65.8, 72.8, 64.9, 64.9, 57.3
270627	Route travel distances [mile]	7.8, 7.8, 2.7, 3.4, 7.8, 7.8, 7.8, 7.8, 2.7, 3.4, 7.8, 7.8, 7.8, 7.8, 2.7, 3.4, 7.8, 7.8, 7.8, 7.8, 2.7, 3.4, 7.8
	Stop time [min]	3.0, 3.0, 0.0, 3.0, 3.0, 3.0, 3.0, 3.0, 0.0, 3.0, 3.0, 3.0, 3.0, 3.0, 0.0, 3.0, 3.0, 3.0, 3.0, 3.0, 0.0, 3.0
	Bus remaining range [mile]	120.0, 112.2, 112.2, 104.5, 111.5, 108.9, 108.9, 105.5, 112.5, 104.6, 104.6, 97.0, 104.0, 96.1, 96.1, 88.5, 95.5, 92.8, 92.8, 89.4, 96.4, 88.6, 88.6, 80.9, 87.9, 80.1, 80.1, 72.4, 79.4, 76.7, 76.7, 73.3, 80.3, 72.5, 72.5, 64.8, 71.8, 64.0, 64.0, 56.3, 63.3, 60.7, 60.7, 57.3, 64.3, 56.4

Block ID	Information	Values
270127	Route travel distances [mile]	3.4, 7.8, 7.8, 2.7, 3.4, 7.8, 7.8, 7.8, 7.8, 2.7, 3.4, 7.8, 7.8, 7.8, 7.8, 2.7, 3.4, 7.8, 7.8, 2.7, 3.4, 7.8, 7.8, 2.7, 3.4
	Stop time [min]	3.0, 3.0, 3.0, 0.0, 3.0, 3.0, 3.0, 3.0, 3.0, 0.0, 3.0, 3.0, 3.0, 3.0, 3.0, 0.0, 3.0, 3.0, 3.0, 0.0, 3.0, 3.0, 3.0, 0.0
	Bus remaining range [mile]	120.0, 116.6, 120.0, 112.2, 112.2, 104.5, 111.5, 108.9, 108.9, 105.5, 112.5, 104.6, 104.6, 97.0, 104.0, 96.1, 96.1, 88.5, 95.5, 92.8, 92.8, 89.4, 96.4, 88.6, 88.6, 80.9, 87.9, 80.1, 80.1, 72.4, 79.4, 76.7, 76.7, 73.3, 80.3, 72.5, 72.5, 64.9, 71.9, 69.2, 69.2, 65.8, 72.8, 65.0, 65.0, 57.3, 64.3, 61.7, 61.7, 58.3
610461	Route travel distances [mile]	4.9, 3.3, 7.6, 7.6, 4.9, 3.3, 7.6, 7.6, 4.9, 3.3, 7.6, 7.6, 4.9, 3.3, 7.6, 7.6, 4.9, 3.3, 7.6, 7.6, 4.9, 3.3, 7.6, 7.6, 4.9
	Stop time [min]	3.0, 0.0, 3.0, 0.0, 3.0, 0.0, 3.0, 0.0, 3.0, 0.0, 3.0, 0.0, 3.0, 0.0, 3.0, 0.0, 3.0, 0.0, 3.0, 0.0, 3.0, 0.0, 3.0, 0.0
	Bus remaining range [mile]	120.0, 115.1, 115.1, 111.7, 111.7, 104.1, 111.1, 103.5, 103.5, 98.6, 98.6, 95.2, 95.2, 87.6, 94.6, 87.1, 87.1, 82.1, 82.1, 78.8, 78.8, 71.2, 78.2, 70.6, 70.6, 65.6, 65.6, 62.3, 62.3, 54.7, 61.7, 54.1, 54.1, 49.2, 49.2, 45.8, 45.8, 38.2, 45.2, 37.6, 37.6, 32.7, 32.7, 29.4, 29.4, 21.8, 28.8, 21.2, 21.2, 16.2
4084	Route travel distances [mile]	8.6, 8.5, 8.6, 8.5, 8.6, 8.5, 8.6, 8.5, 8.6, 8.5, 8.6, 8.5, 8.6, 8.5, 8.6, 8.5, 8.6, 8.5, 8.6, 8.5, 8.6
	Stop time [min]	4.0, 2.0, 4.0, 2.0, 4.0, 9.0, 4.0, 4.0, 4.0, 4.0, 4.0, 5.0, 2.0, 4.0, 2.0, 4.0
	Bus remaining range [mile]	120.0, 111.4, 120.0, 111.5, 116.1, 107.5, 116.8, 108.3, 113.0, 104.4, 113.7, 105.2, 120.0, 111.4, 120.0, 111.5, 120.0, 111.4, 120.0, 111.5, 120.0, 111.4, 120.0, 111.5, 120.0, 111.4, 116.0, 107.5, 116.8, 108.2, 112.9, 104.4, 113.7, 105.1
300530	Route travel distances [mile]	3.4, 4.5, 5.9, 5.8, 7.7, 7.5, 3.4, 4.5, 5.9, 5.8, 3.4, 4.5, 5.9, 5.8, 3.4, 4.5, 5.9, 5.8, 3.4, 4.5, 5.9, 5.8, 7.7, 7.5, 3.4, 4.5, 5.9, 5.8
	Stop time [min]	0.0, 3.0, 0.0, 3.0, 2.0, 3.0, 0.0, 3.0, 0.0, 3.0, 0.0, 3.0, 0.0, 3.0, 0.0, 3.0, 0.0, 3.0, 0.0, 3.0, 0.0, 3.0, 2.0, 3.0, 0.0, 3.0, 0.0
	Bus remaining range [mile]	120.0, 116.6, 116.6, 112.1, 119.1, 113.3, 113.3, 107.6, 114.6, 106.9, 111.6, 104.3, 111.3, 107.9, 107.9, 103.4, 110.4, 104.6, 104.6, 98.9, 105.9, 102.5, 102.5, 98.0, 105.0, 99.2, 99.2, 93.5, 100.5, 97.1, 97.1, 92.6, 99.6, 93.8, 93.8, 88.1, 95.1, 91.8, 91.8, 87.2, 94.2, 88.4, 88.4, 82.8, 89.8, 82.0, 86.7, 79.4, 86.4, 83.0, 83.0, 78.5, 85.5, 79.7, 79.7, 74.0

Block ID	Information	Values
5025	Route travel distances [mile]	8.0, 10.5, 10.6, 8.1, 9.8, 9.7, 8.0, 10.5, 10.6, 8.1, 9.8, 11.2, 8.0, 10.5, 10.6, 8.1
	Stop time [min]	3.0, 3.0, 3.0, 0.0, 3.0, 6.0, 3.0, 3.0, 3.0, 0.0, 3.0, 6.0, 3.0, 3.0, 3.0
	Bus remaining range [mile]	120.0, 112.5, 119.5, 108.9, 115.9, 105.9, 112.9, 104.8, 104.8, 94.9, 101.9, 92.2, 106.2, 98.7, 105.7, 95.2, 102.2, 92.1, 99.1, 91.0, 91.0, 81.2, 88.2, 76.9, 90.9, 83.4, 90.4, 79.9, 86.9, 76.8, 83.8, 75.7
5015	Route travel distances [mile]	10.6, 8.1, 11.4, 9.7, 8.0, 10.5, 10.6, 8.1, 9.8, 9.7, 8.0, 10.5, 10.6, 8.1, 9.8, 9.7
	Stop time [min]	3.0, 0.0, 3.0, 6.0, 3.0, 3.0, 3.0, 0.0, 3.0, 6.0, 3.0, 3.0, 3.0, 0.0, 3.0
	Bus remaining range [mile]	120.0, 109.9, 116.9, 108.8, 108.8, 97.4, 104.4, 94.7, 108.7, 101.1, 108.1, 97.6, 104.6, 94.6, 101.6, 93.4, 93.4, 83.6, 90.6, 80.9, 94.9, 87.4, 94.4, 83.9, 90.9, 80.8, 87.8, 79.7, 79.7, 69.9, 76.9, 67.2
5075	Route travel distances [mile]	11.7, 11.4, 8.0, 10.5, 10.6, 8.1, 9.8, 9.7, 8.0, 10.5, 10.6, 8.1, 9.8, 9.7, 8.0, 10.5
	Stop time [min]	0.0, 9.0, 3.0, 3.0, 3.0, 0.0, 3.0, 6.0, 3.0, 3.0, 3.0, 0.0, 3.0, 6.0, 3.0
	Bus remaining range [mile]	120.0, 108.3, 108.3, 96.9, 117.9, 110.4, 117.4, 106.9, 113.9, 103.8, 110.8, 102.7, 102.7, 92.9, 99.9, 90.2, 104.2, 96.6, 103.6, 93.1, 100.1, 90.1, 97.1, 88.9, 88.9, 79.1, 86.1, 76.4, 90.4, 82.9, 89.9, 79.3
610261	Route travel distances [mile]	7.6, 4.9, 3.3, 7.6, 7.6, 4.9, 3.3, 7.6, 7.6, 4.9, 3.3, 7.6, 7.6, 4.9, 3.3, 7.6, 7.6, 4.9, 3.3, 7.6, 7.6, 4.9, 3.3, 7.6, 7.6, 4.9, 3.3, 7.6, 7.6, 4.9, 3.3, 7.6, 7.6, 7.6
	Stop time [min]	0.0, 3.0, 0.0, 3.0, 0.0, 3.0, 0.0, 3.0, 0.0, 3.0, 0.0, 3.0, 0.0, 3.0, 0.0, 3.0, 0.0, 3.0, 0.0, 3.0, 0.0, 3.0, 0.0, 3.0, 0.0, 3.0, 0.0, 3.0, 0.0, 3.0, 0.0, 3.0, 13.0
	Bus remaining range [mile]	120.0, 112.4, 112.4, 107.5, 107.5, 104.1, 104.1, 96.5, 103.5, 96.0, 96.0, 91.0, 91.0, 87.7, 87.7, 80.1, 87.1, 79.5, 79.5, 74.5, 74.5, 71.2, 71.2, 63.6, 70.6, 63.0, 63.0, 58.1, 58.1, 54.7, 54.7, 47.1, 54.1, 46.5, 46.5, 41.6, 41.6, 38.3, 38.3, 30.6, 37.6, 30.1, 30.1, 25.1, 25.1, 21.8, 21.8, 14.2, 21.2, 13.6, 13.6, 6.0
420342	Route travel distances [mile]	4.6, 6.1, 4.2, 3.9, 8.4, 8.6, 4.4, 3.9, 4.6, 6.1, 4.2, 3.9, 6.2, 5.8, 4.4, 3.9, 4.6, 6.1, 4.2, 3.9, 6.2, 5.8, 4.4, 3.9, 4.6, 6.1, 4.2, 3.9, 8.4, 8.6
	Stop time [min]	0.0, 3.0, 0.0, 3.0, 3.0, 3.0, 0.0, 3.0, 0.0, 3.0, 0.0, 3.0, 0.0, 3.0, 0.0, 3.0, 0.0, 3.0, 0.0, 3.0, 0.0, 3.0, 0.0, 3.0, 0.0, 3.0, 0.0, 3.0, 0.0, 3.0, 0.0, 3.0, 3.0
	Bus remaining range [mile]	120.0, 115.4, 115.4, 109.4, 116.4, 112.2, 112.2, 108.3, 115.3, 106.9, 113.9, 105.2, 112.2, 107.9, 107.9, 104.0, 111.0, 106.4, 106.4, 100.3, 107.3, 103.2, 103.2, 99.3, 106.3, 100.1, 100.1, 94.3, 101.3, 96.9, 96.9, 93.0, 100.0, 95.5, 95.5, 89.4, 96.4, 92.2, 92.2, 88.3, 95.3, 89.2, 89.2, 83.3, 90.3, 86.0, 86.0, 82.1, 89.1, 84.5, 84.5, 78.5, 85.5, 81.3, 81.3, 77.4, 84.4, 76.0, 83.0, 74.3

Block ID	Information	Values
420942	Route travel distances [mile]	12.3, 12.5, 12.3, 12.5, 12.3, 12.5, 12.3, 12.5, 12.3, 12.5, 12.3, 12.5, 12.3
	Stop time [min]	3.0, 3.0, 3.0, 3.0, 3.0, 3.0, 3.0, 3.0, 3.0, 3.0, 3.0, 3.0
	Bus remaining range [mile]	120.0, 107.7, 114.7, 102.4, 109.4, 97.0, 104.0, 91.7, 98.7, 86.4, 93.4, 81.1, 88.1, 75.7, 82.7, 70.4, 77.4, 65.1, 72.1, 59.8, 66.8, 54.5, 61.5, 49.2, 56.2, 43.8
420742	Route travel distances [mile]	12.5, 12.3, 12.5, 12.3, 12.5, 12.3, 12.5, 12.3, 12.5, 12.3, 12.5, 12.3, 12.5
	Stop time [min]	3.0, 3.0, 3.0, 3.0, 3.0, 3.0, 3.0, 3.0, 3.0, 3.0, 3.0, 3.0
	Bus remaining range [mile]	120.0, 107.7, 114.7, 102.4, 109.4, 97.1, 104.1, 91.7, 98.7, 86.4, 93.4, 81.1, 88.1, 75.8, 82.8, 70.4, 77.4, 65.1, 72.1, 59.8, 66.8, 54.5, 61.5, 49.2, 56.2, 43.9
5055	Route travel distances [mile]	10.5, 10.6, 8.1, 9.8, 9.7, 8.0, 10.5, 10.6, 8.1, 9.8, 9.7, 8.0, 10.5, 10.6, 8.1, 9.8, 9.7
	Stop time [min]	3.0, 3.0, 0.0, 3.0, 6.0, 3.0, 3.0, 3.0, 0.0, 3.0, 6.0, 3.0, 3.0, 3.0, 0.0, 3.0
	Bus remaining range [mile]	120.0, 109.5, 116.5, 106.4, 113.4, 105.3, 105.3, 95.5, 102.5, 92.8, 106.8, 99.2, 106.2, 95.7, 102.7, 92.7, 99.7, 91.5, 91.5, 81.7, 88.7, 79.0, 93.0, 85.5, 92.5, 82.0, 89.0, 78.9, 85.9, 77.8, 77.8, 68.0, 75.0, 65.3
5095	Route travel distances [mile]	8.0, 10.5, 10.6, 8.1, 9.8, 9.7, 8.0, 10.5, 10.6, 8.1, 9.8, 9.7, 8.0, 10.5, 10.6, 8.1, 9.8, 6.1
	Stop time [min]	3.0, 3.0, 3.0, 0.0, 3.0, 6.0, 3.0, 3.0, 3.0, 0.0, 3.0, 6.0, 3.0, 3.0, 3.0, 0.0, 3.0
	Bus remaining range [mile]	120.0, 112.5, 119.5, 108.9, 115.9, 105.9, 112.9, 104.8, 104.8, 94.9, 101.9, 92.2, 106.2, 98.7, 105.7, 95.2, 102.2, 92.1, 99.1, 91.0, 91.0, 81.2, 88.2, 78.5, 92.5, 84.9, 91.9, 81.4, 88.4, 78.4, 85.4, 77.2, 77.2, 67.4, 74.4, 68.3
610161	Route travel distances [mile]	3.3, 7.6, 7.6, 4.9, 3.3, 7.6, 7.6, 4.9, 3.3, 7.6, 7.6, 4.9, 3.3, 7.6, 7.6, 4.9, 3.3, 7.6, 7.6, 4.9, 3.3, 7.6, 7.6, 4.9, 3.3, 7.6, 7.6, 7.6
	Stop time [min]	0.0, 3.0, 0.0, 3.0, 0.0, 3.0, 0.0, 3.0, 0.0, 3.0, 0.0, 3.0, 0.0, 3.0, 0.0, 3.0, 0.0, 3.0, 0.0, 3.0, 0.0, 3.0, 0.0, 3.0, 0.0, 3.0, 13.0
	Bus remaining range [mile]	120.0, 116.7, 116.7, 109.0, 116.0, 108.5, 108.5, 103.5, 103.5, 100.2, 100.2, 92.6, 99.6, 92.0, 92.0, 87.1, 87.1, 83.7, 83.7, 76.1, 83.1, 75.5, 75.5, 70.6, 70.6, 67.2, 67.2, 59.6, 66.6, 59.1, 59.1, 54.1, 54.1, 50.8, 50.8, 43.2, 50.2, 42.6, 42.6, 37.6, 37.6, 34.3, 34.3, 26.7, 33.7, 26.1, 26.1, 21.2, 21.2, 17.8, 17.8, 10.2, 17.2, 9.7, 9.7, 2.0

Block ID	Information	Values
610361	Route travel distances [mile]	3.3, 7.6, 7.6, 4.9, 3.3, 7.6, 7.6, 4.9, 3.3, 7.6, 7.6, 4.9, 3.3, 7.6, 7.6, 4.9, 3.3, 7.6, 7.6, 4.9, 3.3, 7.6, 7.6, 4.9, 3.3, 7.6, 7.6, 7.6
	Stop time [min]	0.0, 3.0, 0.0, 3.0, 0.0, 3.0, 0.0, 3.0, 0.0, 3.0, 0.0, 3.0, 0.0, 3.0, 0.0, 3.0, 0.0, 3.0, 0.0, 3.0, 0.0, 3.0, 0.0, 3.0, 0.0, 3.0, 0.0, 3.0, 0.0, 3.0, 13.0
	Bus remaining range [mile]	120.0, 116.7, 116.7, 109.0, 116.0, 108.5, 108.5, 103.5, 103.5, 100.2, 100.2, 92.6, 99.6, 92.0, 92.0, 87.1, 87.1, 83.7, 83.7, 76.1, 83.1, 75.5, 75.5, 70.6, 70.6, 67.2, 67.2, 59.6, 66.6, 59.1, 59.1, 54.1, 54.1, 50.8, 50.8, 43.2, 50.2, 42.6, 42.6, 37.6, 37.6, 34.3, 34.3, 26.7, 33.7, 26.1, 26.1, 21.2, 21.2, 17.8, 17.8, 10.2, 17.2, 9.7, 9.7, 2.0
420142	Route travel distances [mile]	6.2, 5.8, 4.4, 3.9, 4.6, 6.1, 4.2, 3.9, 6.2, 5.8, 4.4, 3.9, 4.6, 6.1, 4.2, 3.9, 6.2, 5.8, 4.4, 3.9, 4.6, 6.1, 4.2, 3.9, 6.2, 5.8, 4.4, 3.9, 4.6, 6.1, 4.2, 3.9, 8.4, 8.6
	Stop time [min]	0.0, 3.0, 0.0, 3.0, 0.0, 3.0, 0.0, 3.0, 0.0, 3.0, 0.0, 3.0, 0.0, 3.0, 0.0, 3.0, 0.0, 3.0, 0.0, 3.0, 0.0, 3.0, 0.0, 3.0, 0.0, 3.0, 0.0, 3.0, 0.0, 3.0, 0.0, 3.0, 0.0, 3.0, 0.0, 3.0, 3.0
	Bus remaining range [mile]	120.0, 113.8, 113.8, 108.0, 115.0, 110.7, 110.7, 106.8, 113.8, 109.2, 109.2, 103.1, 110.1, 106.0, 106.0, 102.1, 109.1, 102.9, 102.9, 97.1, 104.1, 99.7, 99.7, 95.9, 102.9, 98.3, 98.3, 92.2, 99.2, 95.1, 95.1, 91.1, 98.1, 92.0, 92.0, 86.2, 93.2, 88.8, 88.8, 84.9, 91.9, 87.3, 87.3, 81.3, 88.3, 84.1, 84.1, 80.2, 87.2, 81.0, 81.0, 75.2, 82.2, 77.9, 77.9, 74.0, 81.0, 76.4, 76.4, 70.4, 77.4, 73.2, 73.2, 69.3, 76.3, 67.9, 74.9, 66.2
300130	Route travel distances [mile]	5.8, 7.7, 7.5, 3.4, 4.9, 5.9, 5.8, 7.7, 7.5, 7.7, 7.5, 7.7, 7.5, 7.7, 7.5, 7.7, 7.5, 7.7, 7.5, 3.4, 4.5, 5.9, 5.8, 7.7, 7.5, 3.4, 4.5
	Stop time [min]	3.0, 2.0, 3.0, 0.0, 3.0, 0.0, 3.0, 0.0, 3.0, 0.0, 3.0, 0.0, 3.0, 0.0, 3.0, 0.0, 3.0, 0.0, 3.0, 2.0, 3.0, 0.0, 3.0, 0.0, 3.0, 2.0, 3.0, 0.0
	Bus remaining range [mile]	120.0, 114.4, 120.0, 112.3, 116.9, 109.6, 116.6, 113.3, 113.3, 108.3, 115.3, 109.5, 109.5, 103.8, 110.8, 103.1, 103.1, 95.8, 102.8, 95.1, 95.1, 87.7, 94.7, 87.0, 87.0, 79.7, 86.7, 79.0, 79.0, 71.6, 78.6, 70.9, 70.9, 63.6, 70.6, 62.9, 67.5, 60.2, 67.2, 63.9, 63.9, 59.4, 66.4, 60.5, 60.5, 54.9, 61.9, 54.1, 58.8, 51.5, 58.5, 55.2, 55.2, 50.7
6036	Route travel distances [mile]	13.9, 13.3, 13.9, 13.3, 13.9, 13.3, 13.9, 13.3, 13.9, 13.3, 13.9, 13.3, 13.9
	Stop time [min]	3.0, 3.0, 3.0, 3.0, 3.0, 3.0, 3.0, 3.0, 3.0, 3.0, 3.0, 3.0, 3.0
	Bus remaining range [mile]	120.0, 106.1, 113.1, 102.6, 109.6, 95.7, 102.7, 92.3, 99.3, 85.4, 92.4, 81.9, 88.9, 75.0, 82.0, 71.6, 78.6, 64.6, 71.6, 61.2, 68.2, 54.3, 61.3, 50.9, 57.9, 43.9

Block ID	Information	Values
271227	Route travel distances [mile]	5.6, 5.6, 4.3, 4.2, 5.6, 5.6, 4.3, 4.2, 5.6, 5.6, 4.3, 4.2, 5.6, 5.6, 4.3, 4.2, 5.6, 5.6, 4.3, 4.2, 5.6, 5.6, 4.3, 4.2, 5.6, 5.6, 4.3, 4.2, 5.6, 5.6, 4.3, 4.2, 5.6, 5.6, 4.3, 4.2
	Stop time [min]	0.0, 3.0, 0.0, 3.0, 0.0, 3.0, 0.0, 3.0, 0.0, 3.0, 0.0, 3.0, 0.0, 3.0, 0.0, 3.0, 0.0, 3.0, 0.0, 3.0, 0.0, 3.0, 0.0, 3.0, 0.0, 3.0, 0.0, 3.0, 0.0, 3.0, 0.0, 3.0, 0.0, 3.0, 0.0
	Bus remaining range [mile]	120.0, 114.4, 114.4, 108.7, 115.7, 111.4, 111.4, 107.2, 114.2, 108.6, 108.6, 103.0, 110.0, 105.7, 105.7, 101.5, 108.5, 102.8, 102.8, 97.2, 104.2, 99.9, 99.9, 95.7, 102.7, 97.0, 97.0, 91.4, 98.4, 94.1, 94.1, 89.9, 96.9, 91.3, 91.3, 85.6, 92.6, 88.3, 88.3, 84.1, 91.1, 85.5, 85.5, 79.9, 86.9, 82.6, 82.6, 78.4, 85.4, 79.7, 79.7, 74.1, 81.1, 76.8, 76.8, 72.6, 79.6, 73.9, 73.9, 68.3, 75.3, 71.0, 71.0, 66.8, 73.8, 68.2, 68.2, 62.5, 69.5, 65.2, 65.2, 61.0
260526	Route travel distances [mile]	4.3, 3.0, 3.1, 4.2, 4.3, 3.0, 3.1, 4.2, 4.3, 3.0, 3.1, 4.2, 4.3, 3.0, 3.1, 4.2, 4.3, 3.0, 3.1, 4.2, 4.3, 3.0, 3.1, 4.2, 4.3, 3.0, 3.1, 4.2, 4.3, 3.0, 3.1, 4.2, 4.3, 3.0, 3.1, 4.2, 4.3, 3.0, 3.1, 4.2, 4.3, 3.0, 3.1, 4.2, 4.3, 3.0, 3.1, 4.2, 4.3, 3.0
	Stop time [min]	0.0, 3.0, 0.0
	Bus remaining range [mile]	120.0, 115.7, 115.7, 112.9, 119.9, 116.8, 116.8, 112.6, 119.6, 115.4, 115.4, 112.5, 119.5, 116.4, 116.4, 112.2, 119.2, 115.0, 115.0, 112.1, 119.1, 116.1, 116.1, 111.9, 118.9, 114.6, 114.6, 111.7, 118.7, 115.7, 115.7, 111.5, 118.5, 114.2, 114.2, 111.3, 118.3, 115.3, 115.3, 111.1, 118.1, 113.8, 113.8, 111.0, 118.0, 114.9, 114.9, 110.7, 117.7, 113.5, 113.5, 110.6, 117.6, 114.5, 114.5, 110.3, 117.3, 113.1, 113.1, 110.2, 117.2, 114.1, 114.1, 109.9, 116.9, 112.7, 112.7, 109.8, 116.8, 113.8, 113.8, 109.6, 116.6, 112.3, 112.3, 109.4, 116.4, 113.4, 113.4, 109.2, 116.2, 111.9, 111.9, 109.1, 116.1, 113.0, 113.0, 108.8, 115.8, 111.5, 111.5, 108.7, 115.7, 112.6, 112.6, 108.4, 115.4, 111.2, 111.2, 108.3

Block ID	Information	Values
620162	Route travel distances [mile]	3.4, 3.5, 3.4, 3.5, 3.4, 3.5, 3.4, 3.5, 3.4, 3.5, 3.4, 3.5, 3.4, 3.5, 3.4, 3.5, 3.4, 3.5, 3.4, 3.5, 3.4, 3.5, 3.4, 3.5, 3.4, 3.5, 3.0, 3.5, 3.0, 3.5, 3.0, 3.5, 3.0, 3.5, 3.0, 3.5, 3.0, 3.5, 3.0, 2.8, 2.6, 2.8, 2.6, 2.8, 2.6, 2.8, 2.6, 2.8, 2.6, 2.8, 2.6, 2.8, 2.6, 2.8, 2.6, 2.8, 2.6, 2.8
	Stop time [min]	0.0, 3.0, 0.0, 3.0, 0.0, 3.0, 0.0, 3.0, 0.0, 3.0, 0.0, 3.0, 0.0, 8.0, 0.0, 3.0, 0.0
	Bus remaining range [mile]	120.0, 119.2, 119.2, 115.7, 120.0, 119.2, 119.2, 115.7, 120.0, 119.2, 119.2, 115.7, 120.0, 119.2, 119.2, 115.7, 120.0, 119.2, 119.2, 115.7, 120.0, 119.2, 119.2, 115.7, 120.0, 119.2, 119.2, 115.7, 120.0, 119.3, 119.3, 115.8, 120.0, 119.3, 119.3, 115.8, 120.0, 119.3, 119.3, 115.8, 120.0, 119.3, 119.3, 115.8, 120.0, 119.3, 119.3, 115.8, 120.0, 119.3, 119.3, 115.8, 120.0, 119.3, 119.3, 115.8, 120.0, 119.3, 119.3, 115.8, 120.0, 119.3, 119.3, 115.8, 120.0, 119.3, 119.3, 115.8, 120.0, 119.3, 119.3, 115.8, 120.0, 119.3, 119.3, 116.5, 116.5, 116.2, 116.2, 113.4, 113.4, 113.1, 113.1, 110.3, 110.3, 109.9, 109.9, 107.2, 107.2, 106.8, 106.8, 104.1, 104.1, 103.7, 103.7, 100.9, 100.9, 100.6, 100.6, 97.8, 97.8, 97.5, 97.5, 94.7, 94.7, 94.4, 94.4, 91.6, 91.6, 91.2, 91.2, 88.5
4104	Route travel distances [mile]	8.6, 8.5, 8.6, 8.5, 8.6, 8.5, 8.6, 8.5, 8.6, 8.5, 8.6, 8.5, 8.6, 8.5, 8.6, 8.5, 8.6, 8.5, 8.6, 8.5, 8.6, 8.5, 8.6
	Stop time [min]	4.0, 2.0, 4.0, 2.0, 4.0, 9.0, 4.0, 4.0, 4.0, 4.0, 4.0, 6.0, 2.0, 4.0, 2.0, 5.0, 4.0, 4.0, 4.0, 4.0, 4.0, 4.0
	Bus remaining range [mile]	120.0, 111.4, 120.0, 111.5, 116.1, 107.5, 116.8, 108.3, 113.0, 104.4, 113.7, 105.2, 120.0, 111.4, 120.0, 111.5, 120.0, 111.4, 120.0, 111.5, 120.0, 111.4, 120.0, 111.5, 120.0, 111.4, 116.0, 107.5, 116.8, 108.2, 112.9, 104.4, 116.0, 107.4, 116.7, 108.2, 117.5, 108.9, 118.2, 109.7, 119.0, 110.4, 119.7, 111.2, 120.0, 111.4

Block ID	Information	Values
430143	Route travel distances [mile]	3.2, 2.9, 3.8, 5.7, 5.4, 3.6, 3.2, 2.9, 3.8, 5.7, 5.4, 3.6, 3.2, 2.9, 3.8, 5.7, 5.4, 3.6, 3.2, 2.9, 3.8, 5.7, 5.4, 3.6, 3.2, 2.9, 3.8, 5.7, 5.4, 3.6, 3.2, 2.9, 3.8, 5.7, 5.4, 3.6, 3.2, 2.9, 3.8, 5.7, 5.4, 3.6, 3.2, 2.9, 3.8, 5.7, 5.4, 3.6, 3.2, 2.9
	Stop time [min]	0.0, 3.0, 0.0, 5.0, 0.0, 3.0, 0.0, 3.0, 0.0, 5.0, 0.0, 3.0, 0.0, 3.0, 0.0, 5.0, 0.0, 3.0, 0.0, 3.0, 0.0, 5.0, 0.0, 3.0, 0.0, 3.0, 0.0, 5.0, 0.0, 3.0, 0.0, 3.0, 0.0, 5.0, 0.0, 3.0, 0.0, 3.0, 0.0, 5.0, 0.0, 3.0, 0.0, 3.0, 0.0, 5.0, 0.0, 3.0, 0.0
	Bus remaining range [mile]	120.0, 116.8, 116.8, 113.9, 120.0, 116.2, 116.2, 110.5, 120.0, 114.6, 114.6, 111.0, 118.0, 114.8, 114.8, 111.9, 118.9, 115.1, 115.1, 109.4, 120.0, 114.6, 114.6, 111.0, 118.0, 114.8, 114.8, 111.9, 118.9, 115.1, 115.1, 109.4, 120.0, 114.6, 114.6, 111.0, 118.0, 114.8, 114.8, 111.9, 118.9, 115.1, 115.1, 109.4, 120.0, 114.6, 114.6, 111.0, 118.0, 114.8, 114.8, 111.9, 118.9, 115.1, 115.1, 109.4, 120.0, 114.6, 114.6, 111.0, 118.0, 114.8, 114.8, 111.9, 118.9, 115.1, 115.1, 109.4, 120.0, 114.6, 114.6, 111.0, 118.0, 114.8, 114.8, 111.9, 118.9, 115.1, 115.1, 109.4, 120.0, 114.6, 114.6, 111.0, 118.0, 114.8, 114.8, 111.9
300330	Route travel distances [mile]	7.5, 3.4, 4.5, 5.9, 5.8, 7.7, 7.5, 3.4, 4.5, 5.9, 5.8, 3.4, 4.5, 5.9, 5.8, 3.4, 4.5, 5.9, 5.8, 7.7, 7.5, 3.4, 4.5, 5.9, 5.8, 7.7, 7.5, 3.4, 4.5, 5.9, 5.8, 7.7, 7.5, 3.4, 4.5, 5.9, 5.8
	Stop time [min]	3.0, 0.0, 3.0, 0.0, 3.0, 2.0, 3.0, 0.0, 3.0, 0.0, 3.0, 0.0, 3.0, 0.0, 3.0, 0.0, 3.0, 0.0, 3.0, 2.0, 3.0, 0.0, 3.0, 0.0, 3.0, 2.0, 3.0, 0.0, 3.0, 0.0, 3.0, 0.0, 18.0, 0.0, 3.0, 0.0
	Bus remaining range [mile]	120.0, 112.7, 119.7, 116.4, 116.4, 111.8, 118.8, 113.0, 113.0, 107.4, 114.4, 106.6, 111.3, 104.0, 111.0, 107.6, 107.6, 103.1, 110.1, 104.3, 104.3, 98.6, 105.6, 102.2, 102.2, 97.7, 104.7, 98.9, 98.9, 93.2, 100.2, 96.9, 96.9, 92.4, 99.4, 93.5, 93.5, 87.9, 94.9, 87.1, 91.8, 84.5, 91.5, 88.1, 88.1, 83.6, 90.6, 84.8, 84.8, 79.2, 86.2, 78.4, 83.1, 75.8, 82.8, 79.4, 79.4, 74.9, 81.9, 76.1, 76.1, 70.4, 77.4, 69.7, 69.7, 62.4, 104.4, 101.0, 101.0, 96.5, 103.5, 97.7, 97.7, 92.0
270527	Route travel distances [mile]	7.8, 2.7, 3.4, 7.8, 7.8, 2.7, 3.4, 7.8, 7.8, 7.8, 7.8, 2.7, 3.4, 7.8, 7.8, 7.8, 7.8, 2.7, 3.4, 7.8, 7.8, 2.7, 3.4, 7.8, 7.8, 8.5, 8.5, 8.5, 8.5, 8.5, 8.5, 8.5
	Stop time [min]	3.0, 0.0, 3.0, 3.0, 3.0, 0.0, 3.0, 3.0, 3.0, 3.0, 3.0, 0.0, 3.0, 3.0, 3.0, 3.0, 3.0, 0.0, 3.0, 3.0, 3.0, 0.0, 3.0, 3.0, 3.0, 3.0, 3.0, 3.0, 3.0, 3.0, 3.0
	Bus remaining range [mile]	120.0, 112.4, 119.4, 116.7, 116.7, 113.3, 120.0, 112.2, 112.2, 104.5, 111.5, 108.9, 108.9, 105.5, 112.5, 104.6, 104.6, 97.0, 104.0, 96.1, 96.1, 88.4, 95.4, 92.8, 92.8, 89.4, 96.4, 88.5, 88.5, 80.9, 87.9, 80.0, 80.0, 72.4, 79.4, 76.7, 76.7, 73.3, 80.3, 72.5, 72.5, 64.8, 71.8, 69.2, 69.2, 65.8, 72.8, 64.9, 64.9, 57.3, 64.3, 55.8, 62.8, 54.4, 61.4, 52.9, 59.9, 51.6, 58.6, 50.1, 57.1, 48.7, 55.7, 47.2

Block ID	Information	Values
270827	Route travel distances [mile]	7.8, 7.8, 2.7, 3.4, 7.8, 7.8, 2.7, 3.4, 7.8, 7.8, 7.8, 7.8, 2.7, 3.4, 7.8, 7.8, 7.8, 7.8, 2.7, 3.4, 7.8, 7.8, 2.7, 3.4, 8.5, 8.5, 8.5, 8.5, 8.5, 8.5, 8.5, 8.5
	Stop time [min]	3.0, 3.0, 0.0, 3.0, 3.0, 3.0, 0.0, 3.0, 3.0, 3.0, 3.0, 3.0, 0.0, 3.0, 3.0, 3.0, 3.0, 3.0, 0.0, 3.0, 3.0, 3.0, 0.0, 3.0, 3.0, 3.0, 3.0, 3.0, 3.0, 3.0
	Bus remaining range [mile]	120.0, 112.2, 112.2, 104.5, 111.5, 108.9, 108.9, 105.5, 112.5, 104.6, 104.6, 97.0, 104.0, 101.3, 101.3, 97.9, 104.9, 97.1, 97.1, 89.4, 96.4, 88.6, 88.6, 80.9, 87.9, 85.2, 85.2, 81.8, 88.8, 81.0, 81.0, 73.3, 80.3, 72.5, 72.5, 64.8, 71.8, 69.2, 69.2, 65.8, 72.8, 64.9, 64.9, 57.3, 64.3, 61.6, 61.6, 58.2, 65.2, 56.7, 63.7, 55.4, 62.4, 53.9, 60.9, 52.5, 59.5, 51.0, 58.0, 49.7, 56.7, 48.2, 55.2, 46.8
6046	Route travel distances [mile]	9.5, 9.6, 4.4, 4.5, 9.5, 9.6, 4.4, 4.5, 9.5, 9.6, 4.4, 4.5, 9.5, 9.6, 4.4, 4.5, 9.5, 9.6, 4.4, 4.5, 7.8, 7.9, 4.4, 4.5, 7.8, 7.9, 4.4, 4.5, 7.8, 7.9, 4.4
	Stop time [min]	15.0, 3.0, 3.0, 0.0, 15.0, 3.0, 3.0, 0.0, 15.0, 3.0, 3.0, 0.0, 15.0, 3.0, 3.0, 0.0, 15.0, 3.0, 3.0, 0.0, 3.0, 0.0, 3.0, 0.0, 18.0, 0.0, 3.0, 0.0, 18.0, 0.0
	Bus remaining range [mile]	120.0, 110.5, 110.5, 100.9, 107.9, 106.9, 113.9, 109.4, 109.4, 99.9, 99.9, 90.3, 97.3, 96.3, 103.3, 98.8, 98.8, 89.3, 89.3, 79.7, 86.7, 85.7, 92.7, 88.2, 88.2, 78.7, 78.7, 69.1, 76.1, 75.1, 82.1, 77.5, 77.5, 68.0, 68.0, 58.5, 65.5, 64.4, 71.4, 66.9, 66.9, 59.2, 59.2, 51.2, 51.2, 50.2, 57.2, 52.7, 52.7, 44.9, 44.9, 37.0, 37.0, 35.9, 42.9, 38.4, 38.4, 30.6, 30.6, 22.7, 22.7, 21.7
300430	Route travel distances [mile]	7.5, 3.4, 4.5, 5.9, 5.8, 7.7, 7.5, 3.4, 4.5, 5.9, 5.8, 3.4, 4.5, 5.9, 5.8, 3.4, 4.5, 5.9, 5.8, 3.4, 4.5, 5.9, 5.8, 7.7, 7.5, 3.4, 4.5, 5.9, 5.8, 7.7, 7.5, 3.4, 4.5, 5.9, 5.8, 7.7, 7.5, 3.4, 4.5
	Stop time [min]	3.0, 0.0, 3.0, 0.0, 3.0, 2.0, 3.0, 0.0, 3.0, 0.0, 3.0, 0.0, 3.0, 0.0, 3.0, 0.0, 3.0, 0.0, 3.0, 0.0, 3.0, 0.0, 3.0, 0.0, 3.0, 2.0, 3.0, 0.0, 3.0, 0.0, 3.0, 0.0, 5.0, 0.0, 3.0, 0.0, 3.0, 0.0, 18.0, 0.0
	Bus remaining range [mile]	120.0, 112.7, 119.7, 116.4, 116.4, 111.8, 118.8, 113.0, 113.0, 107.4, 114.4, 106.6, 111.3, 104.0, 111.0, 107.6, 107.6, 103.1, 110.1, 104.3, 104.3, 98.6, 105.6, 102.2, 102.2, 97.7, 104.7, 98.9, 98.9, 93.2, 100.2, 96.9, 96.9, 92.4, 99.4, 93.5, 93.5, 87.8, 94.8, 91.5, 91.5, 87.0, 94.0, 88.1, 88.1, 82.5, 89.5, 81.7, 86.4, 79.1, 86.1, 82.8, 82.8, 78.3, 85.3, 79.4, 79.4, 73.8, 80.8, 73.0, 73.0, 65.7, 77.4, 74.0, 74.0, 69.5, 76.5, 70.7, 70.7, 65.0, 72.0, 64.3, 64.3, 57.0, 99.0, 95.6, 95.6, 91.1

Block ID	Information	Values
420642	Route travel distances [mile]	12.3, 12.5, 12.3, 12.5, 12.3, 12.5, 12.3, 12.5, 12.3, 12.5, 12.3, 12.5, 12.3, 4.2, 3.9, 12.5, 12.3, 4.2, 3.9, 12.5
	Stop time [min]	3.0, 3.0, 3.0, 3.0, 3.0, 3.0, 3.0, 3.0, 3.0, 3.0, 3.0, 3.0, 18.0, 0.0, 18.0, 3.0, 18.0, 0.0, 18.0
	Bus remaining range [mile]	120.0, 107.7, 114.7, 102.4, 109.4, 97.0, 104.0, 91.7, 98.7, 86.4, 93.4, 81.1, 88.1, 75.7, 82.7, 70.4, 77.4, 65.1, 72.1, 59.8, 66.8, 54.5, 61.5, 49.2, 56.2, 43.8, 85.8, 81.7, 81.7, 77.7, 119.7, 107.4, 114.4, 102.1, 120.0, 115.8, 115.8, 111.9, 120.0, 107.7
420842	Route travel distances [mile]	12.5, 12.3, 12.5, 12.3, 12.5, 12.3, 12.5, 12.3, 12.5, 12.3, 12.5, 12.3, 4.2, 3.9, 12.5, 12.3, 4.2, 3.9, 12.5, 12.3
	Stop time [min]	3.0, 3.0, 3.0, 3.0, 3.0, 3.0, 3.0, 3.0, 3.0, 3.0, 3.0, 18.0, 0.0, 18.0, 3.0, 18.0, 0.0, 18.0, 3.0
	Bus remaining range [mile]	120.0, 107.7, 114.7, 102.4, 109.4, 97.1, 104.1, 91.7, 98.7, 86.4, 93.4, 81.1, 88.1, 75.8, 82.8, 70.4, 77.4, 65.1, 72.1, 59.8, 66.8, 54.5, 61.5, 49.2, 91.2, 87.0, 87.0, 83.1, 120.0, 107.7, 114.7, 102.4, 120.0, 115.8, 115.8, 111.9, 120.0, 107.7, 114.7, 102.4
5045	Route travel distances [mile]	9.7, 8.0, 10.5, 10.6, 8.1, 9.8, 9.7, 8.0, 10.5, 10.6, 8.1, 9.8, 9.7, 8.0, 10.5, 10.6, 10.5, 10.6, 10.5, 10.6, 10.5, 10.6, 10.5
	Stop time [min]	6.0, 3.0, 3.0, 3.0, 0.0, 3.0, 6.0, 3.0, 3.0, 3.0, 0.0, 3.0, 6.0, 3.0, 3.0, 18.0, 3.0, 3.0, 3.0, 3.0, 3.0, 3.0
	Bus remaining range [mile]	120.0, 110.3, 120.0, 112.5, 119.5, 108.9, 115.9, 105.9, 112.9, 104.8, 104.8, 94.9, 101.9, 92.2, 106.2, 98.7, 105.7, 95.2, 102.2, 92.1, 99.1, 91.0, 91.0, 81.2, 88.2, 78.5, 92.5, 84.9, 91.9, 81.4, 88.4, 78.4, 120.0, 109.5, 116.5, 106.4, 113.4, 102.8, 109.8, 99.7, 106.7, 96.2, 103.2, 93.1, 100.1, 89.6
300230	Route travel distances [mile]	5.9, 5.8, 7.7, 7.5, 3.4, 4.5, 5.9, 5.8, 7.7, 7.5, 7.7, 7.5, 7.7, 7.5, 7.7, 7.5, 7.7, 7.5, 3.4, 4.9, 5.9, 5.8, 7.7, 7.5, 3.4, 4.5, 5.9, 5.8, 7.7, 7.5, 3.4, 4.5, 5.9, 5.8, 7.7, 7.5
	Stop time [min]	0.0, 3.0, 2.0, 3.0, 0.0, 3.0, 0.0, 3.0, 0.0, 3.0, 0.0, 3.0, 0.0, 3.0, 0.0, 3.0, 2.0, 3.0, 0.0, 3.0, 0.0, 3.0, 2.0, 3.0, 0.0, 3.0, 0.0, 3.0, 0.0, 18.0, 0.0, 3.0, 0.0, 3.0, 0.0
	Bus remaining range [mile]	120.0, 114.1, 114.1, 108.5, 115.5, 107.8, 112.4, 105.2, 112.2, 108.8, 108.8, 104.3, 111.3, 105.4, 105.4, 99.8, 106.8, 99.1, 99.1, 91.7, 98.7, 91.0, 91.0, 83.7, 90.7, 83.0, 83.0, 75.6, 82.6, 74.9, 74.9, 67.6, 74.6, 66.9, 71.5, 64.2, 71.2, 67.9, 67.9, 62.9, 69.9, 64.1, 64.1, 58.4, 65.4, 57.7, 62.4, 55.1, 62.1, 58.7, 58.7, 54.2, 61.2, 55.4, 55.4, 49.7, 56.7, 49.0, 49.0, 41.7, 83.7, 80.3, 80.3, 75.8, 82.8, 77.0, 77.0, 71.3, 78.3, 70.6, 70.6, 63.3

Block ID	Information	Values
5035	Route travel distances [mile]	10.6, 8.1, 9.8, 9.7, 8.0, 10.5, 10.6, 8.1, 9.8, 9.7, 8.0, 10.5, 10.6, 8.1, 9.8, 9.7, 7.4, 7.4, 7.4, 7.4, 7.4, 7.4, 7.4, 7.4, 7.4, 7.4, 7.4
	Stop time [min]	3.0, 0.0, 3.0, 6.0, 3.0, 3.0, 3.0, 0.0, 3.0, 6.0, 3.0, 3.0, 3.0, 0.0, 3.0, 3.0, 3.0, 3.0, 3.0, 3.0, 3.0, 3.0, 3.0, 3.0, 3.0, 3.0
	Bus remaining range [mile]	120.0, 109.9, 116.9, 108.8, 108.8, 99.0, 106.0, 96.3, 110.3, 102.8, 109.8, 99.2, 106.2, 96.2, 103.2, 95.1, 95.1, 85.2, 92.2, 82.5, 96.5, 89.0, 96.0, 85.5, 92.5, 82.4, 89.4, 81.3, 81.3, 71.5, 78.5, 68.8, 75.8, 68.4, 75.4, 68.0, 75.0, 67.6, 74.6, 67.1, 74.1, 66.7, 73.7, 66.3, 73.3, 65.9, 72.9, 65.5, 72.5, 65.1, 72.1, 64.7, 71.7, 64.3
5085	Route travel distances [mile]	8.1, 9.8, 9.7, 8.0, 10.5, 10.6, 8.1, 9.8, 9.7, 8.0, 10.5, 10.6, 8.1, 9.8, 9.7, 8.0, 10.5, 10.6, 10.5, 10.6, 10.5, 10.6, 10.5, 10.6
	Stop time [min]	0.0, 3.0, 6.0, 3.0, 3.0, 3.0, 0.0, 3.0, 6.0, 3.0, 3.0, 3.0, 0.0, 3.0, 6.0, 3.0, 3.0, 3.0, 3.0, 3.0, 3.0, 3.0, 3.0
	Bus remaining range [mile]	120.0, 111.9, 111.9, 102.1, 109.1, 99.3, 113.3, 105.8, 112.8, 102.3, 109.3, 99.2, 106.2, 98.1, 98.1, 88.3, 95.3, 85.6, 99.6, 92.0, 99.0, 88.5, 95.5, 85.5, 92.5, 84.3, 84.3, 74.5, 81.5, 71.8, 85.8, 78.3, 85.3, 74.8, 81.8, 71.6, 78.6, 68.1, 75.1, 65.0, 72.0, 61.5, 68.5, 58.4, 65.4, 54.8, 61.8, 51.7
271327	Route travel distances [mile]	4.2, 5.6, 5.6, 4.3, 4.2, 5.6, 5.6, 4.3, 4.2, 5.6, 5.6, 4.3, 4.2, 5.6, 5.6, 4.3, 4.2, 5.6, 5.6, 4.3, 4.2, 5.6, 5.6, 4.3, 4.2, 5.6, 5.6, 4.3, 4.2, 5.6, 5.6, 4.3, 4.2, 5.6, 5.6, 4.3, 4.2, 2.7, 3.4, 5.6, 5.6, 4.3, 4.2, 2.7, 3.4, 5.6, 5.6, 4.3, 4.2
	Stop time [min]	3.0, 0.0, 3.0, 0.0
	Bus remaining range [mile]	120.0, 115.8, 120.0, 114.4, 114.4, 108.7, 115.7, 111.4, 111.4, 107.2, 114.2, 108.6, 108.6, 103.0, 110.0, 105.7, 105.7, 101.5, 108.5, 102.8, 102.8, 97.2, 104.2, 99.9, 99.9, 95.7, 102.7, 97.0, 97.0, 91.4, 98.4, 94.1, 94.1, 89.9, 96.9, 91.3, 91.3, 85.6, 92.6, 88.3, 88.3, 84.1, 91.1, 85.5, 85.5, 79.9, 86.9, 82.6, 82.6, 78.4, 85.4, 79.7, 79.7, 74.1, 81.1, 76.8, 76.8, 72.6, 79.6, 73.9, 73.9, 68.3, 75.3, 71.0, 71.0, 66.8, 73.8, 68.2, 68.2, 62.5, 69.5, 65.2, 65.2, 61.0, 68.0, 65.4, 65.4, 62.0, 69.0, 63.3, 63.3, 57.7, 64.7, 60.4, 60.4, 56.2, 63.2, 60.5, 60.5, 57.1, 64.1, 58.5, 58.5, 52.9, 59.9, 55.6, 55.6, 51.4

Block ID	Information	Values
271127	Route travel distances [mile]	5.6, 4.3, 4.2, 5.6, 5.6, 4.3, 4.2, 5.6, 5.6, 4.3, 4.2, 5.6, 5.6, 4.3, 4.2, 5.6, 5.6, 4.3, 4.2, 5.6, 5.6, 4.3, 4.2, 5.6, 5.6, 4.3, 4.2, 5.6, 5.6, 4.3, 4.2, 5.6, 5.6, 4.3, 4.2, 5.6, 5.6, 4.3, 4.2, 2.7, 3.4, 5.6, 5.6, 4.3, 4.2, 2.7, 3.4, 5.6, 5.6, 4.3, 4.2, 2.7, 3.4, 5.6
	Stop time [min]	3.0, 0.0, 3.0
	Bus remaining range [mile]	120.0, 114.4, 120.0, 115.7, 115.7, 111.5, 118.5, 112.9, 112.9, 107.2, 114.2, 109.9, 109.9, 105.7, 112.7, 107.1, 107.1, 101.5, 108.5, 104.2, 104.2, 99.9, 106.9, 101.3, 101.3, 95.7, 102.7, 98.4, 98.4, 94.2, 101.2, 95.5, 95.5, 89.9, 96.9, 92.6, 92.6, 88.4, 95.4, 89.8, 89.8, 84.1, 91.1, 86.8, 86.8, 82.6, 89.6, 84.0, 84.0, 78.4, 85.4, 81.1, 81.1, 76.8, 83.8, 78.2, 78.2, 72.6, 79.6, 75.3, 75.3, 71.1, 78.1, 72.4, 72.4, 66.8, 73.8, 69.5, 69.5, 65.3, 72.3, 69.6, 69.6, 66.2, 73.2, 67.6, 67.6, 62.0, 69.0, 64.7, 64.7, 60.5, 67.5, 64.8, 64.8, 61.4, 68.4, 62.8, 62.8, 57.1, 64.1, 59.9, 59.9, 55.6, 62.6, 60.0, 60.0, 56.6, 63.6, 57.9
6026	Route travel distances [mile]	13.3, 13.9, 13.3, 13.9, 13.3, 13.9, 13.3, 13.9, 13.3, 13.9, 13.3, 13.9, 13.3, 4.5, 7.8, 7.9, 4.4, 4.5, 7.8, 7.9, 4.4, 4.5, 7.8
	Stop time [min]	3.0, 3.0, 3.0, 3.0, 3.0, 3.0, 3.0, 3.0, 3.0, 3.0, 3.0, 3.0, 3.0, 0.0, 18.0, 0.0, 3.0, 0.0, 18.0, 0.0, 3.0, 0.0
	Bus remaining range [mile]	120.0, 109.6, 116.6, 102.6, 109.6, 99.2, 106.2, 92.3, 99.3, 88.9, 95.9, 81.9, 88.9, 78.5, 85.5, 71.6, 78.6, 68.1, 75.1, 61.2, 68.2, 57.8, 64.8, 50.9, 57.9, 47.4, 54.4, 49.9, 49.9, 42.2, 42.2, 34.2, 34.2, 33.2, 40.2, 35.6, 35.6, 27.9, 27.9, 19.9, 19.9, 18.9, 25.9, 21.4, 21.4, 13.6
5065	Route travel distances [mile]	9.8, 9.7, 8.0, 10.5, 10.6, 8.1, 9.8, 9.7, 8.0, 10.5, 10.6, 8.1, 11.7, 11.4, 8.0, 10.5, 10.6, 10.5, 10.6, 10.5, 10.6, 10.5, 10.6, 10.5
	Stop time [min]	3.0, 6.0, 3.0, 3.0, 3.0, 0.0, 3.0, 6.0, 3.0, 3.0, 3.0, 0.0, 0.0, 9.0, 3.0, 3.0, 18.0, 3.0, 3.0, 3.0, 3.0, 3.0, 3.0
	Bus remaining range [mile]	120.0, 110.2, 117.2, 107.5, 120.0, 112.5, 119.5, 108.9, 115.9, 105.9, 112.9, 104.8, 104.8, 94.9, 101.9, 92.2, 106.2, 98.7, 105.7, 95.2, 102.2, 92.1, 99.1, 91.0, 91.0, 79.3, 79.3, 67.9, 88.9, 81.4, 88.4, 77.9, 84.9, 74.8, 116.8, 106.3, 113.3, 103.2, 110.2, 99.7, 106.7, 96.5, 103.5, 93.0, 100.0, 89.9, 96.9, 86.4
6076	Route travel distances [mile]	13.3, 13.9, 13.3, 13.9, 13.3, 13.9, 13.3, 13.9, 13.3, 13.9, 13.3, 13.9, 13.3, 13.9, 13.3, 13.9, 13.3, 13.9, 13.3, 13.9
	Stop time [min]	3.0, 3.0, 3.0, 3.0, 3.0, 3.0, 3.0, 3.0, 3.0, 3.0, 3.0, 3.0, 3.0, 3.0, 3.0, 3.0
	Bus remaining range [mile]	120.0, 109.6, 116.6, 102.6, 109.6, 99.2, 106.2, 92.3, 99.3, 88.9, 95.9, 81.9, 88.9, 78.5, 85.5, 71.6, 78.6, 68.1, 75.1, 61.2, 68.2, 57.8, 64.8, 50.9, 57.9, 47.4, 54.4, 40.5, 47.5, 37.1, 44.1, 30.1, 37.1, 26.7, 33.7, 19.8

Block ID	Information	Values
6086	Route travel distances [mile]	13.9, 13.3, 13.9, 13.3, 13.9, 13.3, 13.9, 13.3, 13.9, 13.3, 13.9, 13.3, 13.9, 13.3, 13.9, 13.3, 13.9, 13.3
	Stop time [min]	3.0, 3.0, 3.0, 3.0, 3.0, 3.0, 3.0, 3.0, 3.0, 3.0, 3.0, 3.0, 3.0, 3.0, 3.0, 3.0, 3.0
	Bus remaining range [mile]	120.0, 106.1, 113.1, 102.6, 109.6, 95.7, 102.7, 92.3, 99.3, 85.4, 92.4, 81.9, 88.9, 75.0, 82.0, 71.6, 78.6, 64.6, 71.6, 61.2, 68.2, 54.3, 61.3, 50.9, 57.9, 43.9, 50.9, 40.5, 47.5, 33.6, 40.6, 30.1, 37.1, 23.2, 30.2, 19.8
420542	Route travel distances [mile]	4.2, 3.9, 6.2, 5.8, 4.4, 3.9, 4.6, 6.1, 4.2, 3.9, 6.2, 5.8, 4.4, 3.9, 4.6, 6.1, 4.2, 3.9, 6.2, 5.8, 4.4, 3.9, 4.6, 6.1, 4.2, 3.9, 6.2, 5.8, 4.4, 3.9, 4.6, 6.1, 4.2, 3.9, 6.2, 5.8, 4.4, 3.9, 4.6, 6.1, 12.5, 12.3, 4.2, 3.9, 12.5, 12.3
	Stop time [min]	0.0, 3.0, 0.0, 3.0, 0.0, 3.0, 0.0, 3.0, 0.0, 3.0, 0.0, 3.0, 0.0, 3.0, 0.0, 3.0, 0.0, 3.0, 0.0, 3.0, 0.0, 3.0, 0.0, 3.0, 0.0, 3.0, 0.0, 3.0, 0.0, 3.0, 0.0, 3.0, 0.0, 3.0, 0.0, 3.0, 0.0, 3.0, 0.0, 18.0, 3.0, 18.0, 0.0, 18.0, 3.0
	Bus remaining range [mile]	120.0, 115.8, 115.8, 111.9, 118.9, 112.8, 112.8, 106.9, 113.9, 109.6, 109.6, 105.7, 112.7, 108.1, 108.1, 102.1, 109.1, 104.9, 104.9, 101.0, 108.0, 101.8, 101.8, 96.0, 103.0, 98.7, 98.7, 94.8, 101.8, 97.2, 97.2, 91.1, 98.1, 94.0, 94.0, 90.1, 97.1, 90.9, 90.9, 85.1, 92.1, 87.7, 87.7, 83.9, 90.9, 86.3, 86.3, 80.2, 87.2, 83.1, 83.1, 79.1, 86.1, 80.0, 80.0, 74.1, 81.1, 76.8, 76.8, 72.9, 79.9, 75.3, 75.3, 69.3, 76.3, 72.1, 72.1, 68.2, 75.2, 69.0, 69.0, 63.2, 70.2, 65.9, 65.9, 62.0, 69.0, 64.4, 64.4, 58.3, 100.3, 88.0, 95.0, 82.7, 120.0, 115.8, 115.8, 111.9, 120.0, 107.7, 114.7, 102.4

Block ID	Information	Values
430243	Route travel distances [mile]	3.8, 5.7, 5.4, 3.6, 3.2, 2.9, 3.8, 5.7, 5.4, 3.6, 3.2, 2.9, 3.8, 5.7, 5.4, 3.6, 3.2, 2.9, 3.8, 5.7, 5.4, 3.6, 3.2, 2.9, 3.8, 5.7, 5.4, 3.6, 3.2, 2.9, 3.8, 5.7, 5.4, 3.6, 3.2, 2.9, 3.8, 5.7, 5.4, 3.6, 3.2, 2.9, 3.8, 5.7, 5.4, 3.6, 3.2, 2.9, 3.8, 5.7, 5.4, 3.6, 3.2, 2.9, 3.8, 5.7, 5.4, 3.6, 3.2, 2.9, 3.8, 5.7, 5.4, 3.6, 3.2, 2.9
	Stop time [min]	0.0, 5.0, 0.0, 3.0, 0.0, 3.0, 0.0, 5.0, 0.0, 3.0, 0.0, 3.0, 0.0, 5.0, 0.0, 3.0, 0.0, 3.0, 0.0, 5.0, 0.0, 3.0, 0.0, 3.0, 0.0, 5.0, 0.0, 3.0, 0.0, 3.0, 0.0, 5.0, 0.0, 3.0, 0.0, 3.0, 0.0, 5.0, 0.0, 3.0, 0.0, 3.0, 0.0, 5.0, 0.0, 3.0, 0.0, 3.0, 15.0, 5.0, 15.0, 3.0, 0.0, 3.0, 15.0, 5.0, 15.0, 3.0, 0.0, 3.0, 15.0, 5.0, 15.0, 3.0, 0.0
	Bus remaining range [mile]	120.0, 116.2, 116.2, 110.5, 120.0, 114.6, 114.6, 111.0, 118.0, 114.8, 114.8, 111.9, 118.9, 115.1, 115.1, 109.4, 120.0, 114.6, 114.6, 111.0, 118.0, 114.8, 114.8, 111.9, 118.9, 115.1, 115.1, 109.4, 120.0, 114.6, 114.6, 111.0, 118.0, 114.8, 114.8, 111.9, 118.9, 115.1, 115.1, 109.4, 120.0, 114.6, 114.6, 111.0, 118.0, 114.8, 114.8, 111.9, 118.9, 115.1, 115.1, 109.4, 120.0, 114.6, 114.6, 111.0, 118.0, 114.8, 114.8, 111.9, 118.9, 115.1, 115.1, 109.4, 120.0, 114.6, 114.6, 111.0, 118.0, 114.8, 114.8, 111.9, 118.9, 115.1, 115.1, 109.4, 120.0, 114.6, 114.6, 111.0, 118.0, 114.8, 114.8, 111.9, 118.9, 115.1, 120.0, 114.3, 120.0, 114.6, 120.0, 116.4, 120.0, 116.8, 116.8, 113.9, 120.0, 116.2, 120.0, 114.3, 120.0, 114.6, 120.0, 116.4, 120.0, 116.8, 116.8, 113.9, 120.0, 116.2, 120.0, 114.3, 120.0, 114.6, 120.0, 116.4, 120.0, 116.8, 116.8, 113.9
420442	Route travel distances [mile]	4.4, 3.9, 4.6, 6.1, 4.2, 3.9, 6.2, 5.8, 4.4, 3.9, 4.6, 6.1, 4.2, 3.9, 6.2, 5.8, 4.4, 3.9, 4.6, 6.1, 4.2, 3.9, 6.2, 5.8, 4.4, 3.9, 4.6, 6.1, 4.2, 3.9, 6.2, 5.8, 4.4, 3.9, 4.6, 6.1, 4.2, 3.9, 6.2, 5.8, 4.4, 3.9, 4.6, 6.1, 6.2, 5.8, 4.4, 3.9, 4.6, 6.1, 6.2, 5.8, 4.4, 3.9, 4.6, 6.1
	Stop time [min]	0.0, 3.0, 0.0
	Bus remaining range [mile]	120.0, 115.6, 115.6, 111.8, 118.8, 114.2, 114.2, 108.1, 115.1, 111.0, 111.0, 107.1, 114.1, 107.9, 107.9, 102.1, 109.1, 104.7, 104.7, 100.8, 107.8, 103.3, 103.3, 97.2, 104.2, 100.0, 100.0, 96.1, 103.1, 97.0, 97.0, 91.1, 98.1, 93.8, 93.8, 89.9, 96.9, 92.3, 92.3, 86.3, 93.3, 89.1, 89.1, 85.2, 92.2, 86.0, 86.0, 80.2, 87.2, 82.9, 82.9, 79.0, 86.0, 81.4, 81.4, 75.3, 82.3, 78.2, 78.2, 74.3, 81.3, 75.1, 75.1, 69.3, 76.3, 71.9, 71.9, 68.0, 75.0, 70.5, 70.5, 64.4, 71.4, 67.2, 67.2, 63.3, 70.3, 64.2, 64.2, 58.3, 65.3, 61.0, 61.0, 57.1, 64.1, 59.5, 59.5, 53.5, 60.5, 54.3, 54.3, 48.5, 55.5, 51.1, 51.1, 47.3, 54.3, 49.7, 49.7, 43.6, 50.6, 44.4, 44.4, 38.6, 45.6, 41.3, 41.3, 37.4, 44.4, 39.8, 39.8, 33.8

Block ID	Information	Values
430343	Route travel distances [mile]	5.4, 3.6, 3.2, 2.9, 3.8, 5.7, 5.4, 3.6, 3.2, 2.9, 3.8, 5.7, 5.4, 3.6, 3.2, 2.9, 3.8, 5.7, 5.4, 3.6, 3.2, 2.9, 3.8, 5.7, 5.4, 3.6, 3.2, 2.9, 3.8, 5.7, 5.4, 3.6, 3.2, 2.9, 3.8, 5.7, 5.4, 3.6, 3.2, 2.9, 3.8, 5.7, 5.4, 3.6, 3.2, 2.9, 3.8, 5.7, 5.4, 3.6, 3.2, 2.9, 3.8, 5.7, 5.4, 3.6, 3.2, 2.9, 3.8, 5.7, 5.4, 3.6, 3.2, 2.9, 3.8, 5.7, 5.4
	Stop time [min]	0.0, 3.0, 0.0, 3.0, 0.0, 5.0, 0.0, 3.0, 0.0, 3.0, 0.0, 5.0, 0.0, 3.0, 0.0, 3.0, 0.0, 5.0, 0.0, 3.0, 0.0, 3.0, 0.0, 5.0, 0.0, 3.0, 0.0, 3.0, 0.0, 5.0, 0.0, 3.0, 0.0, 3.0, 0.0, 5.0, 0.0, 3.0, 0.0, 3.0, 0.0, 5.0, 0.0, 3.0, 0.0, 3.0, 0.0, 5.0, 0.0, 3.0, 0.0, 3.0, 15.0, 5.0, 15.0, 3.0, 0.0, 3.0, 15.0, 5.0, 15.0, 3.0, 0.0, 3.0, 15.0, 5.0
	Bus remaining range [mile]	120.0, 114.6, 114.6, 111.0, 118.0, 114.8, 114.8, 111.9, 118.9, 115.1, 115.1, 109.4, 120.0, 114.6, 114.6, 111.0, 118.0, 114.8, 114.8, 111.9, 118.9, 115.1, 115.1, 109.4, 120.0, 114.6, 114.6, 111.0, 118.0, 114.8, 114.8, 111.9, 118.9, 115.1, 115.1, 109.4, 120.0, 114.6, 114.6, 111.0, 118.0, 114.8, 114.8, 111.9, 118.9, 115.1, 115.1, 109.4, 120.0, 114.6, 114.6, 111.0, 118.0, 114.8, 114.8, 111.9, 118.9, 115.1, 115.1, 109.4, 120.0, 114.6, 114.6, 111.0, 118.0, 114.8, 114.8, 111.9, 118.9, 115.1, 115.1, 109.4, 120.0, 114.6, 114.6, 111.0, 118.0, 114.8, 114.8, 111.9, 118.9, 115.1, 115.1, 109.4, 120.0, 114.6, 114.6, 111.0, 118.0, 114.8, 114.8, 111.9, 118.9, 115.1, 115.1, 109.4, 120.0, 114.6, 114.6, 111.0, 118.0, 114.8, 114.8, 111.9, 118.9, 115.1, 120.0, 114.3, 120.0, 114.6, 120.0, 116.4, 120.0, 116.8, 116.8, 113.9, 120.0, 116.2, 120.0, 114.3, 120.0, 114.6, 120.0, 116.4, 120.0, 116.8, 116.8, 113.9, 120.0, 116.2, 120.0, 114.3, 120.0, 114.6
420242	Route travel distances [mile]	7.8, 4.2, 3.9, 8.4, 8.6, 4.4, 3.9, 4.6, 6.1, 4.2, 3.9, 6.2, 5.8, 4.4, 3.9, 4.6, 6.1, 4.2, 3.9, 6.2, 5.8, 4.4, 3.9, 4.6, 6.1, 4.2, 3.9, 6.2, 5.8, 4.4, 3.9, 4.6, 6.1, 4.2, 3.9, 6.2, 5.8, 4.4, 3.9, 4.6, 6.1, 6.2, 5.8, 4.4, 3.9, 4.6, 6.1, 6.2, 5.8, 4.4, 3.9, 4.6, 6.1, 6.2, 5.8, 4.4
	Stop time [min]	3.0, 0.0, 3.0, 3.0, 3.0, 0.0, 3.0
	Bus remaining range [mile]	120.0, 112.2, 119.2, 115.1, 115.1, 111.1, 118.1, 109.7, 116.7, 108.1, 115.1, 110.7, 110.7, 106.8, 113.8, 109.3, 109.3, 103.2, 110.2, 106.0, 106.0, 102.1, 109.1, 102.9, 102.9, 97.1, 104.1, 99.8, 99.8, 95.9, 102.9, 98.3, 98.3, 92.3, 99.3, 95.1, 95.1, 91.2, 98.2, 92.0, 92.0, 86.2, 93.2, 88.8, 88.8, 85.0, 92.0, 87.4, 87.4, 81.3, 88.3, 84.2, 84.2, 80.3, 87.3, 81.1, 81.1, 75.3, 82.3, 77.9, 77.9, 74.0, 81.0, 76.5, 76.5, 70.4, 77.4, 73.2, 73.2, 69.3, 76.3, 70.2, 70.2, 64.3, 71.3, 67.0, 67.0, 63.1, 70.1, 65.5, 65.5, 59.5, 66.5, 60.3, 60.3, 54.5, 61.5, 57.1, 57.1, 53.3, 60.3, 55.7, 55.7, 49.6, 56.6, 50.4, 50.4, 44.6, 51.6, 47.3, 47.3, 43.4, 50.4, 45.8, 45.8, 39.8, 46.8, 40.6, 40.6, 34.8, 41.8, 37.4